Monthly Scientific-Technical and Production Journal

The Paton WELDING JOURNAL

November 2001 # 11

English translation of the monthly «Avtomaticheskaya Svarka» journal published in Russian since 1948

The National Academy of Sciences of Ukraine
The E.O. Paton Electric Welding Institute of the NAS of Ukraine
International Association «Welding»

«The Paton Welding Journal»
is published monthly by the
International Association «Welding»

Promotion group:
V.N.Lipodaev, V.I.Lokteva
A.T.Zelnichenko (exec. director)
Translators:
S.A.Fomina, I.N.Kutianova,
T.K.Vasilenko
Editor
N.A.Dmitrieva
Electron galley:
I.V.Petushkov, T.Yu.Snegireva

Editorial and advertising offices
are located at PWI,
International Association «Welding»,
11, Bozhenko str., 03680,
Kyiv, Ukraine
Tel.: (38044) 227 67 57
Fax: (38044) 268 04 86
E-mail: journal@paton.kiev.ua

State Registration Certificate
KV 4790 of 09.01.2001

Subscriptions:
$460, 12 issues per year,
postage and packaging included.
Back issues available

«The Paton Welding Journal» Website:
http://www.nas.gov.ua/pwj

CONTENTS

Residual stresses can be fundamentally decreased by means of initial preheating to a temperature of about 300 °C [7], which is inexpedient in an active pipeline.

CONCLUSIONS

1. Individual pitting defects in active gas and oil pipelines can be repaired by manual arc welding under sparing conditions at a sufficient thickness of root face, H, excluding formation of fracture of the jumper during the welding process by a mechanism of plastic instability under a pressure.

2. Welding up of a pitting defect in pipelines of home-made pipe steels involves a problem of formation of cold (hydrogen) cracks. To avoid such defects, it is necessary to use technological precautions intended for a decrease in the hydrogen content of the welding zone. The content of unfavourable structures (martensite, low-temperature bainite), upon which cold cracking depends, can be decreased by preheating to 150 °C.

REFERENCES

1. *API Standard 1104* (1999) Welding of pipelines and related facilities. Appendix 13. Service Welding. American Petroleum Institute.
2. Burak, Ya.I., Galyuk, V.Kh., Dzhardzhimanov, A.S. *et al.* (1981) Development of parameters for welding repair of cavities in active main oil pipelines. In: *Transport and Storage of Oil and Oil Products*, Issue 1. Moscow.
3. Taliat, V., Zacharia, T., Wang, X.-L. *et al.* (1998) Numerical analysis of residual stress distribution in tubes with spiral weld cladding. *Welding J.*, **8**, 328 – 335.
4. Isachenko, V.P., Osipov, V.A., Sukhomel, A.S. (1975) *Heat transfer*. Moscow: Energia.
5. Erokhin, A.A. (1964) *Kinetics of metallurgical processes of arc welding*. Moscow: Mashinostroyeniye.
6. (1968) *Strength, stability and oscillations*. Handbook. Ed. by I.A. Birger, Ya.G. Panovko. Moscow: Mashinostroyeniye.
7. Makhnenko, V.I. (1976) *Calculation models for investigation of kinetics of welding stresses and strains*. Kyiv: Naukova Dumka.
8. Makhnenko, V.I., Velikoivanenko, E.A., Pochinok, V.E. *et al.* (1999) Numerical methods of the predictions of welding stresses and distortions. *Welding and Surfacing Rev.*, Vol. 13, Part 1. Harwood A.P.
9. Daffy, F., Eiberg, R., McSey, W. (1972) On behaviour of defects in pressure vessels. In: *New methods for estimation of brittle fracture resistance of materials*. Moscow: Mir.
10. Seyffarth, P., Meyer, B., Scharff, A. (1992) Grosser Altas Schwess-ZTU-Schaubilder. Düsseldorf: Dt. Verl. für Schweisstechnik, DVS-Verl.

HEAT INPUT INFLUENCE ON FORMATION OF TEARS IN HIGH-CARBON STEEL BUILDING-UP WITH AUSTENITIC WIRES

V.K. KALENSKY, Ya.P. CHERNYAK, V.G. VASILIEV and **T.G. SOLOMIJCHUK**

The E.O. Paton Electric Welding Institute, NASU, Kyiv, Ukraine

ABSTRACT

Multilayer building-up of worn surfaces of girder tram rails with austenitic wires of PP-06Kh15G15N2MF type is used to demonstrate that deposition of the first bead by one arc with 28 – 30 kJ/cm heat input prevents tears formation in the HAZ metal of difficult-to-weld high-carbon steel M-76.

Key words: *building-up, wear, reconditioning, HAZ metal, tears, twin- and single-arc processes, thermal cycles, structure, hardness*

This study has been performed for the case of building-up worn rails.

Tram rails and wheels, working as a pair, lead to wear of the other part. This process is the most intensive in curvilinear portions of the track, where girder rails are installed. Inner side surfaces of the rail head and lip are mostly worn.

The E.O. Paton Electric Welding Institute experts were requested to develop a technology of building-up side surfaces of worn rails on a tram track in service, without applying any preheating or concurrent heating.

Rails are mainly made of difficult-to-weld steel M-76 (GOST 24182–80) with carbon weight fraction of 0.69 – 0.82 %.

This study was performed using rails of steel M-76, containing, wt.%: C — 0.76; Mn — 0.8; Si — 0.33; S — 0.021; P — 0.017. In building-up rails of this

Figure 1. Macrosection of a built-up rail lip

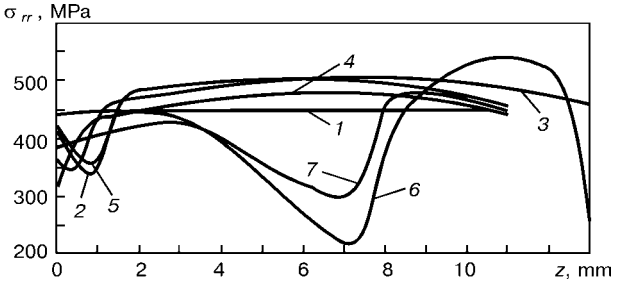

Figure 8. Distribution of residual stresses σ_{rr} depending upon z at $r = 0$ in different variants of welding up of a cavity at $2R = 1020$ mm, $d = 20$ mm and $\delta = 11$ mm: *1* — filling of a cavity with one layer ($h = 6$ mm); *2* — same with three layers at $h = 2$ mm of each layer (main variant); *3* — same with two layers at $h = 4$ mm of each layer; *4* — filling of a cavity with preheating at $T_0 = 150$ °C; *5* — filling of a cavity by the main variant at $P = 0$; *6* — filling of a cavity by the main variant after deposition of the annealing bead; *7* — same after removal of the annealing bead by machining

Picture observed in gas pipelines is approximately the same. However, in this case the process is complicated by the dependence of the intensity of heat exchange between the wall and the transported medium upon the pressure in a pipeline (see Table 1).

Results of the calculations for a velocity of $W = 6$ and 20 m/s, shown in Figure 7, indicate how the critical pressure varies with variations in values H under different welding conditions ($h = 2$ mm) and at different diameters of the cavity. Dependence of the above conditions of heat removal upon the pressure leads to a non-monotonous variation in P_{cr}, depending upon the H values under low pressures.

Along with the above-said, it is necessary also to take into account the probability of fracture of metal caused by the so-called hydrogen (cold) cracks or cracks induced by rapid cooling in welding under the above conditions.

Rapid cooling of metal leads to formation of quenching structures, which, in combination with a certain diffusible hydrogen content and tensile stresses, may create conditions for formation of hydrogen cracks. Different variants of welding up of the cavity, as well as their effect on the level of residual circumferential stresses and presence of quenching microstructures that determine the risk of formation of cold cracks, were studied with allowance for

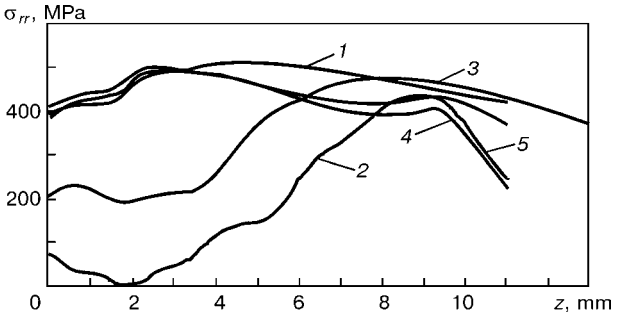

Figure 9. Distribution of residual stresses σ_{rr} depending upon z at $r = 10$ mm in different variants of welding up of a cavity at $2R = 1020$ mm, $d = 20$ mm and $\delta = 11$ mm: *1 – 3* — see explanations to Figure 8; *4* — filling of a cavity by the main variant after deposition of the annealing bead; *5* — same after removal of the annealing bead by machining

a substantial role played by welding stresses and a structural state in formation of hydrogen cracks.

Estimation of a microstructural state of the weld metal and HAZ was made in an assumption that chemical composition of the filler and base metals is identical and corresponds to that of steel 17G1S (GOST 19281–89): C — 0.15 – 0.2; Si — 0.4 – 0.6; Mn — 1.15 – 1.6; Cr — 0.3; Ni — 0.3; Cu < 0.3; P < 0.035; S < 0.04; N > 0.008; As — < 0.08 wt.%.

The diagram of anisothermal decomposition of austentite of a specific steel [10], having chemical composition within the above ranges, was used. A characteristic parameter that determines the thermal cycle of cooling and decomposition of austentite is time $\Delta t_{8/5}$, which corresponds to cooling of a certain point heated to above A_{c_3} within a temperature range of 850 – 500 °C.

The data on the time of dwelling, $\Delta t_{8/5}$, of the weld metal and HAZ within a temperature range of 850 – 500 °C (Table 3 and Figure 8), and on the corresponding microstructures (Table 4) were obtained by calculations for a variant of the oil pipeline with $2R \times \delta = 11 \times 1020$ mm in welding up of a cavity ($d = 20$ mm, $H = 5$ mm) without and with preheating to $T_0 = 150$ °C at $h = 2$ mm and $I_w = 90$ A. The initial microstructure of the base metal comprised 60 % bainite and 40 % ferrite-pearlite. It was found that $\Delta t_{8/5} \approx 6 - 8$ s for a major volume of metal heated to above 850 °C in welding without preheating.

There is a zone of $r \approx 9.5$ mm on the surface of a pipe, where $\Delta t_{8/5} \approx 4$ s. Here the microstructure consists mostly of 70 % bainite and 30 % martensite. However, the martensite content of the indicated individual zones amounts to 70 % and even 85 %, which at substantial tensile residual stresses σ_{rr} may lead to formation of cold cracks near the boundary of fusion with the base metal ($r \approx 6.5 - 10.5$ mm).

The use of local preheating to 150 °C increases $\Delta t_{8/5}$ to 10 – 11 s. Minimum values of $\Delta t_{8/5} \approx 8$ s hold at $r \approx 9.5$ mm, this having a considerable effect on the microstructure. The martensite content is no more than 22 %. The major volume of the zone of a defect repaired by welding has a bainitic structure with a martensite content of about 10 – 15 %. This provides a fundamental decrease in the probability of formation of cold cracks at the presence of tensile residual stresses.

Figures 8 and 9 give an idea of variations in residual circumferential $\sigma_{\beta\beta}$ and radial σ_{rr} stresses in the welded up cavity. Shown are the values of $\sigma_{\beta\beta} = \sigma_{rr}$ through thickness δ along axis z at $r = 0$ and 10 mm, depending upon different conditions of welding up of a cavity in a pipe of the oil pipeline 11×1020 mm in size, made from steel 17G1S, at $I_w = 90$ A, $d = 20$ mm and $H = 5$ mm.

It follows from the above-said that the level of residual stresses in welding up of a cavity is rather insensitive to technological conditions, which is characteristic of welding of steels under consideration [7].

Table 4. Calculated data on relative weight content of martensite in the zone of a defect repaired by welding

z, mm	*Without preheating*												
	r, mm												
	0	*0.5*	*1.5*	*2.5*	*3.5*	*4.5*	*5.5*	*6.5*	*7.5*	*8.5*	*9.5*	*10.5*	*11.5*
11.0	0.38	0.38	0.38	0.39	0.40	0.42	0.46	0.50	0.58	0.69	0.85	0.42	0
10.5	0.38	0.38	0.38	0.39	0.40	0.42	0.45	0.50	0.58	0.69	0.39	0.42	0
10.0	0.38	0.38	0.38	0.38	0.40	0.42	0.45	0.50	0.57	0.69	0.26	0	0
9.5	0.37	0.37	0.37	0.38	0.39	0.41	0.44	0.49	0.56	0.66	0.21	0	0
9.0	0.35	0.35	0.36	0.36	0.38	0.40	0.43	0.47	0.53	0.18	0.02	0	0
8.5	0.34	0.34	0.34	0.35	0.36	0.38	0.40	0.44	0.18	0.63	0.16	0	0
8.0	0.32	0.32	0.32	0.33	0.34	0.35	0.37	0.19	0.46	0.62	0.37	0	0
7.5	0.30	0.30	0.30	0.30	0.30	0.31	0.15	0.37	0.45	0.31	0.35	0	0
7.0	0.26	0.26	0.26	0.26	0.26	0.29	0.32	0.35	0.43	0.17	0.04	0	0
6.5	0.21	0.21	0.21	0.27	0.27	0.28	0.30	0.33	0.13	0.74	0.32	0	0
6.0	0.25	0.25	0.25	0.25	0.25	0.26	0.28	0.29	0.52	0.72	0.60	0	0
5.5	0.24	0.24	0.24	0.24	0.24	0.24	0.24	0.41	0.50	0.30	0.24	0	0
5.0	0.22	0.22	0.22	0.22	0.21	0.21	0.36	0.39	0.47	0.24	0.23	0	0
4.5	0.20	0.20	0.20	0.19	0.18	0.33	0.34	0.37	0.17	0	0	0	0
4.0	0.17	0.17	0.17	0.15	0.33	0.32	0.33	0.33	0	0	0	0	0
3.5	0.12	0.12	0.33	0.33	0.32	0.31	0.30	0	0	0	0	0	0
3.0	0.33	0.33	0.33	0.32	0.31	0.29	0.26	0	0	0	0	0	0
2.5	0.33	0.33	0.32	0.31	0.30	0.27	0	0	0	0	0	0	0
2.0	0.32	0.32	0.31	0.30	0.28	0.24	0	0	0	0	0	0	0
1.5	0.31	0.31	0.30	0.29	0.27	0	0	0	0	0	0	0	0
1.0	0.30	0.30	0.30	0.28	0.25	0	0	0	0	0	0	0	0
0.5	0.30	0.30	0.29	0.27	0.23	0	0	0	0	0	0	0	0
0	0.29	0.29	0.28	0.27	0.21	0	0	0	0	0	0	0	0

Table 4 (cont.)

z, mm	*With preheating at T_0 = 150 °C*												
	r, mm												
	0	*0.5*	*1.5*	*2.5*	*3.5*	*4.5*	*5.5*	*6.5*	*7.5*	*8.5*	*9.5*	*10.5*	*11.5*
11.0	0.09	0.09	0.09	0.09	0.09	0.10	0.10	0.11	0.13	0.16	0.22	0.08	0
10.5	0.09	0.09	0.09	0.09	0.09	0.10	0.10	0.11	0.13	0.16	0.22	0.08	0
10.0	0.09	0.09	0.09	0.09	0.09	0.10	0.10	0.11	0.13	0.16	0.21	0.08	0
9.5	0.09	0.09	0.09	0.09	0.09	0.09	0.10	0.11	0.13	0.15	0.20	0	0
9.0	0.09	0.09	0.09	0.09	0.09	0.09	0.10	0.11	0.12	0.14	0.04	0	0
8.5	0.08	0.08	0.08	0.08	0.08	0.09	0.09	0.10	0.11	0.13	0.20	0	0
8.0	0.08	0.08	0.08	0.08	0.08	0.08	0.09	0.09	0.10	0.12	0.18	0	0
7.5	0.07	0.07	0.07	0.07	0.07	0.08	0.08	0.08	0.02	0.11	0.06	0	0
7.0	0.07	0.07	0.07	0.07	0.07	0.07	0.07	0.06	0.08	0.10	0.01	0	0
6.5	0.06	0.06	0.06	0.06	0.06	0.06	0.05	0.07	0.08	0.05	0.38	0	0
6.0	0.05	0.05	0.05	0.05	0.05	0.06	0.06	0.07	0.07	0.20	0.15	0	0
5.5	0.04	0.04	0.04	0.04	0.06	0.06	0.06	0.06	0.03	0.18	0.12	0	0
5.0	0.06	0.06	0.06	0.06	0.06	0.06	0.05	0.05	0.14	0.17	0.03	0	0
4.5	0.06	0.06	0.06	0.06	0.05	0.05	0.05	0.12	0.13	0.06	0	0	0
4.0	0.06	0.06	0.05	0.05	0.05	0.05	0.04	0.12	0.12	0	0	0	0
3.5	0.05	0.05	0.05	0.05	0.04	0.04	0.12	0.11	0.10	0	0	0	0
3.0	0.05	0.05	0.05	0.04	0.04	0.13	0.12	0.11	0	0	0	0	0
2.5	0.04	0.04	0.04	0.04	0.13	0.12	0.11	0.10	0	0	0	0	0
2.0	0.04	0.04	0.04	0.14	0.13	0.12	0.11	0	0	0	0	0	0
1.5	0.03	0.03	0.14	0.13	0.13	0.12	0.11	0	0	0	0	0	0
1.0	0.14	0.14	0.14	0.13	0.13	0.12	0.10	0	0	0	0	0	0
0.5	0.14	0.14	0.14	0.13	0.13	0.12	0.10	0	0	0	0	0	0
0	0.14	0.14	0.14	0.13	0.13	0.12	0.09	0	0	0	0	0	0

Table 3. Calculated data on $\Delta t_{8/5}$ in the zone of a defect repaired by welding

z, mm	*Without preheating*												
	r, mm												
	0	*0.5*	*1.5*	*2.5*	*3.5*	*4.5*	*5.5*	*6.5*	*7.5*	*8.5*	*9.5*	*10.5*	*11.5*
11.0	6.8	6.8	6.8	6.7	6.6	6.5	6.3	6.0	5.5	4.9	4.0	6.5	0
10.5	6.8	6.8	6.8	6.7	6.7	6.5	6.3	6.0	5.5	4.9	6.7	6.5	0
10.0	6.8	6.8	6.8	6.8	6.7	6.5	6.3	6.0	5.6	4.9	7.8	0	0
9.5	6.9	6.9	6.8	6.8	6.7	6.6	6.4	6.1	5.7	5.1	8.4	0	0
9.0	7.0	7.0	6.9	6.9	6.8	6.7	6.5	6.2	5.8	8.8	14.0	0	0
8.5	7.1	7.1	7.1	7.0	6.9	6.8	6.6	6.4	8.8	5.2	9.0	0	0
8.0	7.2	7.2	7.2	7.2	7.1	7.0	6.9	8.6	6.2	5.3	6.9	0	0
7.5	7.4	7.4	7.4	7.4	7.4	7.3	9.1	6.9	6.3	7.3	7.0	0	0
7.0	7.8	7.8	7.8	7.8	7.8	7.5	7.3	7.0	6.5	8.8	12.1	0	0
6.5	8.3	8.3	8.4	7.7	7.7	7.6	7.4	7.2	9.5	4.6	7.2	0	0
6.0	7.9	7.9	7.9	7.9	7.8	7.8	7.6	7.5	5.9	4.8	5.4	0	0
5.5	8.0	8.0	8.0	8.0	8.0	8.0	8.0	6.6	6.0	7.4	8.0	0	0
5.0	8.2	8.2	8.2	8.3	8.3	8.3	7.0	6.7	6.2	8.0	8.1	0	0
4.5	8.5	8.5	8.5	8.6	8.7	7.1	7.1	6.9	8.8	0	0	0	0
4.0	8.8	8.8	8.9	9.1	7.2	7.2	7.2	7.1	0	0	0	0	0
3.5	9.6	9.6	7.1	7.2	7.2	7.3	7.4	0	0	0	0	0	0
3.0	7.2	7.2	7.2	7.3	7.4	7.5	7.8	0	0	0	0	0	0
2.5	7.2	7.2	7.2	7.3	7.4	7.7	0	0	0	0	0	0	0
2.0	7.3	7.3	7.3	7.4	7.6	8.0	0	0	0	0	0	0	0
1.5	7.3	7.3	7.4	7.5	7.7	0	0	0	0	0	0	0	0
1.0	7.4	7.4	7.4	7.6	7.9	0	0	0	0	0	0	0	0
0.5	7.4	7.4	7.5	7.7	8.1	0	0	0	0	0	0	0	0
0	7.5	7.5	7.6	7.7	8.3	0	0	0	0	0	0	0	0

Table 3 (cont.)

z, mm	*With preheating at T_0 = 150 °C*												
	r, mm												
	0	*0.5*	*1.5*	*2.5*	*3.5*	*4.5*	*5.5*	*6.5*	*7.5*	*8.5*	*9.5*	*10.5*	*11.5*
11.0	10.3	10.3	10.3	10.3	10.2	10.1	10.0	9.8	9.5	9.0	8.2	10.5	0
10.5	10.3	10.3	10.3	10.3	10.2	10.2	10.0	9.8	9.5	9.0	8.2	10.5	0
10.0	10.3	10.3	10.3	10.3	10.3	10.2	10.0	9.8	9.5	9.0	8.3	10.7	0
9.5	10.4	10.4	10.4	10.4	10.3	10.2	10.1	9.9	9.6	9.1	8.4	0	0
9.0	10.5	10.5	10.4	10.4	10.4	10.3	10.2	10.0	9.7	9.2	12.2	0	0
8.5	10.5	10.5	10.5	10.5	10.5	10.4	10.3	10.1	9.8	9.5	8.5	0	0
8.0	10.7	10.7	10.7	10.7	10.6	10.5	10.5	10.3	10.1	9.7	8.6	0	0
7.5	10.8	10.8	10.8	10.8	10.8	10.7	10.7	10.6	13.7	9.8	11.3	0	0
7.0	11.0	11.0	11.0	11.0	11.0	11.0	11.0	11.3	10.5	10.0	16.6	0	0
6.5	11.3	11.3	11.3	11.3	11.3	11.4	11.6	10.9	10.7	11.6	6.8	0	0
6.0	11.6	11.6	11.6	11.7	11.8	11.1	11.1	11.0	10.9	8.5	9.1	0	0
5.5	12.1	12.1	12.2	12.4	11.2	11.2	11.3	11.3	12.7	8.6	9.6	0	0
5.0	11.2	11.2	11.2	11.3	11.3	11.4	11.5	11.6	9.3	8.8	12.9	0	0
4.5	11.3	11.3	11.3	11.4	11.5	11.6	11.8	9.6	9.4	11.4	0	0	0
4.0	11.4	11.4	11.5	11.6	11.7	11.9	12.4	9.7	9.6	0	0	0	0
3.5	11.6	11.6	11.6	11.7	12.0	12.3	9.6	9.8	10.0	0	0	0	0
3.0	11.8	11.8	11.8	12.0	12.3	9.6	9.7	9.9	0	0	0	0	0
2.5	12.0	12.0	12.1	12.4	9.4	9.6	9.8	10.2	0	0	0	0	0
2.0	12.3	12.3	12.5	9.4	9.5	9.6	9.9	0	0	0	0	0	0
1.5	12.8	12.8	9.3	9.4	9.5	9.6	10.0	0	0	0	0	0	0
1.0	9.3	9.3	9.3	9.4	9.5	9.7	10.1	0	0	0	0	0	0
0.5	9.3	9.3	9.4	9.4	9.5	9.7	10.2	0	0	0	0	0	0
0	9.3	9.3	9.4	9.4	9.6	9.7	10.3	0	0	0	0	0	0

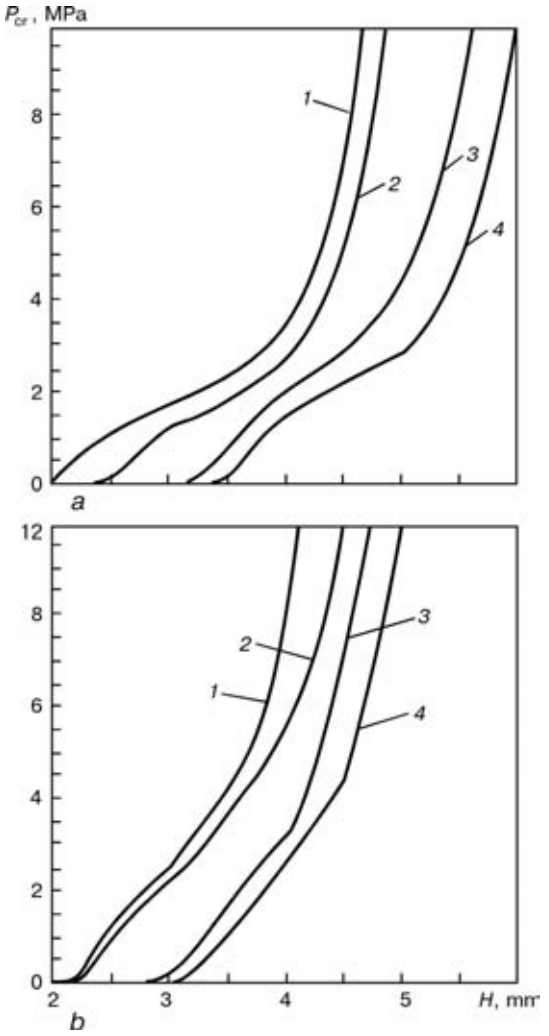

Figure 5. Dependence of critical pressure P_{cr} upon H in welding repair of a cavity with d = 20 (*a*) and 12 (*b*) mm in a pipe of oil pipeline with a diameter of 1020 mm and wall thickness δ = 11 mm: *1*, *2* — I_w = 90 A; *3*, *4* — I_w = 140 A; *1*, *3* — W = 6 m/s; *2*, *4* — W = 2 m/s

the H values up to certain limits, above which the fracture mechanism under consideration is not realized at the above values of I_w, d and W in pipes of steel 17G1S, as the mean temperature through thickness H dramatically decreases and yield strength σ_y increases at a temperature below 700 – 800 °C. A decrease in diameter of the cavity from 20 to 12 mm causes a decrease of about 1 mm in the above H values from 5 – 6 (at d = 20 mm) to 4 – 5 mm (at d = = 12 mm).

The data in Figure 6 are similar to those in Figure 5, *a*, but for a pipe wall thickness of δ = 18 mm. It can be seen from the Figure that an increase in the wall thickness from 11 to 18 mm, other parameters remaining unchanged, causes almost no changes in critical values of P_{cr} and H at I_w = 90 A and an increase of about 1 mm in critical values of H at I_w = = 140 A, which is associated with the thermal state of a jumper, i.e. in the case of low values of the welding current the pipe wall thickness has no marked effect on the temperature field in the jumper at high temperatures.

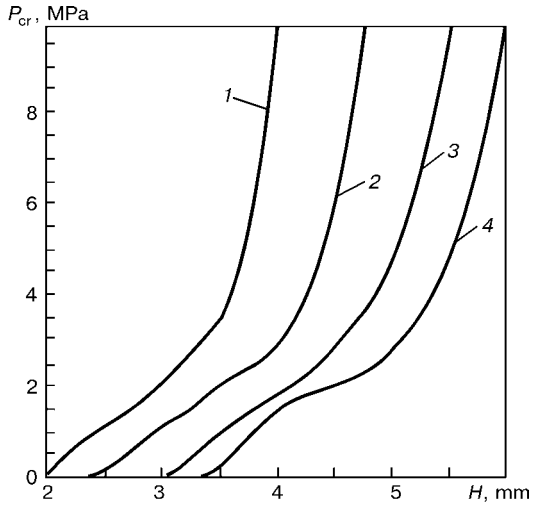

Figure 6. Dependence of critical pressure P_{cr} upon H in welding repair of a cavity with d = 20 mm in an oil pipeline with a diameter of 1440 mm and wall thickness δ = 18 mm (see designations in Figure 5)

It follows from the above-said that in repair of an active oil pipeline, involving welding up of individual pitting defects in the case of welding in layers each with height h, the fracture of the jumper with thickness H and diameter d by the mechanism of plastic instability depends upon specific values of the initial parameters (see Figures 3 and 4), in particular upon the velocity of the oil flow and its pressure.

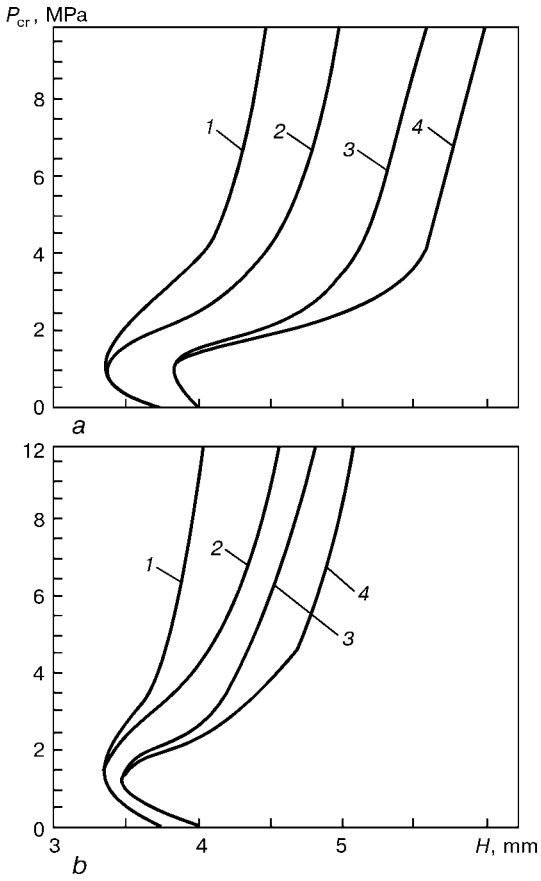

Figure 7. Dependence of critical pressure P_{cr} upon H in welding repair of a cavity with d = 20 (*a*) and 12 (*b*) mm in a pipe of gas pipeline 18 × 1420 mm in size: *1*, *2* — I_w = 90 A; *3*, *4* — I_w = = 140 A; *1*, *3* — W = 20 m/s; *2*, *4* — W = 6 m/s

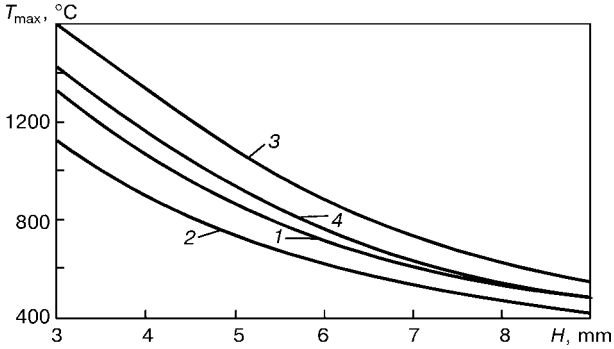

Figure 2. Dependence of a maximum temperature on the inside surface of the pipe ($z = 0$) along axis $r = 0$ upon H and welding parameters: *1, 2* — I_w = 90 A; *3, 4* — I_w = 140 A; *1, 3* — W = = 2 m/s; *2, 4* — W = 6 m/s (D = 1020 mm; δ = 11 mm; d = = 29 mm)

plate δ thick and $2R$ in diameter with hinge-supported edges at $r = B$ and transverse load P. Radius B was selected on the basis of conditions that stresses due to pressure in the defect formation zone are close to those in a pipeline with wall thickness δ, diameter $2R$ and internal pressure P, i.e. according to [6]

$$B = \sqrt{R\delta}\left[\frac{8}{3(3+\nu)}\right]^{0.5} \approx 0.9\sqrt{R\delta},$$

where ν is the Poisson's ratio.

Solving the equation at each step of tracing resulted in the data on tensors of stresses $\sigma_{ij}(r, z, t)$ and strains $\varepsilon_{ij}(r, z, t)$, as well as on displacement vector $U_i(r, z, t)$ at $i = r, z, \beta$. This was done using a procedure taken from [7, 8].

Values of elastic characteristics E, ν and yield strength σ_y, necessary for the calculations, are given in Table 2 and Figure 3. Thus, we can trace development of stresses σ_{ij} and plastic strains ε_{ij}^p at different values of pressure P (Figure 4), i.e. consider variants of welding repair of a defect at P = 0.2 MPa, etc. At a certain value of $P = P_{cr}$ and heating time $t = t_{cr}$, there occurs a critical state of plastic instability characterized by a high level of plastic strains ε_{rz}^p in section

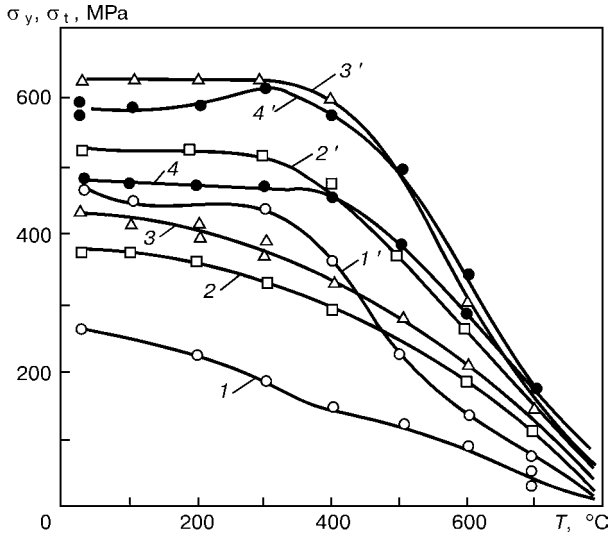

Figure 3. Effect of heating on strength characteristics of steels under investigation: *1, 1′* — St.20; *2, 2′* — 14KhGS; *3, 3′* — 17G1S; *4, 4′* — X60; *1 – 4* — σ_y; *1′ – 4′* — σ_t

Table 2. Mechanical and thermal-physical properties of steel 17G1S

T, °C	*Young modulus,* $E \cdot 10^{-5}$, *MPa*	*Yield strength,* σ_y, *MPa*	*Relative thermal expansion coefficient,* $\alpha \cdot 10^6$, 1/°C	*Thermal conductivity,* $\lambda \cdot 10^2$, *W/(cm·°C)*	*Volumetric heat capacity,* $c\gamma$, *J/(cm³·°C)*
20	1.97	435	11.4	40	3.79
100	1.97	425	11.4	40	3.85
150	1.99	420	11.8	40	3.99
200	2.01	410	12.2	39	4.23
250	1.98	395	12.4	39	4.26
300	1.95	365	12.6	38	4.41
350	1.92	350	12.9	37	4.58
400	1.88	340	13.0	36	4.77
450	1.84	310	13.5	35	5.04
500	1.80	275	13.8	34	5.32
550	1.75	250	13.8	33	5.67
600	1.69	210	13.9	32	6.00
650	1.63	160	14.0	30	6.30
700	1.56	130	14.1	29	6.59
750	1.46	80	16.0	29	11.17
800	1.35	30	18.3	26	6.58
850	1.30	10	18.5	26	5.83
900	1.25	5	18.7	26	5.04
950	1.25	2	19.0	27	4.25
1000	1.25	1	19.4	28	5.04
1050	1.25	1	19.4	28	5.08
1100	1.25	1	19.5	29	5.09
1150	1.25	1	19.5	30	5.17
1200	1.25	1	19.5	30	5.25

$r = r^*$, as shown in Figure 4. Position of section $r = r^*$ is determined by distribution of temperatures and stresses. It is not difficult to see that the achieved limiting state is in good agreement with the known Battelle model [9].

Figure 5 shows results of calculations of critical values of P_{cr} for a pipe of steel 17G1S with wall thickness δ = 11 mm, depending upon the H values at different welding currents and transportation velocities.

It can be seen from the data obtained that critical pressure P_{cr} monotonously grows with an increase in

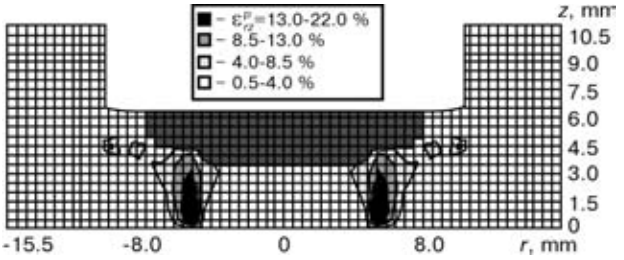

Figure 4. Distribution of plastic strains ε_{ij}^p at the time moment preceding achievement of a limiting state for the next version (pipe 11 × 1020 mm in size, d = 20 mm, I_w = 140 A)

Table 1. Results of calculations of heat transfer coefficient α_k

W, m/s	α_k, J/(cm^2·s·°C)						
	Oil pipeline	Gas pipeline					
	0 – 10 MPa	0.1 MPa	1.0 MPa	2.0 MPa	4.0 MPa	8.0 MPa	10.0 MPa
2	0.0650	0.0058	0.0108	0.0138	0.0167	0.0208	0.0225
6	0.1571	0.0117	0.0242	0.0304	0.0388	0.0496	0.0538
10	0.2367	0.0163	0.0354	0.0450	0.0579	0.1263	0.1367
20	–	0.0267	0.0596	0.0763	0.0996	0.1263	0.1367

oil range normally from 2 to 3, and those for gas — from 6 to 10 m/s.

Nevertheless, the data of Table 1 give a sufficiently full picture of the α_k values at characteristic velocities of oil and gas.

For the outside surface of a pipe the use was made of traditional data on heat exchange with air at α_k = = 0.00208 J/(cm^2·s·°C).

Thermal power q_s of the welding arc was introduced through a filler metal in filling of the cavity being welded up, as well as using a distributed heat flow directly from the arc. The q_s values were determined from the welding parameters of the arc

$$q_s = 0.24 U_a I_w \eta_{work} \ \ [\text{J}/(\text{cm}^2\cdot\text{s}\cdot^\circ\text{C})], \qquad (1)$$

where U_a is the arc voltage; I_w is the welding current and η_{work} is the efficiency of heating of a workpiece. In the case of manual welding using covered electrode of the basic type, U_a was assumed to be equal to 26 V and η_{work} — to 0.8.

Heat q_e introduced by the filler metal per second is determined by temperature T^* and volumetric velocity of its input equal to

$$q_e = \frac{\alpha_d I_w}{3600\gamma},$$

where α_d is the deposition coefficient and γ is the specific mass of a material.

At $T^* \approx 2100$ °C, α_d = 10 g/(A·h) and latent melting heat $\kappa \approx 2080$ J/cm^3, we will have that

$$q_e = \frac{\alpha_d I_w}{3600\gamma}(T^* c\gamma + \kappa) = 4.576 I_w \ [\text{W}], \qquad (2)$$

where $c\gamma$ is the volumetric heat capacity ($c\gamma \approx$ $\approx$ 5.2 J/(cm^3·°C).

It can be seen that q_e is a bit more than 20 % at $q_s = 20.8 I_w$ W, which is characteristic of fusion arc welding [5].

Welding up of a cavity (see Figure 1) is performed in a discrete manner by depositing layers each with height h of not more than 2 mm. After deposition of each layer it is necessary to make an interruption to let them fully cool down. The first layer is most critical.

Taking into account the local character of heating and an actual curvature of the pipe wall, the temperature field was determined by solving axisymmetrical problem of thermal conductivity for a steel plate δ thick with a cavity d in diameter and $\delta - H$ deep (see Figure 1) for a case of filling the cavity with a molten metal layer h high at temperature T^* for a period of time t_0 and under the effect of the arc heat flow equal to $q_s - q_e$.

Time t_0 was found from the preset values of h, D, α_d and I_w:

$$t_0 = \frac{\pi d^2 h \gamma}{4\alpha_d I_w} 3600 \ [\text{s}]. \qquad (3)$$

The non-stationary problem of thermal conductivity under the above conditions was solved by a numerical method using software developed by the E.O. Paton Electric Welding Institute. In this case the account was made of the temperature dependence of thermal-physical coefficients of thermal conductivity λ and volumetric heat capacity $c\gamma$ (Table 2).

Results of numerical solutions for specific source data with respect to temperatures $T(r, z, t)$ were used in the first turn for estimation of a risk of formation of a burn-through at $P = 0$.

The following condition serves as a criterion of the absence of such a defect:

$$T_{max}(r, 0) < T_S,$$

where $T_{max}(r, 0)$ is the maximum temperature on the inside surface at $z = 0$ and T_S is the solidus temperature of the indicated alloy.

Figure 2 shows calculations of the above temperatures T_{max} $(r, 0)$ for pipes of steel of the 17G1S type (δ = 11 mm, d = 20 mm, h = 2 mm) at I_w = 90 and 140 A, depending upon the values of minimum thickness H in the cavity and velocity of the transported oil. It was determined that the welding parameters (h, I_w, H, W) had a substantial effect on $T_{max}(r, 0)$.

If a temperature of 1420 °C is assumed to be T_S, at I_w = 140 A and W = 2 m/s critical values are H_{cr} = = 3.5 mm, and at I_w = 90 A H_{cr} = 2.5 mm.

Elasto-plastic deformation of the zone of a defect being repaired, associated with non-stationary temperature field $T(r, z, t)$ and pressure P, was studied to estimate the critical state at the presence of an internal pressure.

Calculations were made by inducing a successive development of elasto-plastic strains, starting from the moment of the beginning of heating to complete cooling down. Like in the case of calculation of temperatures, this was done using a diagram of a round

MATHEMATICAL MODELLING OF PITTING DEFECTS IN ACTIVE OIL AND GAS PIPELINES AND DEVELOPMENT OF A NUMERICAL METHOD FOR ESTIMATION OF PERMISSIBLE PARAMETERS OF ARC WELDING REPAIR OF DEFECTS

V.I. MAKHNENKO, V.S. BUT, E.A. VELIKOIVANENKO, G.F. ROZYNKA and **N.I. PIVTORAK**
The E.O. Paton Electric Welding Institute, NASU, Kyiv, Ukraine

ABSTRACT

The article considers the possibility of welding repair of pitting corrosion defects 12 – 20 mm in diameter on the outside surface of walls of a main oil pipeline of steel 17G1S without interruption of its operation. Described is the general procedure for selection of parameters of arc welding repair of a defect, which eliminate burn-through and fracture in the welding zone caused by the mechanism of high-temperature plastic instability and cold (hydrogen) cracking.

Key words: *mathematical modelling, thermal-deformation processes, pipeline, pressure, pitting defects, welding repair of defects, plastic instability, microstructural state, cooling time, residual stresses, cold cracks*

The problem of safe welding repair of individual corrosion defects on the outside surface of walls of a pipeline without interruption of its operation attracts rapt attention of specialists throughout the globe. Several fundamental developments covered by the appropriate documents have been made in this area (e.g. at the Edison Welding Institute, USA, etc.) [1 and oth.] for the last 30 years. However, rather big problems arising in reproducing the actual situation in an active pipeline (geometrical factors, conditions of flow on the inside surface by a transported medium, etc.) on a mockup do not allow exhaustive answers to be given to the questions on the possibility of developing a safe technology for repair welding of defects.

In this connection, the calculation methods based on mathematical modelling of thermal-deformation processes which occur during welding up of defects in pipelines, allowing for effective pressure and heat exchange with the oil or gas flow, assume a special significance. It should be noted that an assumption made in [2], that the temperature on the inside surface of the pipe wall in welding up of a defect is constant and equal to the temperature of a transported medium, is oversimplified in terms of safety of repair.

A more substantiated approach is that in which a thermal state is estimated with allowance for convective heat transfer on the inside surface of a pipeline depending upon the corresponding parameters of a transported medium, as it was done in [3] in surfacing of thick-walled pipes.

This work involves a geometrical diagram of welding up of a cavity, taken from [2] and shown in Figure 1, for modelling of temperature fields in welding repair of a pitting defect in the wall of an active main pipeline. This diagram was accepted with allowance for convective heat transfer on the inside surface. Convective heat transfer coefficient α_k was determined, as in [3], using criterial relationships [4] through the appropriate numbers, Reynolds (Re) and Prandtl (Pr), which generalize experimental data on a flow on the pipe wall by fluid or gas in local heating of the wall with a heating spot having diameter D.

Results of the calculation of heat transfer coefficient α_k for transportation of oil and gas, depending upon the velocity of their transportation, W, and pressure P in a pipe at $D < 50$ mm, for the cases under consideration are given in Table 1. For this, the temperature of a transported medium was assumed to be equal to 40 °C.

The range of velocities given in Table 1 is not equally applicable to oil and gas in main pipelines with a diameter of $2R = 1000$ mm. The W values for

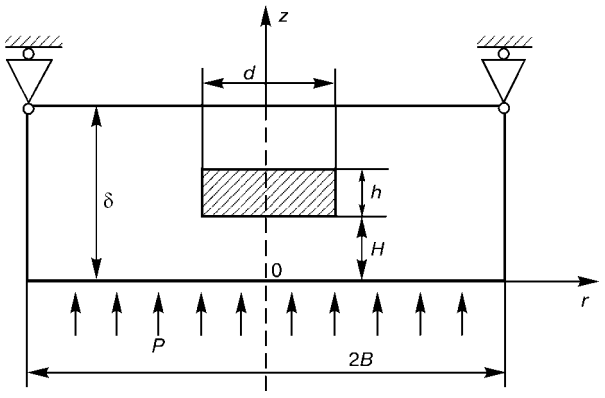

Figure 1. Diagram of welding repair of a cavity in the pipe wall: d — diameter of the cavity; h — thickness of the deposited layer; H — thickness of a jumper; δ — thickness of the pipe wall; P — pressure in the pipe; B — see in the text

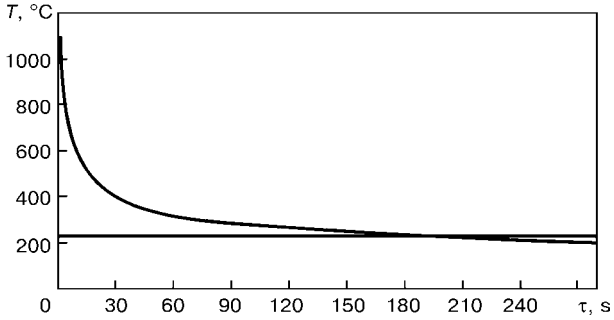

Figure 7. Thermal cycle curve, obtained in single-arc deposition of the first bead with Q = 28.05 kJ/cm

the rate of steel cooling after building-up, i.e. increasing the time of the HAZ metal cooling up to 150 – 250 s. It is known that twin-arc surfacing is an effective method of lowering the rate of cooling of the HAZ metal [6, 7]. Changing the surfacing mode parameters in each arc, as well as their spacing, it is possible to vary the thermal cycle characteristics in a broad range.

In our case the first bead was deposited, using two consecutively located split wires, that were connected to one power source. Flux-cored wire of PP-06Kh15G15N2MF type was selected for experiment performance. The following considerations were taken into account:

- metal, deposited with this wire has the highest CLE ($23 \cdot 10^{-6}$ in the range of 0 – 1000 °C), and, therefore, is the most prone to tear formation;
- it contains a minimal amount of nickel, which is in short supply in Ukraine;
- its as-deposited hardness, equal to about *HRC* 22, rises up to *HRC* 52 after work hardening by tram rails, thus several times increasing the wear resistance of the built-up rails.

Fused pumice-like flux AN-72 was used in experiments. Before building-up was performed, the flux and the wire were thoroughly baked in the furnace. Building-up began at the temperature of 10 °C. The arc spacing in deposition of the first bead was set equal to 90 mm. The second and subsequent beads were deposited with one electrode wire. On the whole, 5 beads were deposited on each specimen, with 10 min intervals after deposition of each bead. Heat input was calculated by the following equation:

$$Q = \frac{60 I_w U_a}{1000 v_b} \text{ [kJ/cm]},$$

where v_b is the building-up speed, cm/min.

Thermal cycles were recorded with KSP-4 chart recorder, using chromel-alumel thermocouples, caulked-in into the base metal on the level of the anticipated fusion line. Results of the conducted experiments are given in Table 1.

Metallographic investigations demonstrated that under the first deposited bead the HAZ metal structure near the fusion line consists almost completely of tempered martensite in the specimen, produced in experiment No.1 (Figure 4, *a*). Its hardness reaches *HV* 413. A tear is visible on the fusion line. With the increase of the heat input, the proportion of tempering martensite is reduced and bainite or even pearlite form in the HAZ metal structure (Figure 4, *b*).

Figure 5 gives the curve of the thermal cycle, obtained in experiment No.3, in twin-arc deposition of the first bead, providing the absence of cracks in the base metal HAZ.

Thus, application of twin-arc surfacing allows solving the problem of building- up tram rails without preheating and without tears in the HAZ metal under the first bead. However, this building-up method makes the technological process much more complicated, as it is more difficult for the operator to monitor two wires, than one (it should be borne in mind, that rail building-up has to be performed in the street at night, when there is no tram traffic).

In view of the above, we chose deposition of the first bead with one wire. Otherwise, the procedure of building-up and recording the thermal cycles remained unchanged. The results of the second test series are given in Table 2.

Building-up with a low heat input (test No.4) similar to the twin-arc process, leads to development of tears. HAZ metal forms martensite which is tempered during deposition of subsequent beads (Figure 6, *a*). Its hardness is *HV* 408. Increase of the heat input up to 28.05 kJ/cm in deposition of the first bead reduces the HAZ metal cooling rate in the temperature range of 300 – 200 °C to 0.50 °C/s, and the maximal hardness — to *HV* 352. Tears are not eliminated. HAZ metal structure consists of bainite and pearlite (Figure 6, *b*). Lower heat input in single-arc building-up markedly refines the metal structure, compared to twin-arc process.

Figure 7 shows a curve of the thermal cycle, obtained in single-arc deposition of the first bead, providing absence of cracks in the base metal HAZ.

Therefore, in order to prevent tears in the HAZ metal of rails of steel M-76 in their building-up with wires of austenitic class, the first bead should be deposited with one arc at the heat input of 28 – 30 kJ/cm.

Flux-cored wire PP-06Kh15G15N2MF is relatively expensive, however, its application for building-up is cost-effective. Calculations that did not take into account the increase of the rails wear resistance, indicated that the cost of building-up rails using the above wire, is 3 – 4 times smaller, than the cost of replacement of the worn rails by new ones.

REFERENCES

1. Frumin, I.I. (1961) *Automatic electric arc surfacing*. Kharkiv: Metallurgizdat.
2. Makarov, E.L. (1981) *Cold cracks in welding of alloyed steels*. Moscow: Mashinostroyeniye.
3. (1974) *Technology of electric arc fusion welding of metals and alloys*. Ed. by B.E. Paton. Moscow: Mashinostroyeniye.
4. Kozlov, R.A. (1986) *Welding of heat-resistant steels*. Moscow: Mashinostroyeniye.
5. Popol, A.A., Popova, L.E. (1965) *Isothermal and thermokinetic diagrams of overcooled austenite decomposition*. Moscow: Metallurgia.
6. Metelev, A.V., Gorbachev, Yu.I. (1984) Regulation of thermal cycle in twin-arc welding of hardenable steels. *Svarochnoye Proizvodstvo*, **2**, 4 – 5.
7. Bursky, G.V., Savitsky, M.M., Novikova, D.P. (1998) Resistance of welded joint HAZ in hardenable high-strength steels to delayed fracture in twin-arc welding. *Avtomaticheskaya Svarka*, **2**, 12 – 15.

posited metal and high-carbon pearlitic M-76 steel, where non-ductile structures developed in the HAZ metal. This study was undertaken to prevent tears. In its first stage, the influence of the cooling rate on austenite decomposition temperature in M-76 steel was determined. For this purpose a quick-action dylatometer of PWI design was used to simulate the thermal cycle of welding, in which the cooling rate in the temperature range of 600 – 500 °C was $w_{6\text{-}5}$ = = 36.0, 20.0 and 8.5 °C/s. At $w_{6\text{-}5}$ = 36 and 20 °C/s the austenite in the steel is completely transformed into martensite. The temperature of the beginning of martensite transformation is about 230 °C. At the cooling rate of 8.5 °C/s martensite transformation M_b is preceded by a slight partial intermediate transformation of austenite into pearlite.

It should be noted that M-76 steel is very close to U8 steel in its composition, also close are the temperature ranges of transformations in these steels, and M_b points coincide completely. Since we did not find a detailed enough thermokinetic diagram of austenite decomposition in steel M-76 in literature, in this work we used the known [5] diagram of austenite transformation in steel U8 (Figure 3). From this diagram it follows, that in order to provide a rather favourable structure of about HV 350 hardness (P = 10 N, t = = 10 – 15 s) in the HAZ metal, it is necessary to «go out» of the martensite region. This requires lowering

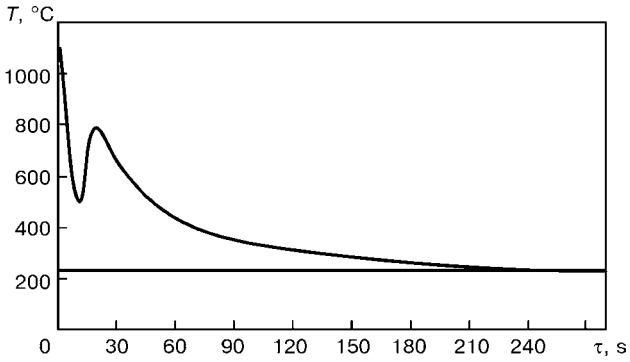

Figure 5. Thermal cycle curve, obtained in twin-arc deposition of the first bead with Q = 33.56 kJ/cm

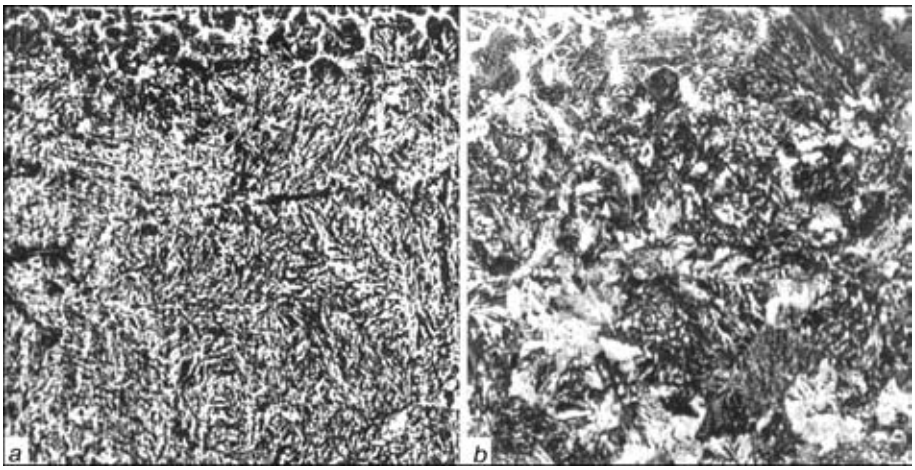

Figure 6. Microstructure of HAZ metal, produced in single-arc deposition of first bead at Q = 11.59 (*a*) and 28.05 (*b*) kJ/cm (×500)

Table 1. Influence of heat input on tear formation under the first bead in twin-arc building-up

Test No.	*Bead*	*Number of arcs*	I_w, *A*	v_b, *m/h*	*Q, kJ/cm*	w_{3-2}, *°C/s*	*Maximal HAZ hardness,* HV_1	*Presence of tears*
1	First,	2	620*	36.8	19.41	1.05	413	Present
	others	1	350	36.8	10.96	Not determ.	–	
2	First,	2	620*	24.8	28.80	0.70	378	None
	others	1	350	36.8	10.96	Not determ.	–	
3	First,	2	620*	21.8	33.56	0.40	348	Same
	others	1	350	36.8	10.96	Not determ.	–	

*Total current of the two arcs; arc voltage is 32 V.

Table 2. Influence of heat input on tear formation under the first bead in single-arc building up*

Test No.	*Bead*	v_b, *m/h*	*Q, kJ/cm*	w_{3-2}, *°C/s*	*Maximal HAZ hardness, HV*	*Presence of tears*
4	First,	36.8	11.59	1.25	408	Present
	others	36.8	11.59	Same	–	
5	First,	19.2	22.20	0.85	368	None
	others	36.8	11.59	Same	–	
6	First,	15.2	28.05	0.50	352	Same
	others	36.8	11.59	Same	–	

*Other parameters of building-up mode are I_w = 370 A, U_a = 32 V.

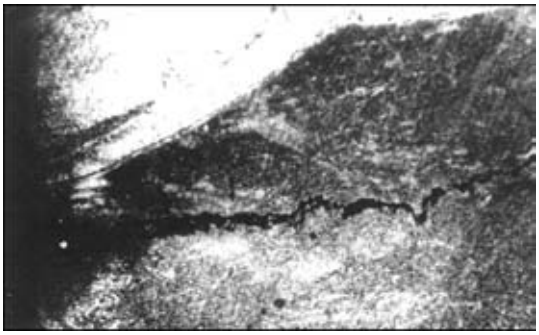

Figure 2. Tear under the first deposited bead (×50)

steel by consumable electrode arc surfacing, when making corner welds, carbon weight fraction in the first deposited bead can be up to 0.45 % due to mixing with the base metal. To avoid formation of cold and hot cracks at such a content of carbon, in practical applications building-up is performed with wires of the ferritic-pearlitic class with mandatory preheating and slower cooling [1, 2]. Since application of preheating was not allowed by the statement of work, in this study building-up was conducted using standard wires of austenitic class Sv-08Kh20N9G7T (C — 0.07; Si — 0.44; Mn — 7.12; Cr — 19.8; Ni — 9.2; Ti — 0.76; Mo — 0.06; S — 0.016; P — 0.32 wt.%), Sv-08Kh21N10G6 (C — 0.06; Si — 0.28; Mn — 5.4; Cr — 20.4; Ni — 9.81; Ti — 0.03; Mo — 0.22; S — 0.018; P — 0.035 wt.%) and test austenitic Cr–Mn flux-cored wire of PP-06Kh15G15N2MF type. It is known [3, 4], that when austenitic class wires are used, that have a lower melting temperature, the HAZ is overheated to a smaller degree, and the amount of hydrogen coming to it from the deposited metal is markedly reduced.

Worn inner surfaces, close to the vertical, were built-up by horizontal beads. They were deposited one onto the other and further formed by AH-72 flux (SiO_2 — 15 – 20; CaO — 15 – 20; Al_2O_3 — 18 – 23; CaF_2 — 35 – 45 wt.%), poured into the rail groove. Building-up mode was as follows: welding current I_w = 350 – 450 A, arc voltage U_a = 30 – 32 V, building-up speed v_b = 28 – 42 m/h, DCRP, flat external characteristic. Transverse macrosection of

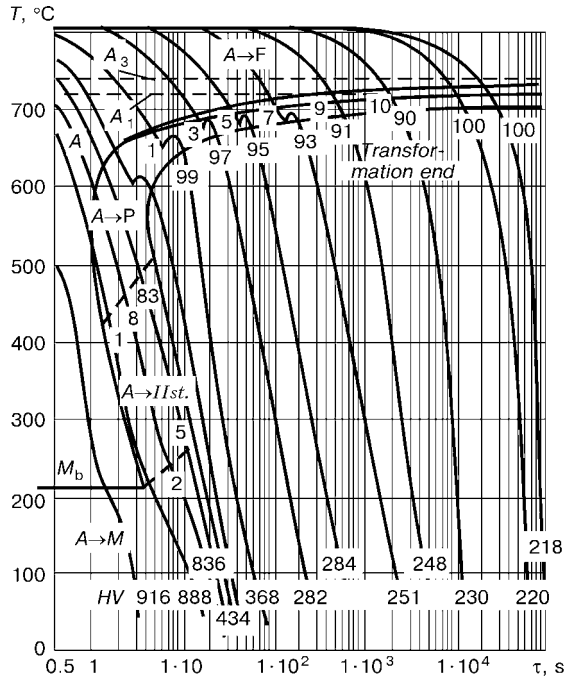

Figure 3. Thermokinetic diagram of austenite transformations in U8 steel (C — 0.76; Si — 0.2; Mn — 0.29 wt.%)

the rail lip, built up by the above process, is shown in Figure 1.

When studying the macro- and microsections, it was found that in all the cases without exception, formation of cold cracks of tear type was observed under the first deposited bead on the fusion boundary or in the HAZ metal, near this boundary, along the length of the deposited section (Figure 2). Crack depth was from 4 to 8 mm, and their opening displacement was up to 0.4 mm. These cracks could not be eliminated by varying the building-up mode in the above ranges. It should be noted, however, that in the HAZ metal of the next beads the cracks were absent, probably, because they were deposited on the base metal already preheated by the heat of the first bead.

The most probable cause for appearance of tears under the first bead is the presence of welding and structural stresses, arising on the fusion line, because of an almost two-times difference between the coefficients of linear expansion (CLE) of austenitic de-

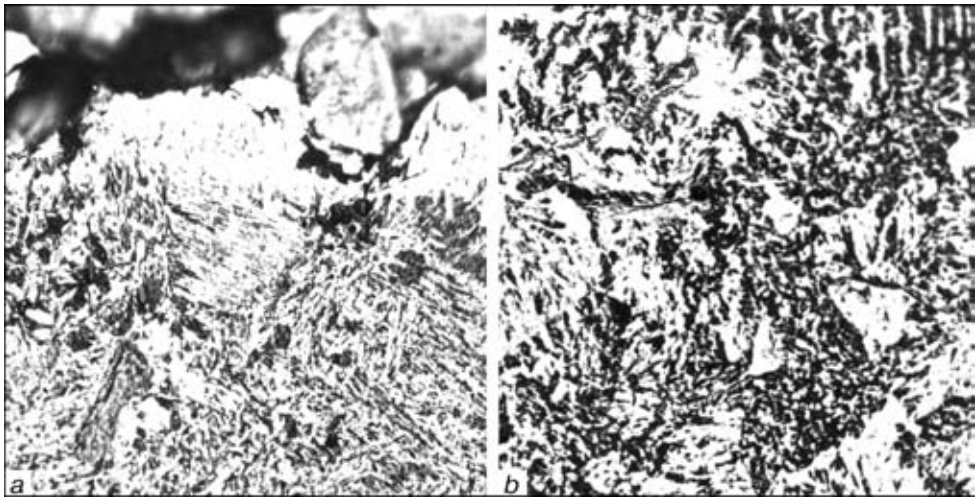

Figure 4. Microstructure of HAZ metal, achieved in twin-arc deposition of the first bead at Q = 19.41 (*a*) and 33.56 (*b*) kJ/cm (×500)

Strength of AMg5/12 vol.% SiC composite and its welded joints made by AAW, using different filler wires

Object of study	*Specimen number*	*Ultimate tensile strength, σ_t, MPa*	*Average value, σ_{av}, MPa*	*Fracture region*
AMg5/12 vol.% SiC (base metal)	1	273.0	278.4	–
	2	273.8		
	3	288.4		
Welded joint (AAW, Sv-AMg63 wire)	4	290.0	267.9	Fusion zone
	5	271.8		
	6	241.8		
Same (AAW, Sv-AK5 wire)	7	183.5	175.3	Weld
	8	180.7		
	9	161.6		

type, the reinforcing phase is non-uniformly distributed in the weld metal, and its hardness is lower, than that of the composite base metal, this being related to the use of non-reinforced filler wire and dilution of the base metal by the filler wire. Hardness profile in the composite welded joints, made by AAW, using Sv-AK5 and Sv-AMg63 filler wires, is given in Figure 8.

In welds, made using Sv-AK5 filler wire, a pronounced non-uniformity of the reinforcing filler distribution is found. These welds have large regions, containing no SiC particles, that are located both in the weld center, and directly at the fusion line (Figure 7, *b*), and accumulation of reinforcing particles is found in the weld root. It is obvious, that a pronounced porosity and non-uniformity of the reinforcing filler distribution, have a strong influence on metal hardness in welds, made using Sv-AK5 filler wire (Figure 8), and, therefore, also on the strength properties of these welded joints (see the Table).

A more uniform distribution of the reinforcing filler and good saturation with it, especially along the fusion line, were found in the metal of welds, made with Sv-AMg63 filler wire (Figure 7, *a*), this also providing their higher hardness. In the weld center, however, matrix saturation with the reinforcing particles is lower — alternation of regions without SiC particles and of their accumulations is observed. Metal hardness in the weld central part is somewhat lower, accordingly (Figure 8). No active interaction on the particle–matrix interface with formation of Al_4C_3 crystals was detected by optical metallography methods in the welds of the composite welded joints.

Mechanical tensile testing of welded joints of AMg5/12 vol.% SiC composite was conducted on flat specimens with reinforcement and back-side bead formation. It is found that the strength of the composite welded joints essentially depends on filler wire selection: the strength is the lowest in the welded joints made with Sv-AK5 filler wire, where fracture runs mostly in the weld. This is attributable to higher porosity of such welds and non-uniform distribution of the reinforcing filler. Strength of welded joints, made using Sv-AMg63 filler wire, is 80 to 100 MPa higher, than the strength of specimens, produced using Sv-AK5 filler wire (see the Table). Ultimate tensile strength of welded joints of AMg5/12 vol.% SiC composite using Sv-AMg63 filler wire is 85 % of the base metal strength.

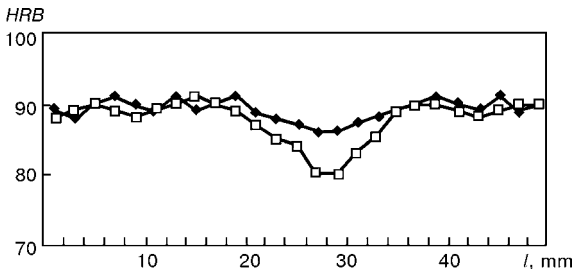

Figure 8. Hardness distribution in the joint of AMg5/12 vol.% SiC composite, made by AAW with Sv-AMg63 (❐) and Sv-AK5 (◆) filler wire (*l* is length of the studied section)

CONCLUSIONS

1. Considered is the influence of non-stationary heating on structural changes in the matrix, behaviour and decomposition of strengthening particles in laser welding, EBW and AAW of dispersion-strengthened Al25/18 vol.% SiC CM. It is found that in laser welding of 5 mm thick specimens, compared to EBW, the degree of SiC particles decomposition becomes greater, forming a rather oversaturated solid solution, thus leading to a greater hardness of the weld metal and lowering of the strength properties of welded joints.

2. It is shown that lowering of temperature and rate of weld pool metal solidification allows the decomposition of the strengthening particles in CM to be greatly reduced.

3. In AAW of AMg5/12 vol.% SiC composite, using Sv-AK5 and Sv-Mg63 filler wires, the welds made with Sv-AMg63 filler wire have a higher strength with a more uniform distribution of the reinforcing filler.

REFERENCES

1. Kreider, K. (1978) *Composite materials with a metal matrix*. Moscow: Mashinostroyeniye.
2. Muravejnik, A.N., Ryabov, V.R., Bogdanova, T.V. (1988) *Fabrication of metallographic sections of composite materials*. Dep. in VINITI on 13.06.88, No.4632-V88. Kyiv.
3. Viala, I.C., Fortier, P., Bouix, I. (1990) Stable and metastable phase equilibria in the chemical interaction between aluminium and silicon carbide. *J. Mater. Sci.*, **25**, 1842.
4. Chernyshova, T.A., Kobeleva, L.I., Shebo, P. *et al.* (1993) *Interaction of metal melts with reinforcing fillers*. Moscow: Nauka.
5. Aksenov, A.A., Churmukov, E.A., Romanova, V.S. (1994) Silicon influence on the processes of interaction on the interface in Al–SiC composite materials. *Izv. Vuzov, Tsvetn. Metallurgia*, **4–6**, 145 – 150.

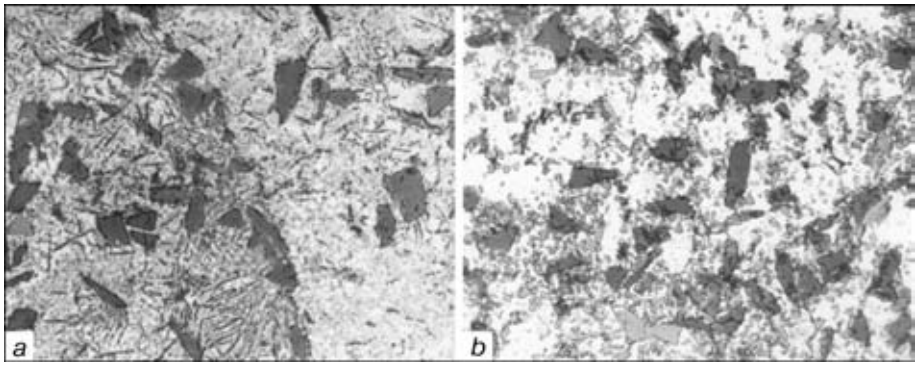

Figure 6. Weld microstructure in Al25/18 vol.% SiC composite penetration in EBW (*a*) and AAW (*b*) (×600)

$$4Al + 3SiC \rightarrow Al_4C_3 + 3Si.$$

At high temperatures (>800 °C), this interaction can proceed up to complete degradation of SiC particles [4]. Apparently, intensive dissociation of SiC particles takes place exactly in the weld central part, directly under the laser beam, where the temperature is maximal during penetration.

The electron beam provides a deeper penetration of the composite, than the laser beam. In both cases, the cast metal of the weld solidifies with formation of a disperse structure, but in laser welding, the dispersity of the eutectic precipitations and dendrites of the aluminium solid solution is higher.

In EBW the reinforcing SiC particles are almost uniformly distributed in the weld metal matrix. An exception is a small section in the central part, closer to the weld surface, where short and fine acicular inclusions of Al_4C_3 are found, located, as a rule, around SiC particles (Figure 6, *a*). It is obvious, that in this region aluminium melt interaction with these particles proceeds by the above reaction. It is less intensive, than under the impact of the laser beam, as the region of interaction, where formation of the new phase inclusions is observed, is smaller. In the considered region, acicular inclusions are finer and shorter, and excess crystals of silicon are absent, this being characteristic of hypoeutectic aluminium alloy, and indicative of the transition of a small amount of silicon into the melt. Microhardness in different weld sections changes only slightly and is equal to *HV* 1500 – 1700 MPa.

In AAW of Al25/18 vol.% SiC composite, the weld pool is characterised by a higher viscosity. The nature of eutectic precipitates in the weld structure changes during recrystallisation. Instead of finely differentiated bulk eutectic colonies, as in the base metal, a range of diverse eutectics of different form of crystallisation and their more uniform distribution are found in the weld metal (Figure 6, *b*). A more uniform arrangement of reinforcing SiC particles in the weld metal should be also noted. Weld metal microhardness increases only slightly up to *HV* 1500 – 2000 MPa at the base metal microhardness of *HV* 1000 – 1500 MPa.

Thus, the nature of weld solidification and the resistance of the reinforcing particles in the aluminium melt in welding, are mainly determined by the temperature-time conditions of the penetration process, related to its main parameters (heat source intensity, welding speed, conditions of heat removal from the fusion zone), as well as thermophysical properties of the metal being welded.

The derived results allowed determination of the conditions of performance and modes of AAW welding of AMg5/12 vol.% SiC composite, produced by the casting method with subsequent extrusion and rolling [5]. Full penetration joints with normal weld formation were made on 3 mm thick specimens of this test alloy by AC AAW welding. A special laboratory unit (v_w = 10 – 12 m/h, I_w = 150 A) and ISVU-315 power source were used for welding.

Welding of butt joints of the above composite was conducted in argon, using Sv-AMg63 (Al–6.3Mg) and Sv-AK5 (Mg — 0.2 – 0.5; Si — 4.5 – 6.5; Cu — 6.0 – 8.0 wt.%) filler wires. The first was selected to improve the weld strength, and the second — to improve the weld pool fluidity. In both cases full penetration welded joints with normal formation of the back-side bead were produced. The structure of the aluminium alloy (matrix) in all the welds is dendritic, typical for the cast condition, with a high dispersity of excess phase precipitates along the boundaries. Equiaxed crystals are found in the weld center, which are somewhat elongated in the solidification direction at the fusion line (Figure 7). The quantity of dispersed precipitates along the boundaries in the weld metal, is greater in welding with Sv-AK5 wire, than Sv-AMg63 wire, this being, probably, related to silicon addition and increase of the amount of eutectic precipitates. Pores are found in all the welds, irrespective of the filler wire type, but their number is much greater in the welds, made with Sv-AK5 wire, than in the case of Sv-AMg63 wire. Regardless of the wire

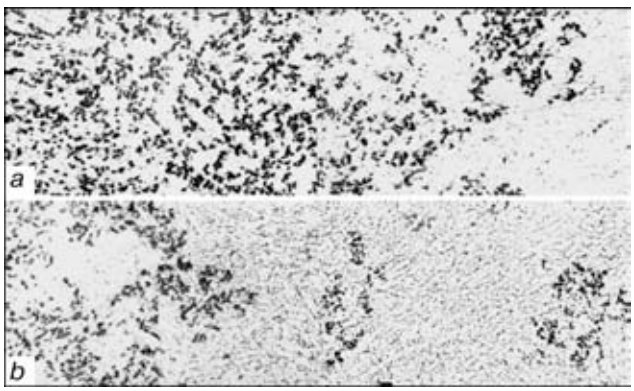

Figure 7. Weld structure in a welded joint of AMg5/12 vol.% SiC composite, produced by AAW with Sv-AMg63 (*a*) and Sv-AK5 (*b*) filler wire (×100)

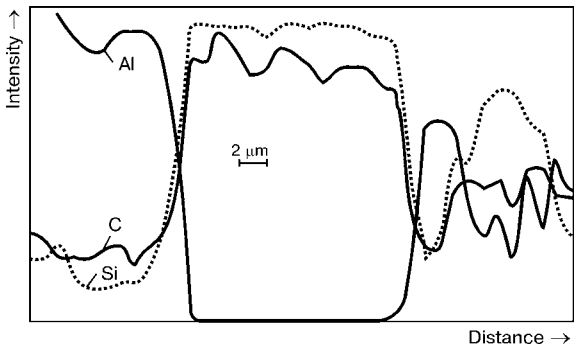

Figure 2. Nature of element radiation intensity distribution in Al25/18 vol.% SiC composite (initial condition)

No pores, discontinuities, products of chemical interaction on the particle–matrix interface were found in the composite in the initial condition, using light metallography methods (see Figure 1).

Figure 2 demonstrates the distribution of element radiation intensity in Al25/18 vol.% SiC composite during successive scanning with the electron probe of the aluminium solid solution, SiC particles and eutectic. Based on the data of X-ray microprobe analysis, grey reinforcing SiC particles have the following fraction by weight, %: Si — 71.4; Al — 1.5; Mg — 0.026; Mn — 0.04; Fe — 0.016; Ni — 0.03; Cu — 0.076; C — 26.6 (balance). The composite density is quite good with just individual micropores present. Its hardness in the initial condition is *HRB* 106 – 107.

Metallographic methods were used to examine in 5 mm specimens of the studied composite the penetration made by the electric arc in argon (I_w = 120 A), CO_2 laser radiation (P = 2.7 kW, v_w = 72 m/h), as well as the electron beam (P = 1.8 kW, v_w = 60 m/h). Investigations showed, that in laser welding at high cooling rates, a much more refined matrix structure is found in the weld metal, than in the base metal. This structure contains fine dendrites of aluminium solid solution and fine eutectic with dispersed inclusions (Figure 3, *b, c*). It should be noted that the individual sections of the weld markedly differ by the nature of the reinforcing phase distribution (Figure 3, *a*). So, a narrow section of the weld adjacent to the fusion line, is almost free of SiC particles, which may be related to the start of weld pool solidification and driving of these particles away by the growing dendrites of α-solid solution. This is followed by a narrow region of the weld, in which dark-grey SiC particles are distributed in a more uniform manner, than in the structure of the initial composite. Now in the weld center, they are present only in some regions over almost the entire depth of the penetration. New phase formation is found in this part: a considerable amount of chaotically located acicular inclusions and large globules of light-grey phase. Simultaneous precipitation of these two phases is also found (Figure 3, *c*).

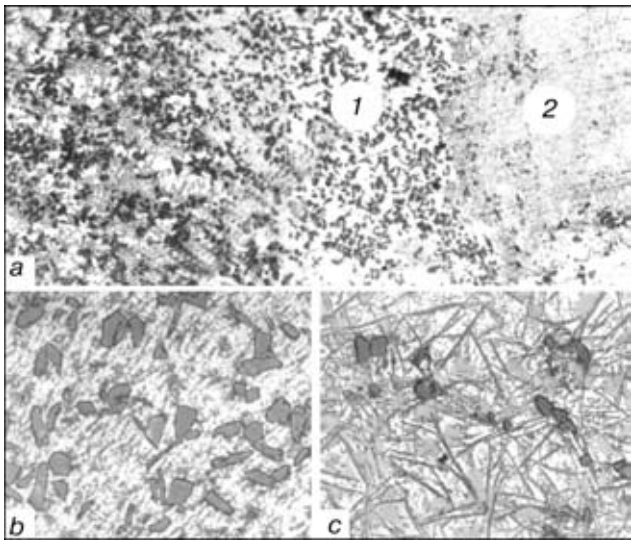

Figure 3. Weld structure in laser welding of Al25/18 vol.% SiC composite (*a*) (×100); *b* — weld periphery (region *1*); *c* — weld center (region *2*) (×600)

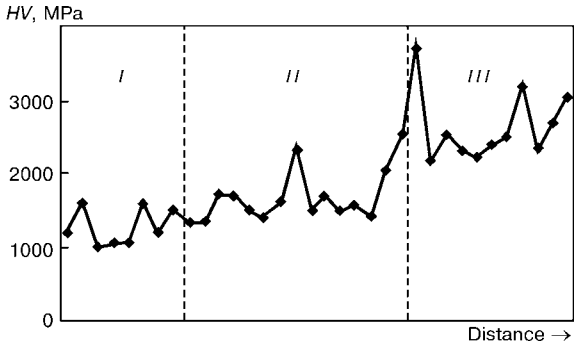

Figure 4. Weld microhardness in laser welding of Al25/18 vol.% SiC composite: *I* — base metal zone; *II* — periphery; *III* — weld center

As is seen from Figure 4, in the case of laser welding the weld metal microhardness is higher, than that of the base metal. However, in the weld metal proper a difference is observed between its values on the periphery and in the central part. In the latter, the microhardness of the regions, where new phase formation is found, can be up to 2500 MPa, and in the areas of the inclusion accumulation, it exceeds 3000 MPa.

Analysis of the curves of element distribution in the weld metal (Figure 5) showed that in scanning of acicular inclusions with the electron probe, increase of weight fraction of carbon and a simultaneous reduction of silicon and aluminium weight fractions, compared to those in the solid solution, are recorded. It is probable, that acicular inclusions are Al_4C_3 phase, and light-coloured globules are silicon crystals, since chemical interaction between silicon carbide and the aluminium melt starts at temperatures above 660 °C and proceeds according to the following reaction [3, 4]:

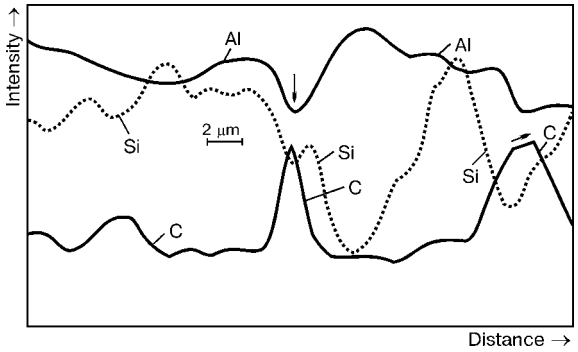

Figure 5. Nature of element distribution in the weld central region in laser welding of Al25/18 vol.% SiC composite (arrow indicates an acicular inclusion)

INVESTIGATION OF WELDABILITY OF DISPERSION-STRENGTHENED Al/SiC COMPOSITE MATERIAL

V.R. RYABOV[1], A.N. MURAVEJNIK[1], V.P. BUDNIK[1], Andr.A. BONDAREV[1], M.M. MONNIN[2], I.S. POLKIN[3], V.Yu. KONKEVICH[3] and E.M. TRUBKINA[3]
[1]The E.O. Paton Electric Welding Institute, NASU, Kyiv, Ukraine
[2]Montpellier University, France
[3]OJSC VILS, Russia

ABSTRACT

The effect of non-stationary heat sources in electron beam, laser and argon-arc welding on structural changes the matrix, behaviour and decomposition of strengthening particles in cast alumocomposite with dispersed SiC ceramic particles was examined. The technology of argon-arc welding of AMg5/12 vol.% SiC composite material is suggested.

Key words: *dispersion-strengthened composite material, matrix, strengthening particles, inclusions, structure, eutectic, hardness, welding, filler wire, strength*

Cast Al-based composites, reinforced by ceramic particles of SiC and Al_2O_3, are promising structural materials, due to their high values of strength, rigidity, high-temperature resistance, dimensional stability and good wear resistance. Owing to a relatively low cost and simplicity of manufacturing methods, they are competing strongly with the traditional alloys in mechanical engineering. However, successful application of composite materials (CM) in modern structures is largely dependent on their weldability [1]. In this connection, application of traditional processes of fusion welding, using widely applied process equipment, is still important for Al-based CM.

In order to select the most rational process of fusion welding, the influence of heating in laser, electron beam (EBW) and argon-arc (AAW) welding of dispersion-strengthened Al25/18 vol.% SiC composite on structural changes in the matrix and the nature of reinforcing particles interaction with the aluminium melt were studied to determine the factors, responsible for welded joint formation. Composite microstructure in the initial condition and after welding was investigated on metallographic sections of the specimens before and after chemical etching in a solution of Keller reagent. Their preliminary preparation for investigations was carried out by grinding on elastic diamond discs of different granularity [2]. Specimen hardness was measured in Rockwell instrument at load F = 600 N, their microhardness — in PMT-3 instrument at F = 0.1 N and the elemental composition of the matrix and the reinforcing phases was determined in Camebax X-ray microanalyser.

The studied composite was made by the casting method, namely mechanical mixing of refractory particles of silicon carbide with the matrix material melt. Used as the composite base was Al25 alloy of the following composition, wt.%: Si — 11.0 – 13.0; Cu — 1.5 – 3.0; Mg — 0.85 – 1.35; Mn — 0.3 – 0.6; Ni — 0.8 – 1.3; Ti — 0.05 – 1.2; Cr — <0.2; Fe — <0.8; Zn — <0.5; Sc — 0.02; Sn — <0.1; Al — balance. It belongs to piston silumins and is a high-alloyed cast alloy. Volume fraction of reinforcing SiC particles in the composite was 18 %.

In the initial condition, the main structural components of the composite (Figure 1) are strengthening SiC particles, dendrites of α-solid solution of aluminium and dispersed (Al + Si) eutectic. With a fine inner structure, the main eutectic colonies have greater dimensions. Found inside them are inclusions of multicomponent eutectics of $FeNiAl_9 + Al_\alpha$, $CuNiAl + Al_\alpha$, $CuSi_4Mg_5Al_4 + Al_\alpha$, etc. Reinforcing particles of silicon carbide are of grey colour, angular shape and 5 – 15 μm size. They are non-uniformly distributed through the matrix bulk (distance between individual particles varies between 3 and 50 μm), and are predominantly located in the eutectics. Apparently, when the composite solidifies, these particles do not become crystallisation centers for the dendrites, but are driven to interdendritic spaces by the growing hard phase.

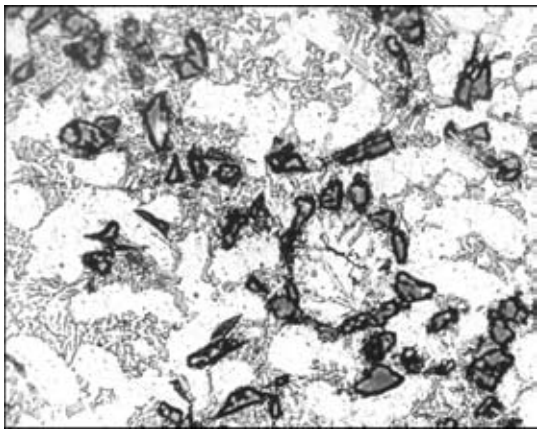

Figure 1. Microstructure of Al25/18 vol.% SiC composite (×600)

The data obtained allow a conclusion that to prevent formation of transverse cracks in welds of alloy 47XD, made by single-pass EBW on metal up to 17 mm thick, it is necessary to subject samples to preheating to 400 – 500 °C and welded joints — to annealing within a temperature range of 800 – 900 °C for 10 – 15 min. Heating of the samples prior to welding and annealing of the welded joints should be performed in a welding chamber using the scanning electron beam as a heat source. Tensile strength of the welded joints made by this technology is 460 – 520 MPa.

In addition, it was of interest to determine the possibility and conditions of prevention of cracks in repair welding of parts of alloy 47XD to eliminate, e.g. surface defects. This was done by making appropriate calculations based on an assumption that a heat source in that case was of a fixed short-time circular type (see Figure 3, sample No.3). Naturally, this heating method will result in a more rigid stressed state formed in a sample than in welding of plates using a linear fast-moving heat source. In this case the probability exists of formation of radial cracks under the effect of stresses $\sigma_{\beta\beta}$ (see Figure 3).

Kinetics of growth of temporary stresses $\sigma_{\beta\beta}$ in the fusion zone ($z = 0$, $r = 15$ mm) at the cooling stage and rate of variation of circumferential plastic strains versus temperature are shown in Figure 7. As it can be seen from the dependencies derived, in this case preheating temperature T_p should be not less than 600 °C, while annealing after welding is imperative, as even at $T_p = 700$ °C a high level of residual stresses persists in a sample. The above conclusions were experimentally verified by weld repair of defects on the surface of samples No.2 of the alloy investigated, involving preheating to $T_p = 850$ °C and annealing after welding at $T_a = 850$ °C directly in the welding chamber. Visual examination and X-ray inspection of weld spots proved that they contained no defects.

CONCLUSIONS

1. Formation of cold cracks in welded joints of γ-alloys based on titanium aluminide is caused by low ductility of these alloys at temperatures below 700 °C and, hence, a high level of longitudinal temporary stresses σ_{yy} formed in cooling of their welded joints.

2. To prevent formation of transverse cracks in EB welded joints of γ-alloy 47XD, it is recommended to use preheating of samples to be welded to a temperature of 400 – 500 °C. For making local welds or building up for repair purposes on parts of alloy 47XD, the temperature of preheating should be not less than 600 °C.

3. The level of residual stresses can be decreased by subjecting welded joints immediately after welding to annealing within a temperature range of 800 – 900 °C. In this case, to avoid formation of extra stresses, it is necessary to provide uniform heating and cooling of the welded joints.

The work was performed with a financial support by the Lawrence Livermore National Laboratory (USA).

REFERENCES

1. Mantle, A.L., Aspinwall, D.K., Wise, M.L.H. (1995) Single point turning of gamma titanium aluminide intermetallic. In: *Proc. of the 8th World Conf. on Titanium'95: Science and Technology*, Birmingham, UK, 22 – 26 Oct. Cambridge: The University Press.
2. Ivanov, V.I., Yasinsky, K.K. (1996) Efficiency of using heat-resistant alloys based on intermetallics Ti_3Al and TiAl for operation at temperatures of 600 – 800 °C in aircraft engineering. *Tekhnol. Lyogk. Splavov*, **3**, 7 – 12, 93.
3. Patterson, R.A., Martin, P.L., Damkroger, B.K. *et al.* (1990) Titanium aluminide: electron beam weldability. *Welding J.*, **1**, 39 – 44.
4. Jensen, C.M., Zhang, H., Baeslack, W.A. et al. (1998) The effect of postweld heat treatment on the structure and properties of electron beam welded Ti–48Al–2Cr–2Nb. In: *Abstr. of papers, presented at 79th AWS Annual Meeting*. Miami: AWS.
5. Makhnenko, V.I. (1976) *Calculation methods for investigation of kinetics of welding strains and stresses*. Kyiv: Naukova Dumka.
6. Hino, N., Nishiyama, Yu. (1990) Application of titanium aluminides. *Metals and Technol.*, **7**, 70 – 74.

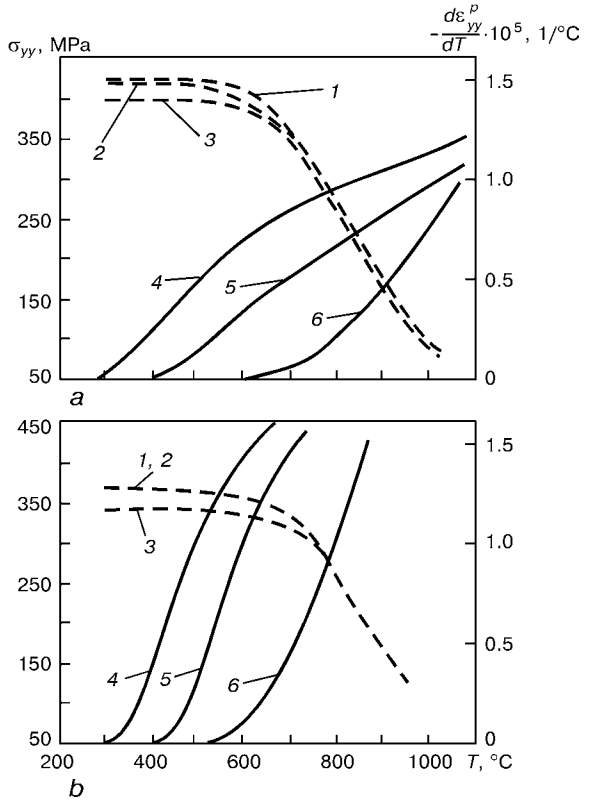

Figure 5. Distribution of longitudinal stresses (dashed lines) and rate of variation of plastic strains (solid lines) along the weld axis in samples No.1 (*a*) and 2 (*b*) after EBW at the cooling stage at T_p = 300 (*1, 4*), 400 (*2, 5*) and 500 (*3, 6*) °C

420 MPa. Therefore, preheating to 400 – 500 °C is an efficient method for decreasing the risk of formation of transverse cracks in EBW of alloy 47XD. As shown by the calculations, the level of transverse stresses σ_{xx} formed during the welding process is much lower than that of longitudinal stresses. Therefore, their role in formation of cracks can be ignored.

An increase in thickness of the plates welded to 17 mm (see Figure 3, samples No.2) and, therefore, heat input in welding does not exert a substantial effect on the processes of plastic deformation and formation of temporary and residual stresses. It might be just noted that in this case an intensive deformation of the plates welded ends at a lower temperature than in welding of samples No.1. For samples No.2 this temperature is equal to 350, 475 and 630 °C, respectively, at a preheating temperature of T_p = 300, 400 and 500 °C.

Also, the level of residual stresses (Figure 5) of these samples in much lower than that of samples No.1.

The calculation results were verified experimentally. Reference samples No.2 were welded using preheating to 400 and 500 °C.

Visual examination and X-ray inspection of welded joints revealed no defects, cracks in particular. Mechanical tests showed that welded joints made with preheating to 400 °C had ultimate strength of 330 – 350 MPa. At T_p = 500 °C the tensile strength of a welded joint is equal to σ_t = 520 MPa, i.e. its strength is equal to that of the base metal. It is likely that this difference in the σ_t values is caused by a higher level

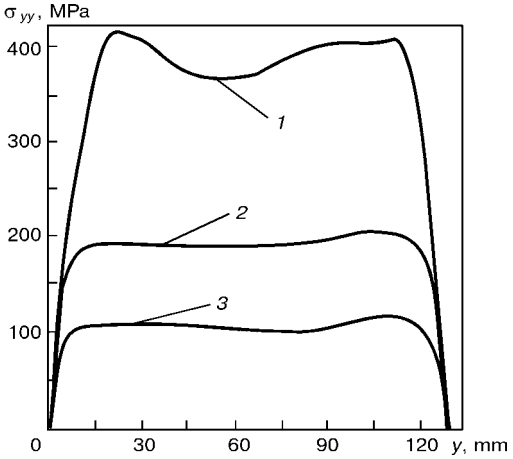

Figure 6. Effect of temperature of annealing after welding on distribution of longitudinal residual stresses in samples No.2 at T_p = 400 °C: *1* — 400; *2* — 880; *3* — 1000 °C

of residual stresses after welding with preheating to T_p = 400 °C. Stresses, which are less significant but still rather high, persist in the samples welded with preheating to T_p = 500 °C (Figure 5). Therefore, further investigations were aimed at identifying parameters for heat treatment of welded joints which would favour a decrease in the level of residual stresses. The calculation methods were employed to study two versions of conditions of cooling after annealing at T_a = = 880 and 1000 °C. The first included electron beam heating of welded joints, holding at a preset temperature and subsequent cooling directly in the welding chamber (α = 42.0 W/(m^2·K)). The second version included the same with cooling outside the welding chamber at the absence of air flows (α = = 21.0 W/(m^2·K)), i.e. annealing in a furnace. As proved by the calculation results, the first version is more favourable for alloy 47XD. According to the data shown in Figure 6, electron beam heat treatment of welded joints in a welding chamber allows residual stresses to be decreased 2 and 4 times, respectively, after annealing at a temperature of 880 and 1000 °C.

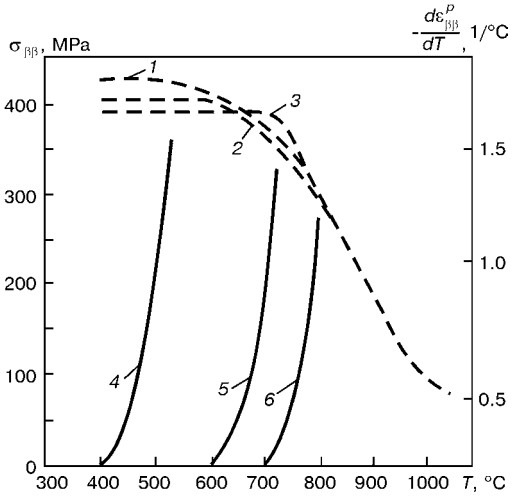

Figure 7. Variation of temporary stresses $\sigma_{\beta\beta}$ (dashed curves) and rate of variation of circumferential plastic strains (solid curves) in samples No.3 of alloy 47XD at T_p = 400 (*1, 4*), 600 (*2, 5*) and 700 (*3, 6*) °C

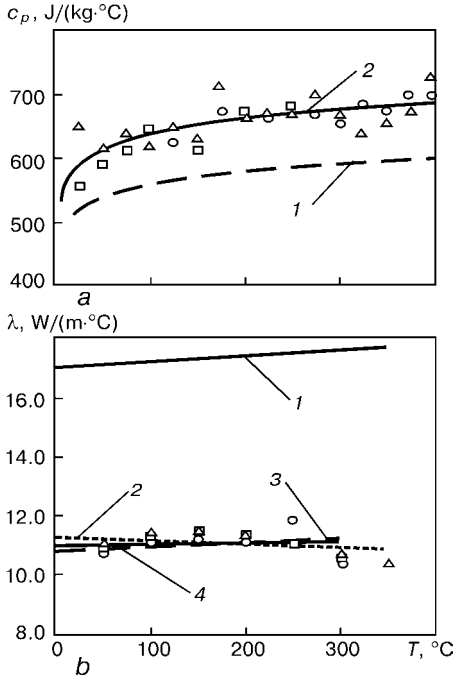

Figure 2. Temperature dependencies of thermal-physical characteristics of the alloys, derived on the basis of three experiments (see Δ, ○, ❐), on specific heat c_p (*a*) and thermal conductivity λ (*b*): *1* — VT1-0; *2* and *2* – *4* — 47XD, respectively

of movement of a heat source along axis *y* were used in the calculations. These temperature values were then used for solving the problem of thermal ductility within the frames of the flat stressed state model [5]. Temperature fields were determined by the numerical method by successively tracing the time development of heating and cooling, starting from the initial state. The spatial range of solution of the problem of propagation of heat was represented by finite elements of a rectangular shape, having the following sizes: Δx = = 1.0 and Δy = 3.5 mm for samples No.1; Δx = 1.0, Δy = 5.0 and Δz = 1.0 mm for samples No.2; and Δr = = 0.5 and Δz = 1.0 mm for samples No.3.

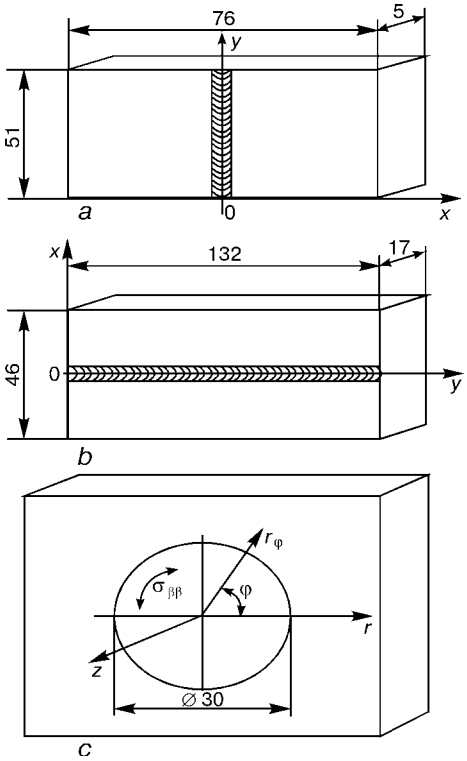

Figure 3. Sizes of samples No.1 – 3 (*a* – *c*) and calculation diagrams

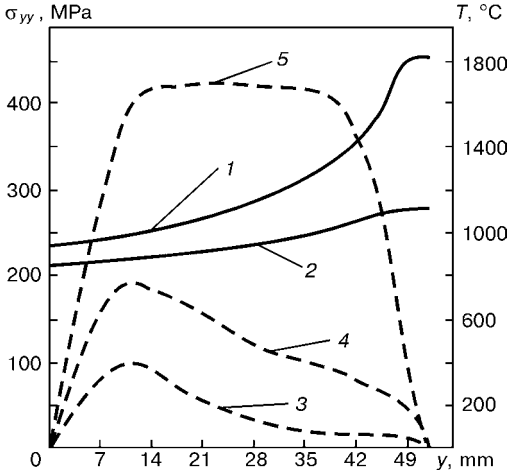

Figure 4. Distribution of temperature (solid curves) and longitudinal stresses σ_{yy} (dashed curves) along the weld axis in samples No.1 after EBW: *1, 3* — after 7.8 s; *2, 4* — after 11.4 s; *5* — after cooling (T_p = 400 °C)

Calculations of temperature fields were performed for welding with T_p = 300, 400 and 500 °C, respectively. The results obtained were used to find the character of variation of temperature along the weld axis and peculiarities of formation of longitudinal temporary and residual stresses σ_{yy}. To illustrate, Figure 4 shows the corresponding data for samples No.1. Relatively low thermal conductivity of the alloy accounts for persistence of non-uniformity of the temperature field in a plate for a long time after the end of welding. Therefore, growth of temporary stresses in the weld metal occurs as a sample cools down to initial temperature T_p (Figure 5). The level of residual tensile stresses along the weld axis at T_p = 400 °C is about 420 MPa and is not in excess of tensile strength of the alloy at a normal temperature. This accounts for the absence of cracks in samples No.1 welded with preheating to T_p = 400 °C.

Analysis of kinetics of plastic strains and temporary tensile stresses of samples No.1 in the central section of a weld at the stage of cooling (Figure 5, *a*) indicates that an increase in the values of T_p from 300 to 500 °C causes the process of intensive longitudinal deformation to shift to a substantial degree to the region of higher temperatures. Thus, if at T_p = = 300 °C the deformation at a rate of more than $0.1 \cdot 10^{-5}$ 1/°C ends at T < 350 °C, at T_p = 400 and 500 °C this occurs at T = 500 and 750 °C, respectively. A marked decrease in the level of temporary and residual stresses σ_{yy} takes place only at T_p = 500 °C. Taking into account the almost absolute absence of plastic flow of the alloy at a temperature below 500 – 600 °C, it can be considered that T_p = 400 °C is that minimum preheating temperature at which growth of plastic tensile strains ends at T > 500 °C, and the maximum level of stresses σ_{yy} is not higher than

SELECTION OF TEMPERATURE OF PREHEATING OF γ-TITANIUM ALUMINIDE IN ELECTRON BEAM WELDING

V.N. ZAMKOV, E.A. VELIKOIVANENKO, V.K. SABOKAR and **E.L. VRZHIZHEVSKY**
The E.O. Paton Electric Welding Institute, NASU, Kyiv, Ukraine

ABSTRACT

Development elasto-plastic strains in welding heating and cooling of samples of γ-titanium aluminide alloy has been analysed using calculation methods. The level of residual longitudinal stresses in the alloy plates 5 – 17 mm thick in EBW, depending upon the temperatures of preheating and annealing of welded joints after welding, has been determined. It has been established that prevention of formation of cold cracks in the 47XD alloy weld made by single-pass EBW on metal up to 17 mm thick is provided by preheating the samples to 400 – 500 °C and annealing of welded joints within a temperature range of 800 – 900 °C for 10 – 15 min.

Key words: *titanium aluminide, cold cracks, temperature fields, elasto-plastic strains, stresses, preheating, annealing*

Interest in γ-alloys based on titanium aluminide TiAl is dictated by their unique properties. They possess high heat resistance and high-temperature stability and, at the same time, low density (3.8 – 3.9 g/cm^3) [1, 2]. However, at a normal temperature these alloys have low ductility ($\delta \leq 2$ %), which makes their technological treatment rather difficult and hampers their commercial application. Therefore, an extensive use of γ-titanium aluminide in various-purpose structures will depend to a great degree upon development of efficient processes for their treatment, including welding.

Because of low ductility (up to a temperature of 700 °C), γ-alloys are very sensitive to stresses formed under conditions of non-uniform heating during welding, and are susceptible to formation of transverse cold cracks in welded joints (Figure 1). It is suggested [3, 4] that preheating should be used to prevent cold cracking, as this method decreases the rate of growth of temporary stresses during welding and lowers the level of residual welding stresses. However, no single-valued recommendations on selection of a temperature of preheating are available in literature and studies [3, 4] give just an interval of its possible values (from 250 to 650 °C) with no explanations.

The purpose of this study was to identify a minimum value of preheating temperature T_p at which no cracks are formed in welded joints of γ-titanium aluminide. Numerical calculation methods were used to solve thermal ductility problems and trace development of elasto-plastic strains during welding heating and cooling [5].

Investigations were conducted on samples of γ-alloy 47XD (Ti–48Al–2Nb–2Mn) [1] cut out from an ingot and subjected to isostatic treatment at a temperature of 1260 °C and pressure of 171 MPa for 4 h, and then to subsequent stabilizing annealing at T_a = = 1015 °C (50 h). Welding and preheating of the plates were performed by electron beam using the UL-144 machine equipped with the ELA-60/60 power supply.

The following characteristics of the alloy were used for the calculations: tensile strength σ_t = 480 – 540 MPa at normal temperature, normal elasticity modulus $E = 1.6 \cdot 10^5$ MPa, Poisson's ratio $\nu = 0.3$ (according to the data of [6]) and coefficient of convective heat transfer in vacuum α = = 21.0 W/(m^2·K). Dependencies of specific heat and thermal conductivity of alloy 47XD upon the temperature were determined experimentally (Figure 2).

Building up with through penetration was preliminarily made on samples No.1 5 mm thick (Figure 3) by measuring the thermal cycle. As experimentally found, a minimum value of T_p at which no cracks are formed is 400 °C. Temperature fields were calculated on this basis and using diagrams shown in Figure 3. Two versions of welding were studied in this case: one using a high-power fast-moving linear source (samples No.1 and 2), and the other using a fixed circular short-time source (samples No.3).

Assuming that electron beam heating provides a uniform heating of flat samples through thickness of the metal, mean values of temperature in the process

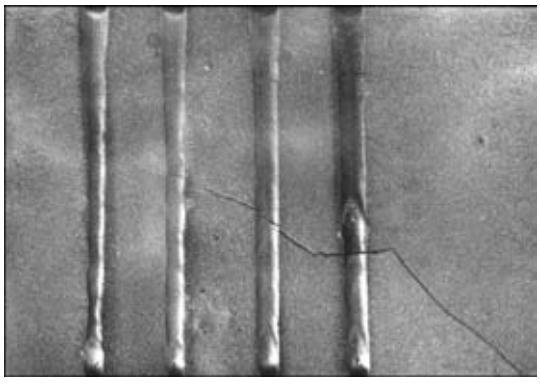

Figure 1. Cold cracks in a welded sample of alloy 47XD made by EBW without preheating

positions for reduction of the surface tension of the metallic melt.

3. To prevent the slag spreading to the weld edges and occurrence of undercuts the welding slags should have surface tension not lower than 300 MJ/m^2. The best welding-technological properties in welding with the self-shielding flux-cored wire in different spatial positions are attained at 300 – 350 MJ/m^2 surface tension of slag.

REFERENCES

1. Kuzmenko, V.G., Galinich, V.I., Tokarev, V.S. *et al.* (1999) Study of properties of slag melts as regards to optimizing the compositions of welding fluxes. Structure. *Avtomaticheskaya Svarka*, **11**, 38 – 41.
2. Podgaetsky, V.V., Kuzmenko, V.G. (1988) *Welding slags*. Kyiv: Naukova Dumka.
3. Sokolov, O.K. (1963) Calculation of surface tension of molten halogenides at the boundary with inert phase at fusion temperature. *Izv. Vuzov, Tsvetn. Metallurgia*, **4**, 55 – 58.
4. Appen, A.A. (1952) Experience in classification of components by their effect on surface tension of silicate melts. *Zhurn. Fiz. Khimii,* **10**, 2215 – 2218.
5. Popel, S.I. (1971) *Theory of metallurgical processes*. Moscow: VINITI.
6. Popel, S.I., Pavlov, V.V. (1965) Thermodynamic calculation of surface tension of solutions. In: *Surface phenomena in melts and solid phase occurring from them*. Nalchik: Kabard.-Balkar. B.P.
7. Podgaetsky, V.V. (1992) Evaluation of surface tension of melts of welding slgs. *Avtomaticheskaya Svarka*, **5**, 26 – 28.
8. Pavlov, V.V., Popel, S.I. (1964) Calculation of surface concentrations of components in oxide melts. *Izv. Vuzov, Tsvetn. Metallurgia*, **6**, 30 – 37.
9. Frenkel, Ya.I. (1945) *Kinetic theory of liquids*. Moscow: AN SSSR.
10. Mojsov, L.P., Burylyov, B.P. (1997) Calculation of properties of metallic and slag systems in the development of welding consumables. *Svarochnoye Proizvodstvo*, **2**, 18 – 20.

LASER BUTT WELDING WITH HIGH-FREQUENCY HEATING OF WELD EDGES

V.Yu. KHASKIN, V.D. SHELYAGIN, V.P. GARASHCHUK, V.N. SIDORETS, A.V. SAKHARNOV and **E.I. GONCHARENKO**

The E.O. Paton Electric Welding Institute, NASU, Kyiv, Ukraine

ABSTRACT

Investigated was the combined effect on steel by laser radiation and high-frequency heating in butt welding. Concurrent high-frequency heating to a temperature on the sample surface equal to 1100 – 1200 °C was established to cause an increase of 1.5 times either in the penetration depth or in the welding process speed. Geometry of the welds is close to that typical for laser welding, although the welds are different in structure (the weld and HAZ metal contains no quenching structures characteristic of laser welding, and values of hardness differ to a lesser degree from those of the base metal).

Key words: *combined welding methods, laser and high-frequency welding, equipment, conditions, structure*

Much consideration has been given to investigation of the combined effect on metal by radiation of laser and other heat sources in welding, for example, by arc discharge [1, 2] or high-frequency current [3], in order to increase penetration depth or process productivity.

Welding using a highly concentrated heat source, such as laser, is characterized by a rigid thermal cycle, which in a number of cases is a negative factor, leading to formation of cracks and undesirable brittle quenching structures [4]. We investigated laser butt welding, involving concurrent high-frequency heating with a purpose to avoid this drawback and increase the penetration depth (or welding speed). For this we welded the prepared butt joints, other than a joint described in [3], which was formed during longitudinal welding of a pipe, where high-frequency currents were concentrated at a butt joint point to form a high-intensity heat source.

For experiments we used the technological laser LT 104 with a radiation power of up to 10 kW [5] and high-frequency welding unit IV120-160/0.44 with a power of 160 kW and a working frequency of 0.44 MHz. A reequipped turning and screw-cutting machine was used as a welding post, where a column with laser radiation focusing optics was installed instead of a cutter holder, and a mobile high-frequency welding head rigidly connected to a support was used instead of a tailstock [6]. A single-winding work coil that heated a joint welded was attached to the head. The coil was made from a copper tube 6 and 8 mm in diameter. The gap between the coil and samples welded was 3 mm. The temperature of high-frequency heating on the external and internal surfaces of the tubular samples welded was measured with the optical pyrometer «Spektropir P1-003» (1986, Research and Production Association «Lenteplopribor»), having a temperature measurement range of 600 – 1800 °C and a main instrumental reduced error of ±1 %.

Butt welding of tubular samples with a wall thickness of δ = 15 mm was performed in CO_2. It was fed so that the plasma flame over the weld pool, caused by a break-down occurring in the plasma and formation of the arc discharge between the coil and a sample,

where x_i is the content of the i-th component, mole %.

The equation (5) does not take into account the effect of the dissolved sulphur, nitrogen and oxygen, but makes it possible to evaluate the change in the surface tension of the molten metal at small variations in the content of the above-mentioned impurities.

The calculations showed that aluminium and manganese have the highest influence on the surface tension (Figures 1, 2).

In welding with experimental wires in vertical plane this influence became evident, as at 1.6 % Al content the metal is flowing down. Here, the metal has a low surface tension (≈ 1670 MJ/m^2). At about 0.9 – 1.1 % Al and 1.0 – 1.2 % Mn content in metal (surface tension is 1690 – 1695 MJ/m^2) a good weld formation is observed in case of the vertical welding. To evaluate the effect of the surface tension of the molten metal on the welding-technological properties of the flux-cored wire the alloying with manganese and aluminium is admitted within the established limits.

Curves of changing the surface tension of slag of the salt-oxide BaF_2–LiF–MgO system at 1673 and 1873 K temperature, calculated by formula (3), are shown in Figure 3. For slags of all the systems the surface tension is reduced with the temperature increase that proves about the decrease in interparticle interaction and it is increased monotonically with the increase of MgO concentration in melt. The absence of maximums and minimums on the isolines of the surface tension indicates the absence of the complex ions. Therefore, the slag system BaF_2–LiF–MgO represents a solid solution within the entire field of solidification (see Figure 3). The fact, that the surface tension does not depend on the temperature, proves the absence of the structural changes in the mentioned slag system during solidification.

The compositions of slags forming in fusion of experimental flux-cored wires and their surface tension at temperature 1673 K are given in the Table.

The surface tension of welding slags influence greatly their covering power. The quality weld formation, as well as its formation in vertical and overhead welding depend on it to a great extent. In this case it is desirable that the slag had a high surface tension to maintain the weld pool, however, the covering power of the slag is here deteriorating. To increase the latter it is necessary to provide low values of the slag surface tension. However, it should be taken into account that at very low surface tension the slag is flowing down to the weld edges. The experimental check-out of effect of surface tension of slags on the welding-technological properties was performed using experimental wires, whose main slag composition is given in the Table.

With wires No.1 – 5 the slags have the low surface tension. In welding with these wires a slag spreading along the weld surface is observed. At very low (about 250 MJ/m^2) surface tension the fusion of the welding edge is occurred with the formation of undercuts. Thus, in welding with experimental wires No.1 and 2, whose slags have the surface tension of 213 and 223 MJ/m^2, respectively, the appearance of undercuts is observed. When the wires No.4 and 5 are used, whose slags have surface tension in the ranges of 263 – 271 MJ/m^2, the regions of undercuts are negligible. In welding with wires No.6 and 7 (slags surface tension is 325 – 345 MJ/m^2) the weld is almost completely covered with the slag and undercuts are not formed. When wire No.8 is used (surface tension of the slag is 385 MJ/m^2) the undercuts are not observed, but the slag covering power is insufficient.

Surface tension of slags at 1673 K temperature

No. of wire	Content of components in slag, wt.%						σ, MJ/m^2
	BaF_2	LiF	MgO	ZrO_2	KF	Al_2O_3	
1	61	15	15	3.0	3.5	–	213
2	57	14	16	6.4	3.2	–	223
3	55	13	25	3.0	1.5	–	253
4	50	15	27	3.5	1.0	–	263
5	50	13	30	4.0	1.0	–	271
6	40	10	45	3.0	1.0	–	325
7	45	5	40	1.0	–	9	345
8	35	4	55	1.0	–	5	385

Thus, in welding with wires whose slags have a low surface tension, the slags are spreading at the weld edges, while in using wires whose slags have high surface tension, the slags do not cover weld surface completely that deteriorates its appearance and formation. It was established as a result of the carried out investigations that the best welding-technological properties are attained in welding with flux-cored wires whose slags of the given salt-oxide system have the surface tension in the range of 300 – 350 MJ/m^2.

Thus, knowing surface tension of slag and molten metal, it is possible to predict the welding-technological properties of the self-shielding flux-cored wires by such characteristics as the covering power of the slag and weld formation in the vertical plane.

CONCLUSIONS

1. The dependence of the surface tension of slag of the salt-oxide BaF_2–LiF–MgO system on the composition and melt temperature was investigated. The absence of maximums and minimums on the isolines of the surface tension indicate the absence of complex ions. Therefore, the BaF_2–LiF–MgO system represents a solid solution in the entire field of solidification. As the surface tension does not depend on the temperature it is possible to state about the absence of structural changes in the slag system above the line of liquidus. The surface tension of the slag melt is increasing monotonically with the increase in concentration of the manganese oxide.

2. It is desirable to limit the content of aluminium to 1.5 % and manganese to 2.0 % in the self-shielding flux-cored wires used for welding at different spatial

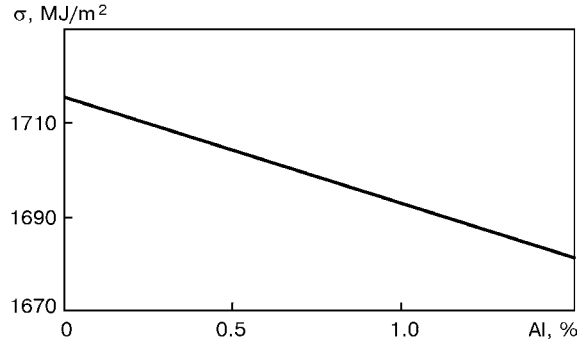

Figure 1. Dependence of surface tension of metal (C — 0.07; Si — 0.1; Mn — 1.0; Ni — 1.0; S — 0.005; P — 0.01; N — 0.02; O — 0.02 wt.%) on the content of aluminium at temperature 1823 K

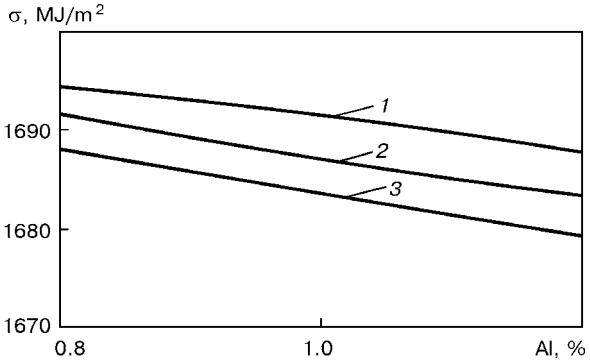

Figure 2. Dependence of surface tension of metal (C — 0.1; Si — 0.3; S — 0.02; P — 0.02; N — 0.02; O — 0.02 wt.%) on content of aluminium and manganese at temperature 1823 K: *1* — 0.5 Mn; *2* — 1.0 Mn; *3* — 1.5 Mn

$$\sigma = \sigma_i - \frac{RT}{\omega} \ln \sum_{i=1}^{k} F_i N_i, \qquad (3)$$

where σ_i is the surface tension of pure i-th component; R is the gas constant; ω is the molar surface (area occupied by one mole of solution); F_i is the surface activity of the i-th component in the solution depth; N_i is the molar fraction of the i-th component.

As the molar surface of salt-oxide system is changed negligibly, then the molar surface can be taken approximately constant for the wide range of concentrations of components of the salt-oxide melts. The value $\omega = 3.3 \cdot 10^8$ cm^2 has a good correlation with experimental data obtained after measuring the surface tension of the slag [9]. The slag base of the self-shielding flux-cored wires of a tubular design represents salt-oxide systems on the base of fluorides of barium, lithium, potassium and oxides of magnesium, aluminium and zirconium.

When the surface tension [2, 3] of melts of slags of the salt-oxide systems is determined the following values of constants F_i are derived: $F_{MgO} = 1.5$; $F_{LiF} = 3.2$; $F_{BaF_2} = 2.9$; $F_{ZrO_2} = 2.1$; $F_{KF} = 3.4$; $F_{Al_2O_3} = 3.4$.

The equation (1) was derived for oxides and fluorides of MeO and MeF type, respectively. To use it for oxides and fluorides of Me_xO_y and Me_xF_y, it is necessary to replace molar fractions N_i by concentration N_i' characterizing the equal amounts of gram-ion fractions of oxygen in different oxides [10], according to the equation

$$N_i' = \frac{\gamma_i N_i}{\sum_i^k \gamma_i N_i}, \qquad (4)$$

where γ_i is the amount of oxygen atoms in the oxide molecule.

The properties of slag and metallic phase influence most significantly on the weld geometry at temperature 1700 – 1400 °C. The use of deoxidizing and alloying with aluminium, manganese, nickel at a small content of silicon is typical of the self-shielding flux-cored wires with slag of the salt-oxide system. In case of the multicomponent slag system Fe–Ni–Mn–Si–Al at 1823 K the surface tension can be described by the equation [10]

$$\sigma = 1735x_{Fe} + 1700x_{Ni} + 1030x_{Mn} + 720x_{Si} - 630(x_{Fe} + x_{Mn})x_{Si} + 800x_{Al} - 200x_{Fe}x_{Al}, \qquad (5)$$

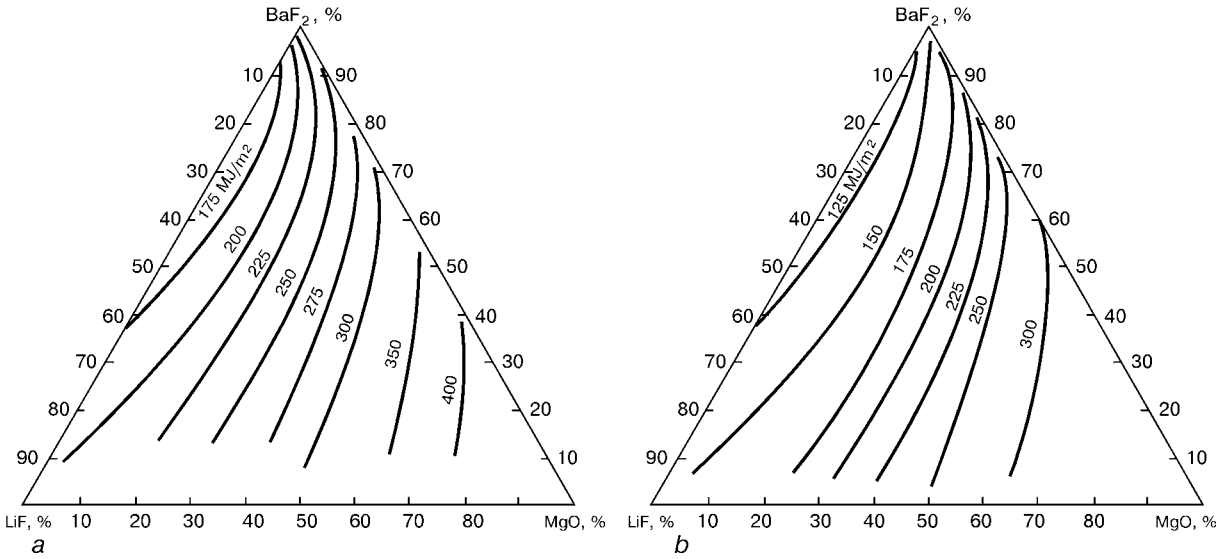

Figure 3. Dependence of surface tension of slag of the BaF_2–LiF–MgO salt-oxide system on their composition at temperature 1673 (*a*) and 1873 (*b*) K

EFFECT OF SURFACE TENSION OF WELDING SLAGS OF SALT-OXIDE SYSTEM ON CHARACTERISTICS OF WELDING-TECHNOLOGICAL PROPERTIES OF SELF-SHIELDING FLUX-CORED WIRE

V.N. SHLEPAKOV and **S.M. NAUMEJKO**
The E.O. Paton Electric Welding Institute, NASU, Kyiv, Ukraine

ABSTRACT

Dependence of surface tension of slag of the salt-oxide BaF_2–LiF–MgO system on its composition and temperature was investigated. The effect of surface tension on the welding-technological properties of the flux-cored wires in welding in various spatial positions is considered.

Key words: *arc welding, flux-cored wire, welding fluxes, salt-oxide systems, surface tension, welding-technological properties, covering power, undercuts*

The development of the new welding consumables with the required technological properties for arc welding is an actual scientific problem of the welding manufacturing. Conceptions about the interrelation of the conditions of producing quality welded joints with main physical-chemical properties of slags are shown in some publications [1, 2]. They outline the effect of the surface tension of slag and metallic phases on the welding-technological properties of welding consumables in case of arc fusion welding, in particular the covering ability of the slag. At a low covering power the slag does not cover the weld completely, thus deteriorating its appearance, formation of weld and slag removal. The surface tension of the molten metal, conditions and technology of welding also affect the smooth transition to the parent metal and favourable shape of the weld. The weld formation in vertical and overhead positions depends greatly on the surface tension of the slag and metallic phases.

The interfacial tension defines the peculiarity of proceeding metallurgical reactions, stability and rate of removal of non-metallic inclusions from the molten metal, adhesion of slag and metal. The interfacial tension characterizes the energy of the interaction of iron atoms with slag ions which has a certain effect on the strength of slag adhesion with metal, and, consequently, the slag crust removal. The chemical adhesion of slag and metal are greatly affected by the surface and interfacial tension at the metal–slag interface on which the metal wetting with molten slag depends. With increase in value of the interfacial tension the metal wetting with the slag is deteriorated, the adhesion strength is decreased. The closer the melt and metal surface in their molecular nature, the lower the interfacial tension at the melt–metal interface and higher adhesion.

The interfacial tension is characterized by the equation

$$\sigma_{Me-s} = \sigma_{Me} + \sigma_s \cos \theta, \quad (1)$$

where σ_{Me-s} is the interfacial tension of molten slag at the boundary with weld metal; σ_{Me}, σ_s is the surface tension, respectively, of molten metal and molten slag; θ is the angle of wetting.

On the basis of the second law of thermodynamics the spontaneous proceeding of process of wetting of hard surface of metal with slag is possible in that case when the following condition is kept

$$\sigma_{Me} \geq \sigma_{Me-s} + \sigma_s, \quad (2)$$

i.e. the spreading is accompanied by the decrease in a free energy of the system. It follows from this expression that the weld metal surface is wetted better with the slag when the surface tension of the slag and interfacial surface tension of metal–slag are lower and the surface tension of the metal is higher. Thus, coming from the surface tension of the slag and weld metal it is possible to evaluate wettability, and, thus, the covering power of the slag.

The surface tension of metallurgical and welding slags was investigated by many scientists [3 – 6]. The experimental data about the surface tension of the molten slag are limited by the definite systems, therefore, in practice the change in some properties of welding consumables are not taken into account when the slags are selected. The calculation methods of evaluation of the surface tension of slags [5 – 8] give an opportunity to obtain the information on the basis of a limited experimental material.

To evaluate the surface tension of the molten welding slag a method of approximated calculation of the surface tension of multicomponent solutions, developed in [7, 8], was used. According to model-thermodynamic equation the surface tension, σ, is equal to

primary austenite grains and in the bulk of the grains. The grain index is ≈5.

Structure of the weld metal in the case of combined welding at a speed of 90 m/h is characterized by coarser components and a reduced amount of pearlite, as compared with the similar case at a speed of 120 m/h. Microhardness of ferrite is given in the Table. Microhardness of pearlite was not measured, as the pearlitic regions were too small. Structure of the overheated region is ferritic-pearlitic. The amount of ferrite increased and became dominant. Ferrite is precipitated along the boundaries of primary austenite grains and in the bulk of the grains. An insignificant amount of ferrite has a Widmanstaetten orientation [4]. Grain has index 6. Structure of the complete recrystallization region is fine-grained (index 9 – 10), ferritic-pearlitic, with dominating ferrite, and that of incomplete recrystallization is also ferritic-pearlitic.

In a sample welded by the combined method at a speed of 120 m/h, the weld metal structure is a mixture of ferrite and pearlite. Here the ferrite amount is dominant. The structure is finely dispersed and oriented along the boundaries of crystalline grains. The overheated region consists of pearlite grains surrounded by ferritic precipitates along the boundaries. The amount of the pearlitic component decreases and structure is refined with a distance from the fusion line. Grain in this region has index 5 – 6. The region of complete recrystallization has a fine-grained (index 9 – 10) ferritic-pearlitic structure with a dominating ferritic component. The incomplete recrystallization region has a similar structure with the grain index similar to the complete recrystallization region.

The following trends of variation of structure of the weld metal were fixed. Like in the case of laser welding, an increase in the welding speed is accompanied by an increase in the degree of dispersion of the structure, which still remains coarser, and a decrease in size of the cast zone and the HAZ metal. In the case of a maximum speed an insignificant increase in microhardness of the weld metal is fixed. This is attributable to the fact that the share of the ferritic component of the weld and HAZ metal increases with an increase in the welding speed. However, in all the cases the structure is ferritic-pearlitic, rather soft and ductile. Unlike laser welding, the combined welding process results in the HAZ which preserved all the zones, independently of the welding speed.

It can be concluded from the results of investigations of microstructures that high-frequency heating of the samples welded provides structures of the weld and HAZ metal which are close to those of the base metal. In addition, this heating allows avoidance of hard and brittle martensitic structures, which in laser welding may lead to cracking and decrease in impact toughness and ductility [6]. Besides, as proved by experiments, concurrent high-frequency heating provides a substantial decrease in the probability of formation of pores and improvement of formation of the top bead.

Despite differences in design between our experiments and those described in [3], it is appropriate to note some points they share. Within a high-frequency heating temperature range of 20 to 1200 °C an increase in the welding speed [3] and penetration depth in our case (see Figure 2) has a similar trend. Like in study [3], the weld and HAZ metal had a structure close to that of the base metal. The issues of the shielding gas feed and elimination of the plasma flame also turned out to be important. As noted in [3], the welding process is considerably affected by the accuracy of alignment of the weld edges.

CONCLUSIONS

1. Concurrent high-frequency heating to 1100 – 1200 °C on the sample surface allows an increase of about 1.5 times in either the penetration depth or the welding speed.

2. Welds made by using high-frequency heating are close in shape to typical laser welds, but differ in structure.

3. The weld and HAZ metal contains no quenching structures characteristic of laser welding, microhardness of the metal becomes much more uniform and close to that of the base metal, which is a positive factor, promoting an increase in ductility of the welds.

4. Drawbacks of the weld and HAZ structure in the case of combined welding include coarsening of grains.

REFERENCES

1. Dilthey, U., Lueder, F., Wieschemann, A. (1999) Technical and economical advantages by synergies in laser arc hybrid welding. *Welding in the World*, Vol. 43, 141 – 152.
2. Nagata, S., Katsumura, M., Matsuda, J. *et al.* (1985) Laser welding combined with TIG or MIG. *IIW Doc. IV-390–85.*
3. Hayasi, T. (1998) Use of welding with preliminary high-frequency heating for production of thick-walled medium-diameter pipes. *Transact. of Laser Treatment Society*, **7**, 137 – 144.
4. Grabin, V.F. (1982) *Metals science of fusion welding.* Kyiv: Naukova Dumka.
5. Garashchuk, V.P., Shelyagin, V.D., Nazarenko, O.K. *et al.* (1997) Technological CO_2-laser LT 104 with power of 10 kW. *Avtomaticheskaya Svarka*, **1**, 36 – 39.
6. Khaskin, V.Yu., Pavlovsky, S.Yu., Garashchuk, V.P. *et al.* (2000) Laser heat hardening of complex-alloyed steels with a low and medium carbon content. *Dopovidi NAN Ukrainy*, **2**, 36 – 39.
7. Kovalenko, V.S., Golovko, L.F., Merkulov, G.V. *et al.* (1981) *Hardening of parts by a laser beam.* Kyiv: Tekhnika.

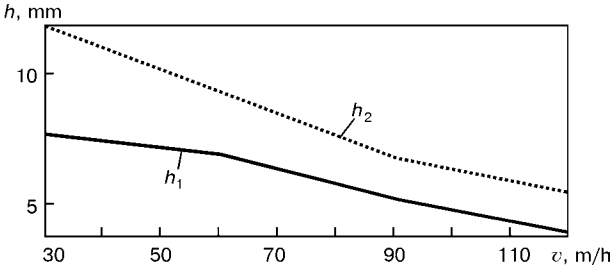

Figure 3. Dependence of variation of laser penetration depth h_1 and penetration depth h_2 with concurrent high-frequency heating to 1100 – 1200 °C upon the welding speed

laser welding at a speed of 30 m/h. Structure of the weld metal consisted of bainite with rare regions of martensite. Ferritic regions and a small amount of pearlite were detected along the boundaries of crystalline grains. The HAZ was 1.6 mm wide, including the overheated region 0.9 mm, fine-grained region 0.3 mm and incomplete recrystallization region 0.38 mm wide. Structure of the overheated region metal is a fine-acicular mixture of martensite and bainite regions, as well as local precipitates of pearlite and ferrite. In the overheated region the grains had index 5, and some rare grains had index 4. In the fine-grained region the structure was refined to index 10.

Structure of the weld and HAZ metal in a sample welded by using laser radiation at a speed of 90 m/h is similar to the above one, although it is more finely dispersed. Metal of the HAZ 0.68 mm wide consists of regions of overheating (0.25 mm), fine grains (0.13 mm) and incomplete recrystallization (0.3 mm). In the overheated region it corresponds to index 5, more rarely — to index 6. The grain is refined to index 7 – 8 with distance from the fusion line.

In laser welding at a speed of 120 m/h the weld metal is characterized by the most finely dispersed structure consisting of martensite, bainite and fine precipitates of pearlite along the crystalline grain boundaries. Martensite has different etchability, which is associated with its carbon content (lighter regions are likely to be more finely dispersed and low-carbon martensite [7]). The HAZ is 0.15 – 0.2 mm wide and consists of the overheated region. Structure of the region is a fine-acicular martensite and local pearlite precipitates (see the Table).

The following trends of variation of the weld metal structure can be seen. An increase in the welding speed is accompanied by an increase in the degree of dispersion of the structure, decrease in size of the cast zone and HAZ, and an increase in their microhardness. The latter is attributable to an increase in the share of a martensite component and a decrease in the amount of pearlite and ferrite up to their complete disappearance. The zone of fine and coarse grains merge in the HAZ metal, while at a maximum welding speed the HAZ is an overheated region.

Structure of the weld metal resulting from the combined method laser + high-frequency heating at a welding speed of 30 m/h is ferritic-pearlitic with a small amount of ferrite characteristic of the Widmanstaetten structure [4]. Structure of the overheated

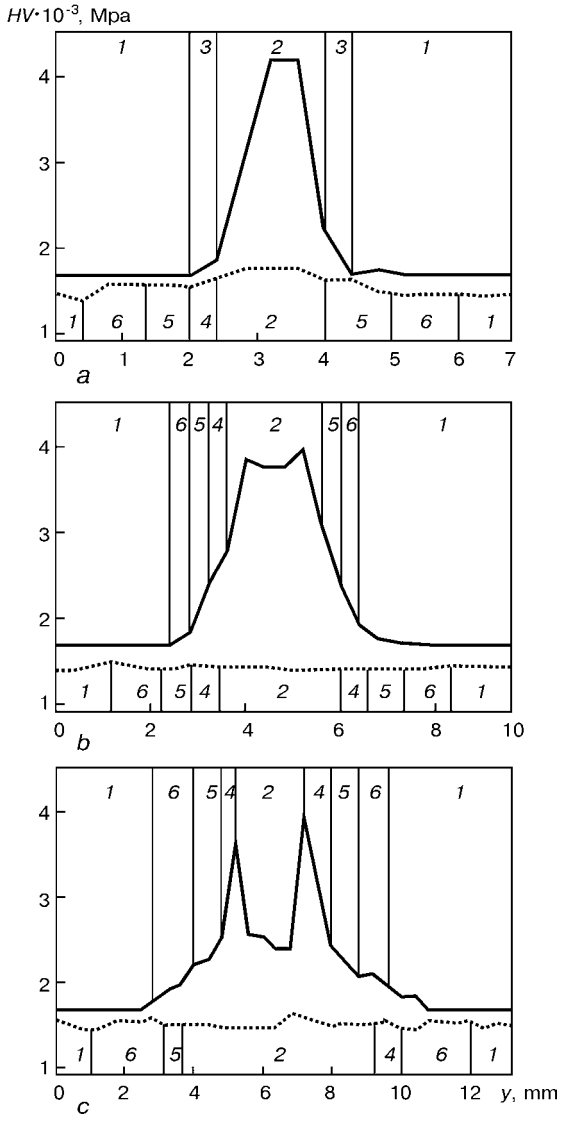

Figure 4. Distribution of microhardness HV in direction y, normal to the plane of the joint welded, at depth $h/3$ for laser welding (solid curve) and combined welding (dotted curve) with high-frequency heating to 1100 – 1200 °C at a speed of 120 (*a*), 90 (*b*) and 30 (*c*) m/h: *1* — base metal; *2* — weld; *3* — HAZ; *4* – *6* — regions of coarse and fine grains and incomplete recrystallization, respectively

zone is more coarsely dispersed than in all other samples welded using laser radiation and high-frequency heating. Primary grain of austenite becomes coarser (index 4 – 5). Ferrite is precipitated along the grain boundaries and in the bulk of the grains (see the Table). The amount of pearlite increases, as compared with the bead-on-plate welds made at a speed of 60, 90 and 120 m/h.

Microstructure of the weld metal in the case of the combined method at a welding speed of 60 m/h consists of coarser laminae than at a welding speed of 90 m/h, but is more finely dispersed than at a welding speed of 30 m/h. The amount of pearlite decreases, and its precipitates are very fine. Hardness of pearlite in the weld metal was not determined, while that of ferrite is given in the Table. Structure of the overheated zone is also ferritic-pearlitic. Here the amount of pearlite is insignificant. Ferrite is precipitated along the boundaries of

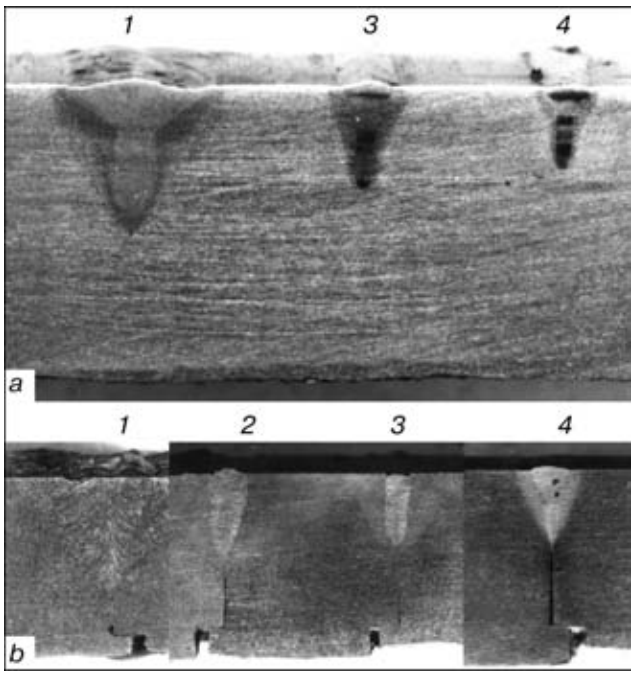

Figure 1. Macrosections of laser bead-on-plate welds made using no filler (*a*) and butt welded joints made by the combined method (*b*) on a wall of δ = 15 mm of St.3 tubular samples at a speed of 30 (*1*), 60 (*2*), 90 (*3*) and 120 (*4*) m/h

was eliminated. Material of the samples was semi-killed steel St.3. For comparison, four bead-on-plate samples were welded, using no filler, by laser radiation (simulation of laser welding) without and with high-frequency heating at a speed of 30, 60, 90 and 120 m/h. In all the cases the laser radiation power was 3 kW, focus immersion depth was 2 mm, focal distance of the lens was 300 mm, and temperature of concurrent high-frequency heating was varied from 800 to 1500 °C.

According to the accepted experimental design, high-frequency heating of circumferential butt joints was done on the side of the external surface of a sample. Walls of the tubular samples were 15 mm thick. Temperature gradient through this thickness was 500 – 800 °C, which exerted a substantial effect on the penetration depth.

The most characteristic macrosections of the welds are shown in Figure 1. Dependencies of geometry of the welds upon some parameters of the combined welding process are shown in Figures 2 and 3. The

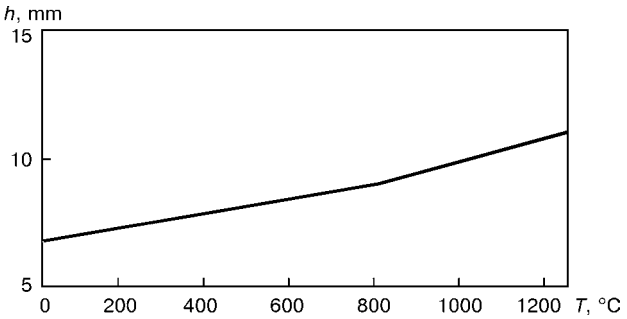

Figure 2. Dependence of variation of penetration depth h upon temperature T of concurrent high-frequency heating at a welding speed of 60 m/h

experiments showed that high-frequency heating of the steel sample surface to 1100 – 1200 °C allowed the penetration depth to be increased approximately 1.5 times, as compared with conventional laser welding. In addition, the knife penetration was preserved in this case.

Microstructures of the welds were investigated from microsections etched in 4 % alcohol solution of nitric acid for 5 s. Examinations were carried out using the optical microscope «Neophot-32» at ×50 – 250, the grain size was measured according to GOST 5639–82, and microhardness was determined using the LECO hardness meter under loads of 0.1, 0.25, 2.0 and 10.0 N.

The base metal had a ferritic-pearlitic structure. Ferritic grains had index 7 – 8, microhardness was *HV* 1660 – 1800 MPa at 10 N. After laser welding, as it might be expected and which is in agreement with the results of study [7], structures of bainite and martensite, in addition to ferrite and pearlite, were detected in the weld and HAZ metal. After combined laser welding with high-frequency heating, only ferritic-pearlitic structures were fixed in the weld and HAZ metal, which are indicative of the absence of a rigid thermal cycle [4], i.e. of a considerable decrease in the cooling rates. Results of measuring microhardness of structural components of the weld and HAZ metal for both cases are given in the Table.

Distribution of microhardness (load *HV* 10 N) in the weld and near-weld zone metal at a welding speed of 30, 90 and 120 m/h is shown in Figure 4.

The most coarsely dispersed structure of metal of the laser bead-on-plate welds was fixed in the case of

Microhardness of structural components of the weld and HAZ metal in laser and combined welding, MPa

Welding speed, m/h	*Laser welding, HV 0.1*				*Combined welding, HV 0.25*	
	Ferrite	*Pearlite*	*Bainite*	*Martensite*	*Ferrite*	*Pearlite*
30	1680 – 1750 / 1810 – 2050	1980 – 2290 / 1850 – 2050	2050 – 2570 / 2290 – 2580	3030 – 3220 / 3300 – 3780	876 – 891 / 805 – 839	– / 1160 – 1200
60	–	–	–	–	958 – 940 / 824 – 839	–
90	1810 – 1850 / 2050	1810 / 2270	2740 – 3300 / 3000 – 3250	3780 – 4510 / 3850 – 4290	772 – 876 / 805 – 1050	–
120	–	– / 2030 – 2380	2900 – 3030 / –	3960 – 4130 / 5930	997 – 1050 / 925 – 1050	1220 – 1360 / 1050 – 1220

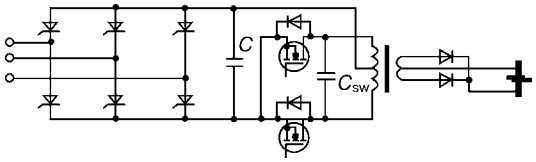

Figure 10. Converter with a rectifier in the welding transformer secondary circuit: C_{sw} — switching capacitor

quency, and a transformer with two valves. This converter differs from that considered in Figure 8, only by valves in the secondary circuit, which allows it to operate at higher frequencies. The width-pulse control of the polarity switch transistors provides the most complex cycles of welding current variation, also ensuring a stable quality of welded joints.

This type of converters are especially promising for microwelding, when additional power losses in the valves are not important. They are indispensable for suspended machines, operating in robotic lines and performing welding of metal parts with protective metal coatings. In this case, the converter allows reducing the weight and changing the machine overall dimensions, as well as increasing electrode resistance.

When selecting a particular machine type, it should be borne in mind, that any machine with the converter of frequency and phase number, is much more expensive, than a simple single-phase machine with a thyristor contactor. While a single-phase machine can be acceptable in terms of technology, its connection to the distribution network runs into problems. Thus, the rationality of investing additional means into purchase of a machine with a converter, should be analysed. Increasing the set power of the distribution network section may involve less expense.

CONCLUSIONS

1. Achievements in power semiconductor engineering open up great prospects for application of converters of frequency and phase number for resistance welding.

2. Evaluation of the advantages of applying a machine, fitted with a converter, should take into account not only the possible power effect, but also the process advantages, that can be provided by energy conversion.

3. Single-phase machines with thyristor contactors will still remain to be the most widely accepted, but the fields of their application will be limited to simple processing problems and relatively low power, the limiting value of which can be determined in each specific case, based on power supply conditions.

4. Machines, incorporating 30 Hz converters without valves in the welding machine secondary circuit, will become applied for resistance and flash-butt welding. These machines have both process and power advantages, compared to the simplest single-phase machines, and are superior to DC machines in efficiency and some other characteristics.

5. Converters with an intermediate higher-frequency unit should be applied in machines for spot and seam microwelding, and butt welding of thin strip. Converters of such a type with valves in the welding transformer secondary circuit are promising for machines, operating as part of robotic lines for producing items of coated steel and aluminium alloys, as well as machines designed for welding various extra thin-walled parts, including those with conducting coatings.

REFERENCES

1. Paton, B.E., Lebedev, V.K. (1969) *Electric equipment for resistance welding*. Moscow: Mashinostroyeniye.
2. Kuchuk-Yatsenko, S.I. (1992) *Flash-butt welding*. Kyiv: Naukova Dumka.
3. (1986) *Flash-butt welding of pipelines*. Ed. by S.I. Kuchuk-Yatsenko. Kyiv: Naukova Dumka.
4. Podola, N.V., Kuchuk-Yatsenko, S.I. (1957) Flash-butt welding by high-frequency currents. *Avtomaticheskaya Svarka*, **1**, 63 – 72.
5. Lebedev, V.K., Pismenny, A.A. (1998) Improvement of power systems for resistance welding machines. In: *Proc. of Int. Conf. on Welding and Allied Technologies into the XXI Century*. Kyiv: PWI.
6. Lebedev, V.K., Dubko, A.G. (1998) Improvement of the process of flash-butt welding of thin strip. *Avtomaticheskaya Svarka*, **11**, 48 – 50.
7. Lebedev, V.K. (1992) Effectiveness of application of DC machines for resistance welding. *Ibid*., **11/12**, 3 – 6.
8. Bokshtein, O.N., Kanin, A.M. (1976) *Equipment for DC resistance welding*. Leningrad: Energia.
9. Thamodharan, M., Beck, H.P., Wolf, A. (1999) Steady and pulsed direct current welding with a single converter. *Welding J*., **3**, 75 – 79.

current frequency of 30 Hz [5]. A quasisymmetrical operating mode is understood to be such a mode, in which the symmetrical load of the three-phase mains is recorded, on average, over three half-waves of low-frequency current. Deviations from symmetry were found within the same half-wave.

In terms of technology, machines with such a converter, have indubitable advantages, compared to a single-phase machine, as well as machines, fitted with a three-phase half-wave converter. When operating at 30 Hz frequency, one can use practically the same transformers, as in commercial frequency AC machines, because in the frequency range of 50 to 30 Hz, the machine short-circuiting impedance drops almost in proportion to frequency, and the voltage, required for welding, decreases.

A similar welding converter with a polarity switch, using bipolar transistors with an insulated gate, should be regarded as more perfect (Figure 8). Transistors, suitable for this purpose, already are available. However, the features of their operation in power circuits of welding converters of a rather high power, have not been sufficiently well studied, especially at welding current frequency below the mains frequency. Such a study could be aimed at frequency optimisation.

Such converters, using transistors that operate at a higher frequency, are especially promising for low-power machines. Given an appropriate control equipment, they provide welding current variation cycles that are the most favourable for producing the joint. By their process properties, machines with the above converters, are superior to widely accepted capacitor-type machines. Machines, fitted with converters, that are shown in Figures 7 and 8, will find an application also for butt welding, including thin strip [6].

Over the last decade, some companies developed resistance and flash-butt welding machines, with a three-phase group of transformers (Figure 9). Secondary windings of these transformers are connected to valves, that form a six-phase rectification system. The parts to be welded are heated by direct current. These machines are characterised by good process properties in resistance welding, which is described in information leaflets. We believe, that the processing effect is achieved chiefly due to minimal ripple of welding current. Application of direct current in flash-butt welding was studied in [7 – 9]. However, convincing evidence on process advantages of direct current application for this welding process is not available.

DC machines provide a symmetrical load for the AC mains phases, have a relatively high power factor and in this respect, are superior to other machine types with converters of frequency and phase number. They, however, have a very significant drawback of a low efficiency. So, in resistance welding of steel parts, the voltage drop on them is seldom more, than 1.5 V. The voltage drop across silicon valves in the machine secondary circuit during welding is approximately the same, or even higher. More power is removed with the cooling water, than is used for welding. Relative

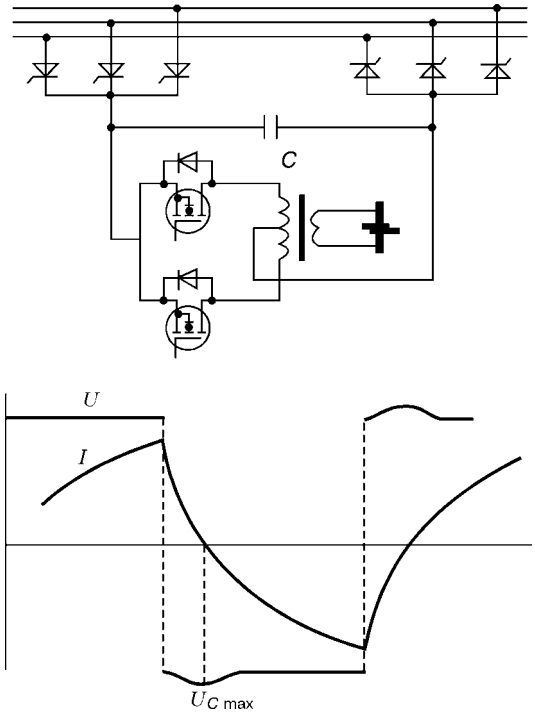

Figure 8. Converter with a higher frequency intermediate unit and polarity switch, using bipolar transistors: C — capacitor; $U_{C\,max}$ — maximal voltage of the capacitor

power losses are even higher in welding aluminium alloy parts.

In continuous flash-butt welding without resistance preheating, the losses in the valves are relatively lower, because of a higher resistance of the welding contact. Valves, however, create additional ohmic resistance, that affects flashing stability. Therefore, flashing is to be conducted at a higher voltage, thus leading to lower thermal efficiency, equipment efficiency and additional metal loss. In this connection, the rationality of applying DC machines for flash-butt welding is open to question.

A converter, shown in Figure 10, includes a rectifier, smoothing capacitor, inverter, converting direct current into alternating current of a higher fre-

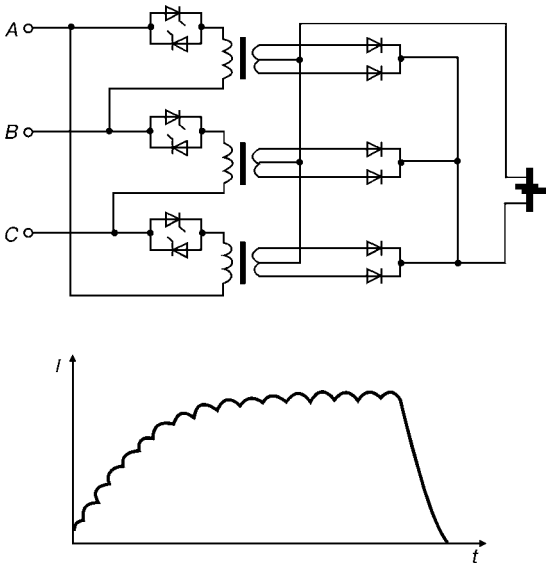

Figure 9. Power system for DC welding

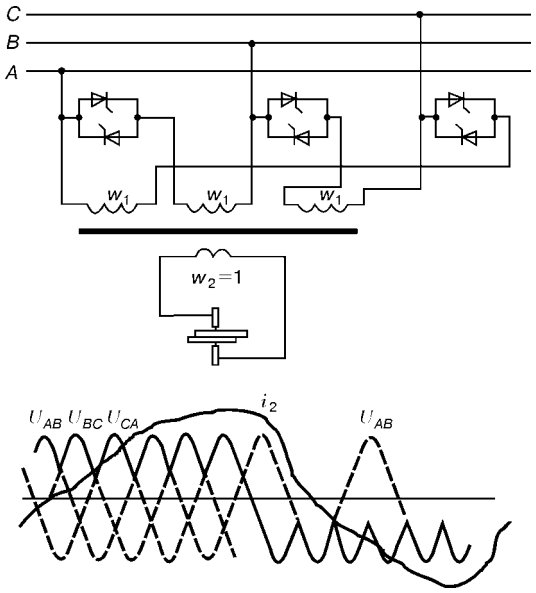

Figure 5. Converter of frequency and phase number: *A, B, C* — mains phases; w_1, w_2 — primary and secondary windings of welding transformer; i_2 — secondary current

The efforts of developers of this kind of electrical engineering equipment are currently focused on development of various converters, that is, without doubt, promoted by the progress in the field of power semiconductor devices. The devices considered below do not incorporate converters with energy storage, the most widely accepted of which are capacitor-type storages. Machines with such converters have good power characteristics, but are inferior to the machines with modern converters of frequency and phase number, as to their processing capabilities.

Application of rotary converters is sometimes necessary for energy storage and its subsequent pulsed application during welding. Study [3] reports the use of unipolar DC generators for supplying power to machines, designed for thousands of amperes. Self-sufficient welding machines of the type of rail- and pipe-welding machines, operated in the field conditions, are fitted with mobile electric power plants with commercial frequency three-phase generators. Only semiconductor converters of frequency and phase number are considered below, and machines fitted with such converters are compared with the simplest and most widely used single-phase machines (see Figure 4). In the general form, they can be compared by quality characteristics. Quantitative characteristics are determined not only by selection of a particular converter, but also by the actual modification of the machine.

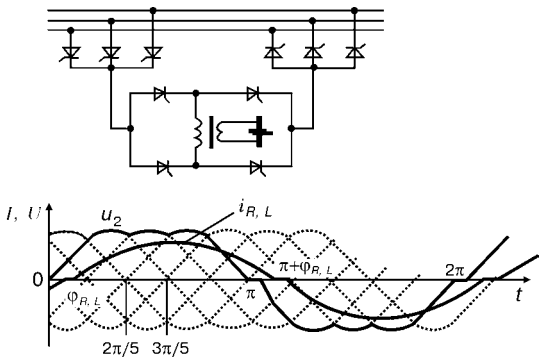

Figure 6. Converter of frequency and phase number with current polarity switch: u_2 — secondary voltage; $i_{R,L}$ — ohmic-inductive current value; $\varphi_{R,L}$ — phase shift in the case of ohmic-inductive load

One of the first converters of frequency and phase number was developed by Sciaky Company more than half a century ago (Figure 5). It also includes six thyristors (ignitrons), as well as a special transformer with three primary windings, designed for secondary current frequency of 5 Hz. Three thyristors operate in each low frequency half-period, that kind of simulate three-phase half-wave rectification of commercial frequency current in relation to the secondary circuit. Process advantages of a machine with such a transformer include:

- a much more sloping external characteristic due to a low frequency and low reactive voltage drop in the current-carrying secondary circuit;
- blunted secondary current shape, compared to the sinusoidal one.

Power-related advantages are as follows:

- sufficiently high power factor;
- practically uniform load in the three-phase distribution network;
- smaller power losses in massive secondary circuit elements, as a result of a more uniform current distribution in them.

A drawback of the machines is a cumbersome and heavy transformer [4], because of a very low frequency, which it would be rational to increase to a certain extent. However, other characteristics will become lower. Machines with such converters, designed for welding steel structures of sheets and profiles with up to 10 – 12 mm wall thicknesses, found only limited application. Use of arc welding is more advantageous for the above structures.

A fundamental difference of the converter, presented in Figure 6, consists in that its main elements are a three-phase full-wave rectifier and a standard two-winding transformer. Its disadvantage consists in that ten thyristors are required instead of six. Four complementary thyristors form the current polarity switch. A variant with a three-winding transformer and two (instead of four) complementary thyristors is possible (Figure 7). Full-wave rectification provides additional capability as regards frequency selection. Such a converter operates with good power characteristics in a quasisymmetrical mode at welding

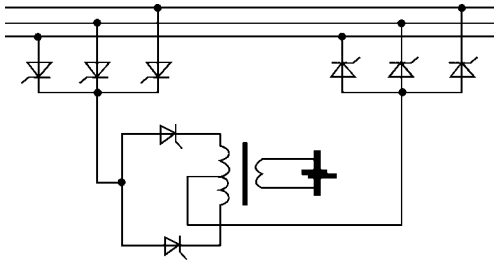

Figure 7. Variant of the converter (see Figure 6) with a reduced number of thyristors

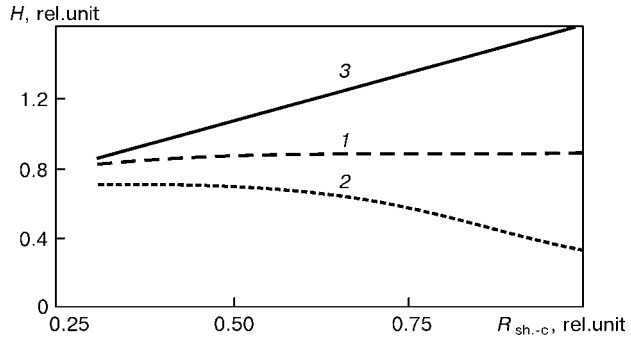

Figure 2. Dependence of height H_1 of spot nugget with a new electrode and H_2 with a worn electrode on short-circuiting impedance $R_{sh.-c}$: *1* — H_1; *2* — H_2; *3* — U

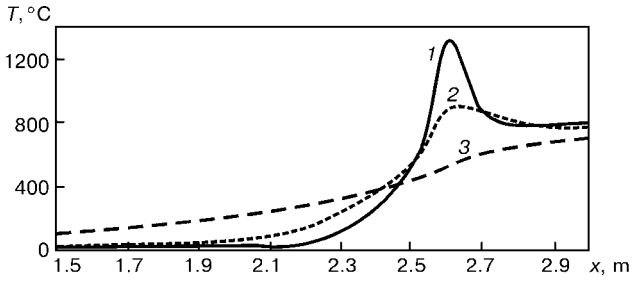

Figure 3. Temperature distribution in electrode–part contact, depending on current pulse duration at unchanged energy: *1* — 0.4; *2* — 2.0; *3* — 20.0 ms (x is contact length)

antee the minimal required nugget height with a worn electrode. The same is also true for shunting: the external characteristic shape still influences welded joint formation even with this disturbance.

There is no doubt, that electrode wear depends on the electrode–part contact temperature at the start of the welding process, when this contact has not yet formed, and the microcontacts have not deformed. Machine short-circuiting impedance also has its role: the lower it is, the lower the probability of overheating of the microcontacts with all its negative consequences.

Figure 3 shows the approximate distribution of temperature in the contact of a copper electrode with a steel part, where the surface layer is characterised by a higher resistance, as a result of the presence of films and surface roughness. Temperature distribution corresponds to the moment following the passage of current pulses of different duration, but the same energy, through the welding contact. The «softer» the pulse, the lower the temperature on the material interface. In this connection, overheating of this interface should be influenced by welding current ripple. Deep ripple can lead to melting of microvolumes with formation of alloys, differing by increased electrical resistance and increasing sticking of such an alloy to the electrode surface. Such a phenomenon is recorded in welding steels with anti-corrosion coatings, in particular zinc coating. If the electrode melting temperature is higher, than the melting temperature of the part metal, electrode metal transfer onto the welded joint surface is possible. For the case, when the electrode–part contact can be overheated, alternating current of commercial frequency is unfavourable. It is obvious, that the smaller the difference between the current amplitude and its root-mean-square value, the better.

The influence of other disturbances can be compensated, in part, by the automatic adjustment system, if it is sufficiently well-developed.

In flash-butt welding, the short-circuiting impedance, that determines the shape of the external characteristic, has a great influence on the stability of the process and its thermal efficiency This issue is described in detail in [1, 2] and is not considered here.

Any resistance welding machine with one pair of electrodes, is a single-phase machine (Figure 4), if it is not fitted with a special converter. Electrodes are connected to a transformer, that is connected to the mains by a thyristor contactor. A drawback of this type of machines consists in that they provide a non-uniform load for the three-phase distribution network. The current in the loaded phases is $\sqrt{3}$ times higher, that at symmetrical load of the same power. For this reason, the asymmetrical load leads to a greater voltage drop in the distribution network, this being detrimental for the radiation of the lighting fixtures. This impact is especially noticeable in connection with the intermittent cycle of welding equipment operation.

Asymmetrical load leads to distortion of the three-phase voltage star. Finally, in the electric mains, this gives rise to a three-phase voltage system with the reversed phase sequence, causing additional power losses in asynchronous motors. If the power of the single-phase welding machine is not more than 2/3 of the power of the distribution transformer, then, as shown by theoretical evaluation, these additional losses are not great, and hardly should be taken into account. Single-phase machines have a relatively low power factor, because of a considerable reactance in the machine secondary circuit. Power factor also lowers phase control of the thyristors. And one more drawback of all the resistance welding machines, related to intermittent operation cycle, necessitates development of distribution networks «with a margin».

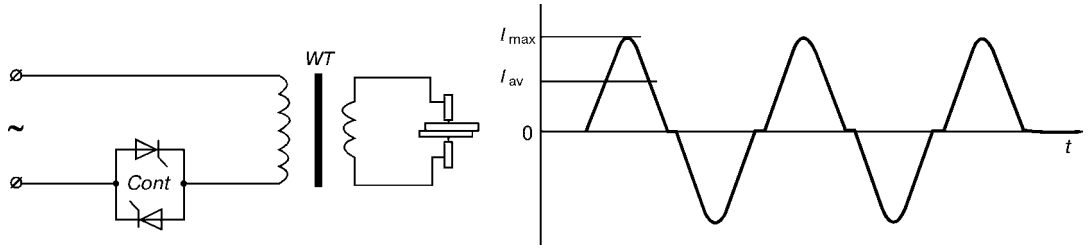

Figure 4. Power circuit of AC machine: *WT* — welding transformer; *Cont* — thyristor contactor; t — time

POWER SYSTEMS OF RESISTANCE WELDING MACHINES

V.K. LEBEDEV and **A.A. PISMENNY**
The E.O. Paton Electric Welding Institute, NASU, Kyiv, Ukraine

ABSTRACT

Power systems of resistance welding machines are analysed, including single-phase machines of commercial frequency and three-phase machines with converters of frequency and phase number. Qualitative comparison of seven power systems is performed in terms of their technological properties, influence of disturbances on the joint quality, electrode wear, as well as power characteristics.

Key words: *resistance welding, power systems, converters of frequency and phase number, DC machines, power characteristics*

Resistance welding is one of the most widely spread methods of joining metals, applied in automotive industry and instrument making, production of diverse appliances, control, measurement and communication systems, metal mesh and frames, construction and repair of railway tracks, as well as many other areas. Resistance welding is used to make products of steels and non-ferrous metal based alloys. Thickness of parts that can be joined by spot welding, varies from several microns up to several millimeters, and in butt welding the joint cross-sectional area varies from several fractions to hundred thousand square millimetres. Therefore, resistance welding equipment is highly diverse, both as to its design, and as to its power and overall dimensions.

Considered below are the features of power systems in resistance welding machines, that determine their power characteristics and to a great extent also their process properties.

When selecting a power system, it is necessary to determine, whether an optimal welding mode can be reproduced, using a particular system, and which of them enables doing it in the simplest and the most reliable manner. As regards such pulsed processes, as resistance spot, projection or seam welding, the goal here should be the minimal required process time and possibility of reproducing the most suitable current cycle. But even that is insufficient — it is also necessary to analyse the possible influence of disturbances, arising during welding, on the joint quality.

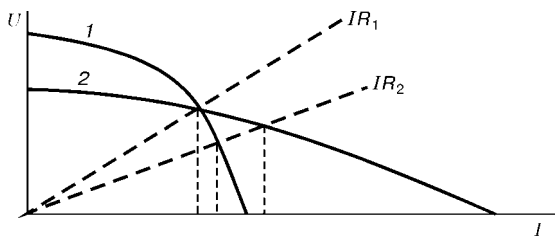

Figure 1. External characteristic of resistance welding machines and voltage drop across the welding contact ($R_2 < R_1$); *1, 2* — flat and sloping characteristics

In resistance welding of parts from metal sheets, the main disturbances are as follows:

- electrode wear, leading to greater of the electrode–part contact surface;
- bridging of welding contact by the earlier welded spots or random contacts;
- mechanical shunting by the earlier welded spots, hindering formation of the welded contact; a similar effect can be also produced by inaccurate fit-up;
- mains voltage fluctuation;
- item surface contamination or their poor preparation for welding;
- electrode surface contamination.

The influence of a number of disturbances on the joint quality is largely related to the external characteristic (Figure 1), the shape of which depends not only on the machine short-circuiting impedance, but also on the power system, primarily, on welding current frequency. The features of the power system to a certain extent determine also the conditions at the electrode–part interface, that are responsible for the operational stability of the electrodes.

The most probable disturbance is electrode wear, leading to lowering of the welding contact resistance, as well as current rise, which is the higher, the more sloping is its external characteristic. As a result, the probability of incomplete penetration becomes smaller, when machines with more flat external characteristics are used. In practice, welding modes with a greater margin are often selected to avoid this kind of defects. This, however, results in extra power consumption.

Figure 2 shows dependencies of the weld spot nugget height H on the machine short-circuiting impedance, $R_{sh.-c}$. Voltage is selected to be such as in welding with an unworn electrode and then remains constant. Height H_1 refers to the new electrode, and H_2 — to the electrode, in which the contact surface diameter is increased by 20 % through wear. As is seen, lowering of the short-circuiting impedance is favourable for dimensional stability of the welded spot cast nugget. There is no need to apply additional energy to guar-

Taking into account all parameters for experimental electrodes

$$[\%CIP]_{max} = \frac{0.12 - \frac{5.2[Mn]}{[\%\ ilm]}}{0.006}. \quad (16)$$

Results of calculation $(\%CIP)_{max}$ using formula (16) are given in Figure 2, *b*.

To check the calculation method of determination of equilibrium content [C] and [Mn] and maximum possible adding of cast iron (at different mass fractions of ilmenite in coating) the real content of carbon and manganese in the deposited metal of experimental electrodes, containing 5, 10 and 15 % of CIP, 30 – 60 % ilmenite and 15 % FeMn in the coating, was established. The results of chemical analysis of experimental deposits are given in Figure 3.

The data obtained show that at similar mass fractions of FeMn and cast iron powder in the coating the content of [C] and [Mn] are changed depending on the oxidizing ability of the coating, determined by the amount of ilmenite, thus confirming the validity of the given calculation method.

Thus, with use of the calculation method it is possible to establish the optimum content of cast iron powder in the coating depending on its oxidizing ability, determined by the content of ilmenite at different adding of FeMn or preset content of [Mn]. The feasibility of calculation of equilibrium content of [C] depending on the content of ilmenite and FeMn in the coating, and also [Mn] in the deposited metal was also obtained.

CONCLUSIONS

1. The feasibility of use of carbon in the fixed state (in the form of a ferro-carbon alloy) was established as a deoxidizer and the validity of calculation method for determination of its maximum content in the coating of the ilmenite-type electrodes was confirmed.

2. Method of calculation of equilibrium content of [C] and [Mn] has been developed, which makes it possible to determine the allowable amount of carbon in the form of cast iron powder in electrode coatings at different mass fractions of ilmenite, FeMn and [Mn].

REFERENCES

1. Efimenko, N.G., Kalin, N.A. (1978) Oxidizing ability of rare-earth metals in comparison with known deoxidizers. *Svarochnoye Proizvodstvo*, **10**, 3 – 4.
2. Alov, A.A. (1947) *Electrodes for arc welding and surfacing*. Moscow: Mashgiz.
3. Penkov, V.B., Potapov, N.N., Kakovkin, O.S. (1990) Estimation of metallurgical role of FeO in the development of electrodes for manual arc welding. *Svarochnoye Proizvodstvo*, **10**, 38 – 39.
4. Lyubavsky, K.V. (1961) *Metallurgy of fusion welding*. Moscow: Znanie.
5. Kazachkov, E.A. (1978) *Calculations on the theory of metallurgical processes*. Moscow: Metallurgia.
6. Medzhibozhsky, M.Ya. (1986) *Fundamentals of thermodynamics and kinetics of steel melting processes*. Kyiv-Donetsk: Vyshcha Shkola.
7. (1974) *Technology of electric fusion welding of metals and alloys*. Ed. by B.E. Paton. Moscow: Mashinostroyeniye.
8. Petrov, G.L. (1972) *Welding consumables*. Leningrad: Mashinostroyeniye.
9. Erokhin, A.A. (1973) *Fundamentals of fusion welding*. Moscow: Mashinostroyeniye.

FUNCTIONAL AND TEST DIAGNOSTICS OF WELDING EQUIPMENT

A.E. KOROTYNSKY

The E.O. Paton Electric Welding Institute, NASU, Kyiv, Ukraine

ABSTRACT

The paper deals with the problems of orginizing a diagnostic support of welding equipment. Procedures of functional diagnostics of inverter and resonance arc welding sources are described. It is shown that the resonance arc welding sources require test temperature diagnostics of the capacitance reactor condition. Procedures with a partial and complete diagnostics of the latter are presented. Also considered is a scheme of the resonance source with a functional-test diagnostics.

Key words: *arc welding, functional and test diagnostics, scheme of built-in control*

Technical diagnostics of control is one of the most important trends in improvement of effectiveness and quality of service of the welding equipment. Its application increases significantly the repair intervals, prevents timely the failures and, thus, reduces considerably the labour consumption and expenses for the technical maintenance and repair.

The assurance of high characteristics of quality and reliability of the welding equipment requires the use of many measures, connected with the selection and training of electronic components, separate units and completed functional blocks, as well as selection of mild conditions of their operation. However, even the above-mentioned measures make not it possible to reach the high safety level.

$$[\%C] = \frac{13.7[Mn]}{K_{tr}^{Mn} K_{c.m} [Mn]_{FeMn} [\% \text{ ilm}]}. \quad (13)$$

Based on numerous experiments it was established that K_{tr}^{Mn} in the ilmenite-type electrodes is on average 0.07. In accordance with equation (13) and using definite values of K_{tr}^{Mn}, $K_{c.m}$, $[Mn]_{FeMn}$, we shall obtain the calculation formula for determination of $[\%C]_{eq}$ in electrodes of the experimental batch:

$$[\%C]_{eq} = \frac{5.2[Mn]}{[\% \text{ ilm}]}. \quad (14)$$

Results of calculation by formula (14) are given in Figure 2, *a*. The content of [Mn] is assumed to be within 0.5 – 0.7 % which is typical of the ilmenite-type electrodes.

Calculation of adding the maximum possible fractions of cast iron powder into the composition of the electrode coating at a preset content of [Mn] and keeping conditions $[\%C] \le 0.12$ %, is performed by expression (10) using formula (13):

$$[\%CIP]_{max} = \frac{0.12 - \dfrac{13.7[Mn]}{K_{tr}^{Mn} K_{c.m} [Mn]_{FeMn} (\% \text{ ilm})}}{K_{tr}^{C} K_{c.m} \dfrac{[C]_{CIP}}{100}}. \quad (15)$$

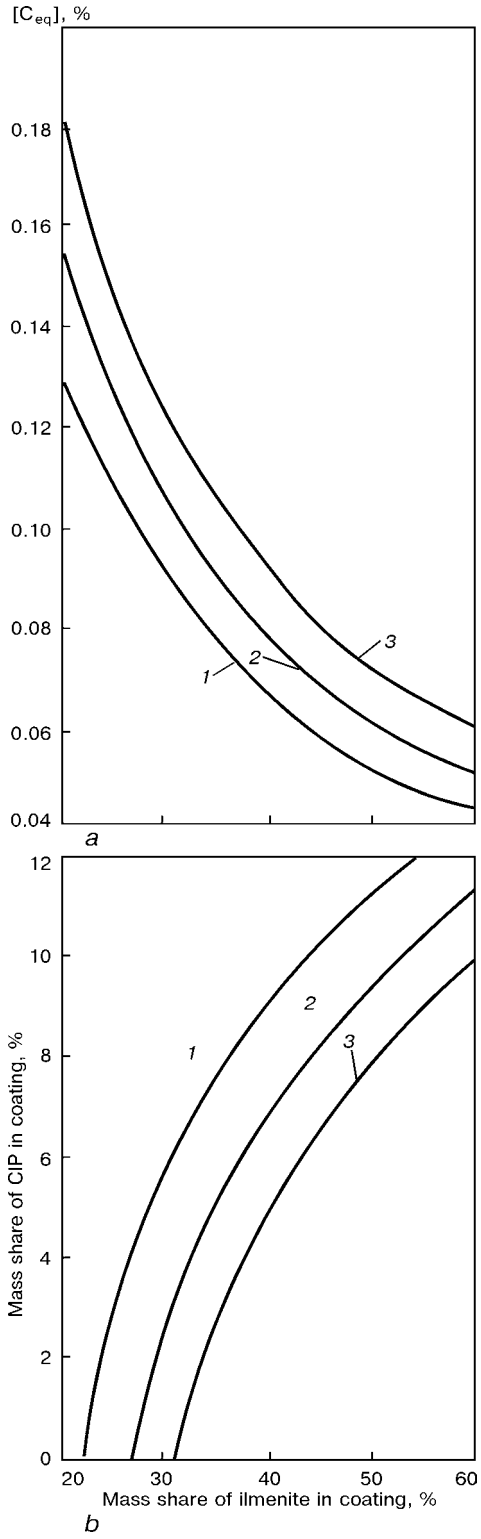

Figure 2. Dependence of equilibrium content of carbon in the deposited metal (*a*) and maximum content of cast iron powder in coating (*b*) on mass fraction of ilmenite in coating at different concentrations of manganese in the deposited metal: *1* — 0.5; *2* — 0.6; *3* — 0.7 %

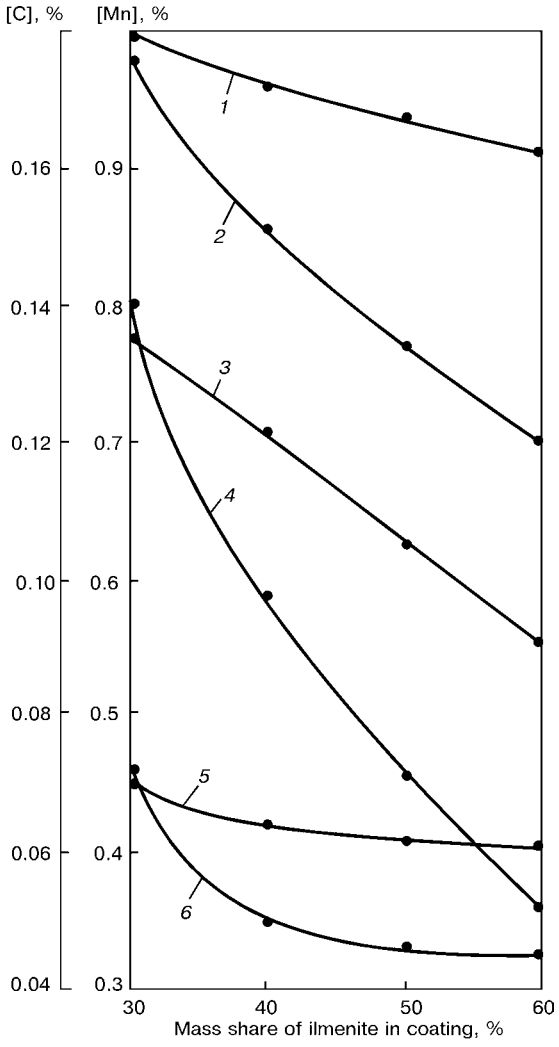

Figure 3. Dependence of content of carbon and manganese in the deposited metal on the ilmenite amount in coating at different mass fractions of CIP and 15 % FeMn: *1, 3, 5* — [Mn]; *2, 4, 6* — [C] at 15, 10 and 5 % of CIP, respectively

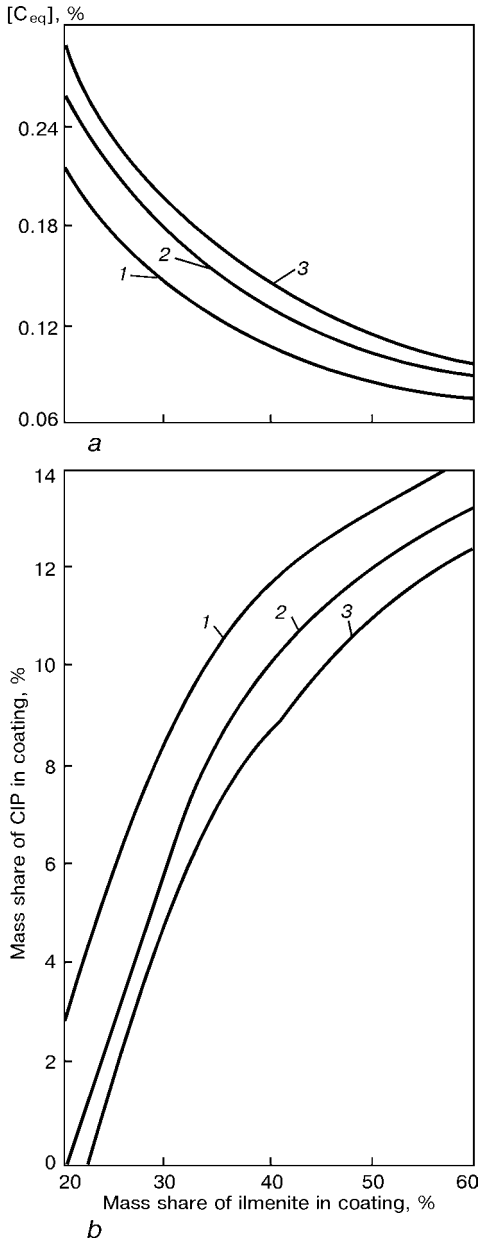

Figure 1. Dependence of equilibrium content of carbon in the deposited metal (*a*) and maximum content of cast iron powder in coating (*b*) on mass fraction of ilmenite in coating at different amount of FeMn: *1* — 15; *2* — 18; *3* — 20 %

$$[\%C]_{eq} = \frac{[\%Mn]f_O^{Mn}}{K_C K'_{Mn}}. \quad (6)$$

Changing [%Mn] in equation (6) by expression (2) we shall obtain

$$[\%C]_{eq} = \frac{(\%MnO)f_O^{Mn}}{(\%FeO)K_{Mn} K_C K'_{Mn}}. \quad (7)$$

Calculation of parameters f_O^{Mn}, K_{Mn}, K_C, K'_{Mn} at the moment of solidification at temperature 1810 K gives $f_O^{Mn} = 0.97$, $K_{Mn} = 4.055$, $K'_{Mn} = 0.00845$, $K_C = 519$.

Substituting values of the mentioned parameters to formula (7), the equation for the calculation of dependence of the equilibrium carbon content in the deposited metal on the ratio of manganese and iron ratio in slag will take a form

$$[\%C]_{eq} = 0.054 \cdot 5 \frac{[\%MnO]}{[\%FeO]}. \quad (8)$$

In practical calculations of compositions of electrode coatings it is more convenient to use components, used in the electrode manufacture. As a result of recalculation of oxides of manganese and iron in FeMn (80 % Mn) and ilmenite (40 % FeO) we shall obtain formula for calculation $[\%C]_{eq}$ depending on the content of FeMn and ilmenite in the coating of electrodes, taking into account the coating mass factor $K_{c.m}$.

$$[\%C]_{eq} = 0.137 \frac{[\%FeMn\ ]}{K_{c.m}[\%\ ilm]}. \quad (9)$$

Calculation $[\%C]_{eq}$ by formula (9) for variants of experimental electrodes taken for the experiment is given in Figure 1, *a*. Here, FeMn is taken in mass fractions 15, 18 and 20 % which are most often used in electrodes of the ilmenite type.

Taking into account that the carbon content in deposited metal of the ilmenite-type electrodes should not exceed 0.12 % [7], we shall obtain the equation for calculation of maximum amount of cast iron powder in the composition of coating in accordance with [8]

$$[\%CIP]_{max} = \frac{0.120 - 0.137 \dfrac{[\%FeMn]}{[\%\ ilm]}}{K_{tr}^C K_{c.m} \dfrac{[C]_{CIP}}{100}}, \quad (10)$$

where K_{tr}^C is the coefficient of carbon transfer, taken equal to 0.37 [9] for ilmenite-type electrodes; $[C]_{CIP}$ is the carbon content in CIP, %.

Substituting definite values of K_{tr}^C, $K_{c.m}$ and $[C]_{CIP}$ for the variants of electrodes investigated to formula (10) we shall find estimated relation

$$[\%CIP]_{max} = \frac{0.120 - 0.137 \dfrac{[\%FeMn]}{[\%\ ilm]}}{0.006}. \quad (11)$$

Results of calculation using formula (11) are given in Figure 1, *b*.

Similar calculations depending on the content of manganese in the deposited metal at a preset its concentration present a practical interest.

The content of FeMn in the coating of electrodes is as follows:

$$[\%FeMn] = \frac{[Mn]}{K_{tr}^{Mn} K_{c.m} [Mn]_{FeMn}} \cdot 100, \quad (12)$$

where K_{tr}^{Mn} is the coefficient of manganese transfer; $[Mn]_{FeMn}$ is the mass fraction of manganese in FeMn.

The content of $[\%C]_{eq}$ will be calculated using expressions (9) and (10):

CALCULATION OF OPTIMUM CONTENT OF CARBON AND MANGANESE IN ELECTRODE ILMENITE-TYPE COATINGS

N.G. EFIMENKO and **N.A. KALIN**
Ukrainian Engineering-Pedagogical Academy, Kharkov, Ukraine

ABSTRACT

Use of carbon in the composition of the ferro-alloy, in particular cast iron, as a deoxidizer in welding ilmenite-type electrodes is suggested. The method of calculation of equilibrium content of carbon and manganese in the deposited metal has been developed that makes it possible to determine the maximum admissible amount of carbon, added with a cast iron powder into the electrode coatings at different shares of ilmenite, FeMn and [Mn].

Key words: *electrode coating, slag, carbon, cast iron powder, deoxidizing ability, equilibrium content, manganese, oxygen*

The use of carbon as a deoxidizer in welding electrodes presents a practical interest, because it is readily available. At the welding arc temperature of more than 2800 K the carbon is the most active deoxidizer, capable to recover oxides of all known elements [1].

However, the use of carbon in a free state [2, 3] requires increase in an oxidizing potential of the coating for its complete oxidizing that deteriorates the welding-technological properties of the electrodes.

The aim of the present work is to study the feasibility of using the fixed carbon (in the form of a ferro-carbon alloy) as a deoxidizer for the electrode coatings of the ilmenite type.

For investigations the 4 mm diameter electrodes on wire Sv-08A (C — 0.1; Si — 0.03; Mn — 0.35 – 0.65 wt.%; Fe — balance) were manufactured using the extrusion method. A cast iron powder (CIP), containing 3.5 % C, was used as a ferro-carbon alloy. The coating mass factor $K_{c.m}$ of electrodes was 0.47. The FeMn content varied within the range of 15 – 20 %, while that of ilmenite concentrate was 30 – 60 % at 5, 10 and 15 % mass fraction of the CIP. To define the amount of carbon and manganese in the deposited metal the surfacing was performed at DCRP (160 – 180 A) in accordance with GOST 9466–60.

To compare the deoxidizing ability of carbon and manganese in each concrete case it is necessary to calculate their equilibrium content in the deposited metal, which is determined by a similar residual mass fraction of oxygen in the molten iron, being deoxidized by these elements at the moment of solidification:

$$[\%O]^{C}_{eq} = [\%O]^{Mn}_{eq}. \quad (1)$$

The residual content of manganese in metal is calculated using equation given in [4]:

$$[\%Mn] = \frac{[\%MnO]}{K_{Mn}\,[\%FeO]}, \quad (2)$$

where [%MnO], [%FeO] are the mass fractions of oxides of manganese and iron in slag, %; K_{Mn} is the constant of equilibrium of reaction which is calculated by equation $\lg K_{Mn} = (6440/T) - 2.95$.

Equilibrium concentration of oxygen in metal, deoxidized by manganese, is determined by formula given in [5]:

$$[\%O]^{Mn}_{eq} = \frac{K'_{Mn}}{[\%Mn]\,f^{Mn}_{O}}, \quad (3)$$

where K'_{Mn} is the constant of equilibrium of deoxidation reaction, calculated by formula $\lg K'_{Mn} = (-15065/T) + 6.25$; f^{Mn}_{O} is the coefficient of oxygen activity determined by formula $\lg f^{Mn}_{O} = e^{Mn}[\%Mn]$.

Carbon containing in drops of the electrode metal and transferring to them from the cast iron powder, is oxidized by oxygen, being dissolved in molten iron or available in it in the form of oxides, and also at metal interaction with slag and oxygen-containing gases of the arc atmosphere at the metal–slag and metal–gas interface.

To calculate the equilibrium content of oxygen in metal deoxidized by carbon (C = 0.02 – 2.00 %), and a partial pressure CO in the gas phase, equal to the atmospheric pressure, the expression given in [6] is used:

$$[\%O]^{C}_{eq} = \frac{1}{K_{C}\,[\%C]}, \quad (4)$$

where K_C is the constant of equilibrium of carbon oxidation, determined by formula $\lg K_C = (1160/T) + 2.01$.

Substituting equations (3) and (4) to (1) we shall obtain

$$\frac{1}{K_{C}\,[\%C]} = \frac{K'_{Mn}}{[\%Mn]\,f^{Mn}_{O}}, \quad (5)$$

hence, the equilibrium carbon content is equal to

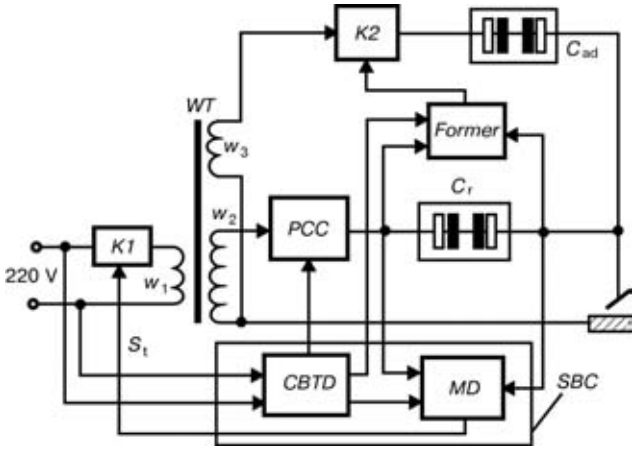

Figure 3. Scheme of complete test diagnostics of capacitance reactor of the resonance welding source

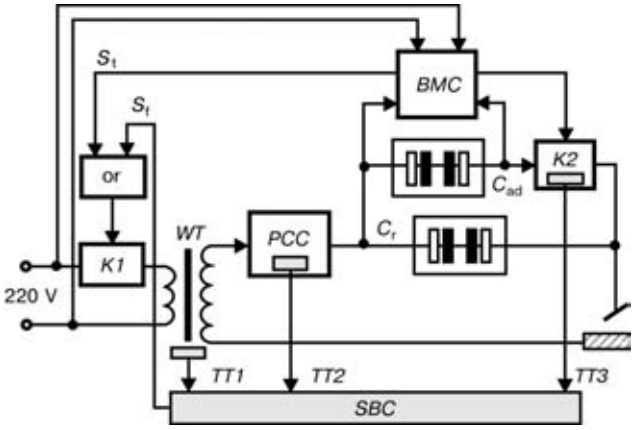

Figure 4. Scheme of functional-test diagnostics of the resonance welding source

The drawback of schemes with an indirect temperature diagnostics is the fact that, here, the operating life of the main reactor is predicted by the results of control of the additional reactor operation. It is more desirable to use the welding units with a full temperature diagnostics of the main reactor, whose idea of operation is as follows.

Let us consider the scheme of the resonance welding source (Figure 3), whose secondary circuit is made according to a two-circuit diagram. The main circuit includes a winding w_2, *PCC* and reactor C_r. The additional circuit is made on winding w_3 which with the help of key *K2*, being controlled by a *Former*, is connected to the additional reactor C_{ad}. In this circuit a base current 15 – 20 A is formed during one period when the main circuit is switched off. The algorithm of *SBC* operation is preset by a control block of the temperature diagnostics *CBTD*. Procedures, realized by this unit, are as follows:

- first the block *PCC* is locked and the main welding current passing in the circuit of the main reactor is interrupted;
- reactor C_r is charged until voltage U_0 = const;
- then, C_r is discharged through a reference resistance R_0 (constant of time of discharge circuit is equal to $t_d = C_r R_0$);
- a definite threshold $U_{dis} = \lambda U_0$, is set in a discriminator of the measuring device *MD* similar to the described device. When this threshold is attained a single-vibrator is operated forming a pulse whose duration is associted functionally with a value of the controllable capacitance of the reactor.

Therefore, the algorithm of the temperature diagnostics of the main reactor C_r can be obtained from formula (3) taking into account that $k_h = 1$, i.e.

$$t_d = R_0 [C_r(1 + \alpha T_{adm})]. \quad (4)$$

In accordance with (4) a signal is generated at exceeding the admissible temperature in *MD* which closes key *K1* and the welding machine is disconnected from the mains.

The resonance welding sources with a functional-test diagnostics can be manufactured, for example, on the base of combination of scheme solutions, presented in Figures 1, *b* and 2, *a*. In one of the feasible variants of such unit, given in Figure 4, the functional diagnostics is performed using *SBC*, and the temperature testing is realized by *BMC* in the condition of the indirect control. As a result, the signals S_f and S_t are formed by these blocks. The disjunction of signals defines the function of diagnostics:

$$F_d = S_f \vee S_t, \quad (5)$$

where $S_f = x_1 \vee x_2 \vee x_3$.

Similarly, the scheme of a resonance welding machine with a functional-test diagnostics can be made, in which the temperature test is realized in the conditions of a complete diagnostics. However, the scheme-technical solution of the power block should be selected so that to provide pauses in its operation during which the testing could be performed. As our experience showed, the resonance welding sources with a discrete-time adjustment of the welding current are suitable for this purpose [8]. In this case, the pause duration of not less than one period of mains frequency ($t_{meas} \geq 20$ ms) is quite sufficient for conductance of all the procedures of the complete temperature testing.

It should be noted in conclusion that the problems of the diagnostic support of the modern welding equipment should be solved in parallel with the development of the power units and blocks of control of the power sources. This will make it feasible to increase their safety and service life.

REFERENCES

1. Parkhomenko, P.P., Sogomonyan, E.S. (1981) *Fundamentals of technical diagnostics*. Moscow: Energia.
2. Sogomonyan, E.S. (1972) Principles of construction of systems of functional diagnosis of technical condition of complex objects. *Voprosy Sudostroyeniya*, Series 5, Issue 1.
3. Kolchin, A.V. (1984) *Transducers of systems for diagnostics of machines*. Moscow: Mashinostroyeniye.
4. Sogomonyan, E.S. (1968) About one approach to the problem of construction of tests. *Avtomatika i Telemekhanika*, **10**, 137 – 146.
5. Korotynsky, A.E. (1996) Automated bench for testing welding equipment. *Avtomaticheskaya Svarka*, **12**, 21 – 24.
6. Savchenko, Yu.G., Svistelnik, A.A. (1987) *Methodological bases of creation of diagnostic support of ACS*. Kyiv: Znaniye.
7. Skobelev, O.P. (1980) Methods of transformation of information on the basis of test transition processes. *Izmereniye, Kontrol, Avtomatizatsiya*, **1/2**, 11 – 17.
8. Korotynsky, A.E. (2000) Discrete-time control of welding current in power sources of LC type. *The Paton Welding Journal*, **6**, 42 – 44.

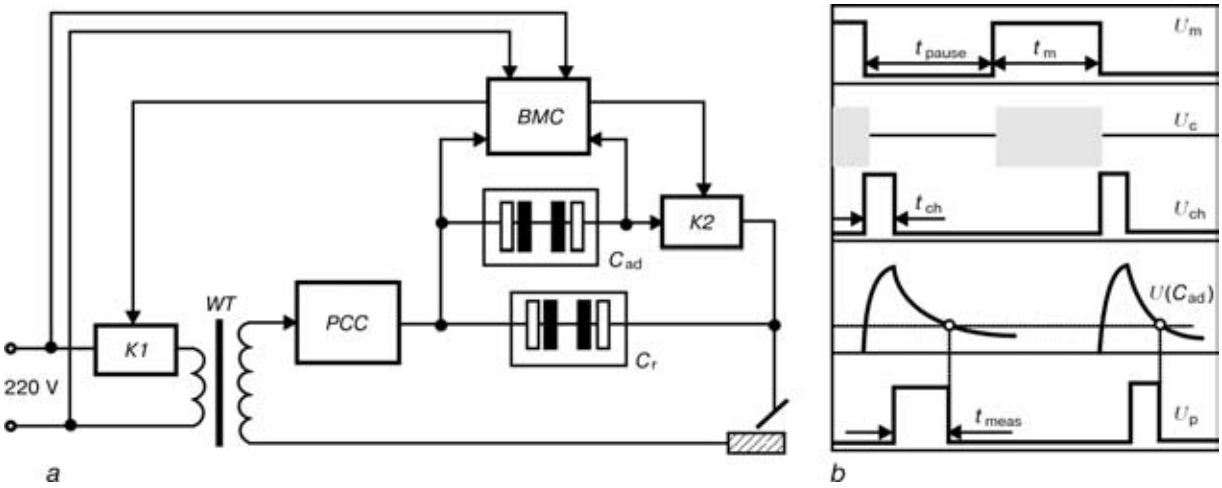

Figure 2. Scheme of test diagnostics of resonance welding source (*a*) and time diagram of its operation (*b*): U_m — voltage of modulation; U_c — voltage at additional circuit; $U(C_{ad})$ — voltage at capacitance discharge; U_p — voltage of measuring pulse

$$F_d = x_1 \vee x_2 \vee x_3 \vee x_4 \vee x_5,$$

where x_1, x_2, x_3, x_4, x_5 are the output signals of appropriate transducers, which are equal to 0 within the operating conditions and 1 — beyond the allowances.

Therefore, it is enough for one of the transducers to come out of order, that F_d will become equal to 1. In this case a signal is formed at the *SBC* output, which switches off *HFC* via *CU* and, consequently, the welding machine as a whole.

Somewhat another scheme is used for the functional diagnostics of resonance welding sources with a smooth adjustment of the welding current (Figure 1, *b*). Here, only three thermoelectric transducers are used for the thermal diagnostics, which are mounted directly on the secondary winding of the welding transformer *WT*, on the radiators of triacs, included into the composition of the phase controller of welding current *PCC*, and on the capacitance reactor C_r. The function of diagnostics for the given device is written in the form of $F_d = x_1 \vee x_2 \vee x_3$. When 1 is appeared at the *SBC* output the key *K* is closed and the welding device is disconnected from the mains.

However, the described diagram of diagnostics of the resonance welding machines is characterized by one essential drawback which consists in complexity and ambiguity of heat control of capacitance reactors. This is due to the fact that the reactor consists of a large number of separate capacitors whose characteristics can be essentially different. Depending on the capacity of the power source the number of these capacitors can be from 16 to 42. It is naturally, that the functional diagnostics of their condition requires the similar quantity of transducers, and this complicates *SBC* significantly. In addition, using this approach it is possible to control only the surface temperature of the capacitors that does not always correspond to the reality. It is possible to apply another approach, i.e. to distinguish a group of capacitors (additional reactor C_{ad}), with the help of which to perform the modulation of the welding current, as is shown in Figure 2, *a*. This not only improves the welding-technological properties of the source, but will also make it possible to control the change in capacitance C_{ad} in the pauses of the modulated action t_{pause} using the method of a rated discharge [7]. And it is important that in this case the inner temperature of the reactor C_{ad} will be estimated.

The algorithm of diagnostics is realized as follows. With the help of the key *K2* the reactor C_{ad} is connected periodically in parallel to the main reactor C_r for the period of a modulating action t_m, during which its heating occurs. Then, during pause (Figure 2, *b*) C_{ad} is charged to the voltage U_{ch} = const. Then, it is discharged through the resistance R_0 until some preset level — λU_{ch}. If to select $\lambda = 0.373$, then it is possible to write

$$t_{meas} = R_0 C_{ad}(T) = R_0 [C_{ad0}(1 + \alpha T)], \qquad (2)$$

where t_{meas} is the time of measurement; $C_{ad}(T)$ is the capacitance depended functionally on temperature; C_{ad0} is the initial value of capacitance at room temperature; α is the temperature coefficient of capacitance. If to come to the time representation, then the expression (2) can be presented in the form of

$$t_{meas} = t_0 + \Delta t\ (T).$$

Then the admissible time of C_{ad} reactor can be found from inequality

$$t_{adm} \le t_0 + \Delta t(T_{adm}).$$

As the reactor C_{ad} operates in a mild temperature condition, as compared with C_r, then its coefficient of heat load k_h can be preset by the expression

$$k_h = t_m/(t_m + t_{pause}).$$

Consequently, the predicted time of operation of the main reactor, when the condition of a safe operation is ensured, should be reduced by k_h times, i.e.

$$t_d = t_{meas} k_h = R_0 [C_{ad0}(1 + \alpha T_{adm})] k_h. \qquad (3)$$

The expression (3) is the algorithm of an indirect temperature diagnostics of the resonance welding source. It is realized by a block of measurement and control (*BMC*), in which a reference pulse of duration t_0 is formed in each cycle of measurement. At $t_d \ge t_0$ *BMC* a signal is generated which locks the key *K1* and, thus, disconnects the power source from the mains.

This problem can be solved radically only by the development of built-in systems of diagnostics of technical condition of either of all or the critical units in the welding equipment which are subjected to the most loaded state. There is a complete or partial diagnostics [1]. The complete diagnostics is usually used for complicated technical complexes, whose failure can lead to the serious consequences. The partial diagnostics is used for separate most critical units, therefore, it is more preferable in welding manufacturing.

In complex technical systems the methods of functional or test diagnostics are realized depending on their purpose [2]. In the welding equipment, as will be shown below, it is rational, sometimes, to use a combined approach, i.e. creation of systems of functional-test diagnostics. In the systems of a functional diagnostics (SFD) no special signals are fed to the welding machine blocks and units. In this case the welding equipment is functioning in the conditions which are preset by its working algorithm, and the SFD is used only for control of the correctness of operation of its separate units, finding of their parameters in the zone of the set allowances, and also revealing the elements and units which are beyond the admissible deviations.

The hardware of SFD is, as a rule, incremental transducers [3], mounted in the controllable points of separate blocks and units, whose outputs are connected to the block of a logic output. The combination of the mentioned hardware is accepted to call schemes of a built-in control (*SBC*). During recently a large attention is paid to the problems of development and creation of self-checking *SBC*, i.e. schemes which detect not only the faults of the objects being controlled, but also the own errors. However, their practical realization requires the obligatory adding of computational units, equipped with appropriate sensors, into the welding equipment.

When developing the test diagnostics systems (TDS) [4], the mathematical models of troubles of selected units are used. In *SBC* the transducers are used not of a relay type, but those which operate within the wide range of changing the controllable signals. As the test diagnostics is usually made at a disconnected block, then it is rationally to use it in welding equipment with a redundancy. In devices with a modulation (PLM-controllers) and periodic action the test diagnostics can be realized at the moments of pauses, however, this requires the use of quick-response measuring units. In some cases the continuous test diagnostics can be made at higher frequencies. As an example, a temperature test of the welding transformer by changing the inner resistance of the winding can be illustrated when its value is determined at sufficiently high frequencies, exceeding 50 Hz by many times [5].

Let us consider the statement of the problem of a functional diagnostics of the welding equipment. The management of system of the welding equipment diagnostics is started with a distinguishing of separate components in its structure, for which the fields of admissible parameters are established. In literature they are called changeable blocks [6]. From the technical point of view the welding machine can be presented by a set E, whose elements are some collection of sound e_0 and unsound e_1 conditions. Usually, such parameter is preset as a depth of diagnostics, g, which determines the subdivision of set E into several nonintersecting subsets E_j ($j = 1, 2, \ldots, g$). These subsets describe naturally the technical condition of changeable blocks of the welding machine.

If to assume that the transducers with a relay characteristics are used for diagnostics, when 0 corresponds to the sound condition of the block and 1 — to the unsound block, then their disjunction can be determined by the expression:

$$F_{\text{d}} = x_1 \vee x_2 \vee \ldots \vee x_g. \qquad (1)$$

$$F_{\text{d}} = 0 \text{ at } x_1 = x_2 = \ldots = x_g = 0,$$
$$F_{\text{d}} = 1 \text{ at } x_j = 1.$$

In expression (1) the function of diagnostics F_{d} is determined, which is equal to 0, if all the signals are equal to 0, and becomes equal to 1, if at least one of the signals is equal to 1.

Let us consider the realization of the function of diagnostics in a disjunctive form for a welding inveter and a resonance source (Figure 1).

The modular design of a classic inverter, designed for welding with rod electrodes, consists of a high-voltage rectifier *HVR*, a filter *F*, a high-frequency converter *HFC*, a welding rectifier *Rect* with a choke *Ch* at the output and a control unit *CU*. Usually in this class of devices a heat state of the distinguished blocks is controlled. This control is most often performed using bimetal thermoelectric transducer *TTj* with a relay output characteristic. The latter are mounted in points of a maximum heat generation (radiators of rectifying diodes and transistor switches — *TS*, as well as on ferritic magnetic cores of the transformers *Tr — HFC*), and their outputs are connected to a diagram of the built-in control. *SBC* hardware realizes the function of diagnostics in the form of a disjunction of input signals *TT1 – TT5*

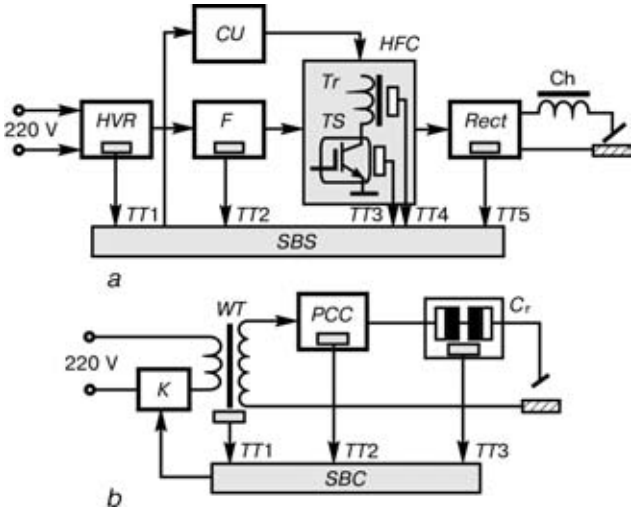

Figure 1. Schemes of functional diagnostics of welding inveter (*a*) and resonance welding source (*b*)

Results of tests of the metal deposited by the submerged-arc hard-facing method using wires Sv-08A and Sv-10GN and flux ZhSN-5, as well as strip 18Kh3GMFA and flux AN-60

Property of deposited metal	*Type of deposited metal (hard-facing consumable)*		
	18KhMFS (Sv-08A, flux ZhSN-5)	*22Kh6MFN (Sv-10GN, flux ZhSN-5)*	*18Kh3GMF (18Kh3GMFA, flux AN-60)*
Wear, mg	26.5 – 30.1	22.3 – 26.0	36.7 – 40.3
Heat resistance (number of heating-cooling cycles to formation of a visible crack)	1230 – 1320	890 – 1020	1510 – 1590
Hardness at 20 °C, *HRC*	38 – 39	41 – 42	32 – 36
Hardness at 500 – 550 °C, *HRC*	27 – 30	26 – 29	26 – 30
Index of technological strength, mm/min	11.9 – 12.3	9.5 – 10.1	13.2 – 13.8

resistant hard-facing of rolling mill rolls and roll-table rollers. Samples of the metal were tested to heat and wear resistance at increased temperatures, and to resistance to solidification cracking during hard-facing. Its hardness at normal and increased temperatures and mechanical properties, including after tempering, were evaluated and metallographic studies were conducted. The samples were made by depositing five layers on steel 50 (C — 0.3 wt.%; Fe — balance) plates 40 mm thick, which were preheated prior to deposition to a temperature of 300 – 350 °C. For comparison, investigations were conducted on the deposited metal produced by the submerged-arc hard-facing method using wires of the Sv-08A (C — 0.1; Si — 0.03; Mn — 0.35 – 0.65 wt.%; Fe — balance) and Sv-10GN (C — 0.1; Mn — 1.0; N — 0.8 wt.%; Fe — balance) grades and ceramic flux ZhSN-5. Results of these comparative tests are given in the Table.

As shown by laboratory investigations, the deposition process performed by the submerged-arc hard-facing method using steel 18Kh3GMFA strip and fused flux AN-60 is characterized by high welding-technological properties, such as stable arc burning, good formation of the deposited metal, absence of pores and undercuts, and good detachability of the slag crust. As it can be seen from the data given in the Table, the metal deposited by the submerged-arc hard-facing method using strip 18Kh3GMFA and flux AN-60 exhibits very high service properties (first of all, increased ductility and crack resistance), which is especially important for metal operating under conditions of cyclic variations in loads and temperatures.

Results of the investigations performed are indicative of technical feasibility and promising future of using the cold-rolled alloyed strip manufactured by the Plant for hard-facing of rolling mill rolls and roll-table rollers. Hard-facing was done on a pilot-commercial batch of rolls of the slabing-1150 mill (horizontal and vertical rolls), NShS-1700 hot rolling mill (roughing stand backing-up and working rolls) and TLS-3000 roll-table rollers. The process of hard-facing using the alloyed strip is characterized by a high stability and consistency, good detachability of the slag crust and high quality of formation of the treated surface.

Operation of the hard-faced rolls of the slabing-1150 mill showed that the working layer met all requirements of the technology of rolling the slabs, i.e. absence of slipping and frictional sliding of metal and improvement of bite of slabs. The rate of wear of the working surface is not in excess of the specified one and amounts to 1 mm per 150,000 – 170,000 t of rolled products (at minimum fire cracking). Operation of the hard-faced NShS-1700 mill rolls and TLS-3000 roll-table rollers proved high properties of the working layer deposited with the alloyed strip. Analysis of strength of the rolling mill rolls showed that their service reliability was higher than that of standard steels. In addition, wear resistance of the working layer deposited by the submerged-arc hard-facing method using flux AN-60 is not higher than that using flux ZhSN-5, which is attributable to a lower degree of alloying of the strip. However, in addition to an increase in productivity of the hard-facing process, the economical expediency of using the alloyed strip made by the Plant allows its wide application to be recommended for repair and hardening of rolling mill rolls and roll-table rollers.

The Plant is currently involved in further collaborative R&D efforts intended for production of hard-facing strip with a different degree of alloying. This will enable solution of the problem of providing the required and relatively inexpensive hard-facing consumables for high-productivity processes of repair and hardening of wearing parts by the electric submerged-arc hard-facing method using the electrode strip and ceramic flux under the domestic production conditions.

MASTERING THE TECHNOLOGY FOR MANUFACTURE OF COLD-ROLLED ALLOYED HARD-FACING STRIP AT THE OJSC «ILYICH MARIUPOL METALLURGICAL WORKS»

V.N. MATVIENKO, K.K. STEPNOV, V.P. IVANOV, N.G. ZAVARIKA, A.I. OLDAKOVSKY and **V.P. ERMOLOV**
Priazovsky State Technical University, Mariupol, Ukraine

ABSTRACT

Described are peculiarities of development of composition and manufacture of cold-rolled alloyed strip at the Open Joint-Stock Company «Ilyich MMW», intended for deposition of a wear-resistant metal layer by the electric-arc hard-facing method to repair and harden parts of rolling and metallurgical facilities.

Key words: *electric submerged-arc hard-facing, cold-rolled alloyed strip, deposited metal, parts of rolling and metallurgical facilities*

The Ilyich Mariupol Metallurgical Works is an enterprise which is capable of using a complete metallurgical cycle, and which manufactures a wide range of products. One of the main areas of its activity is manufacture of high-quality plates of a different thickness. The enterprise extensively employs the process of electric-arc hard-facing of parts of metallurgical and rolling equipment. Hard-facing consumables are in high demand. At present there is a shortage of electrode materials for mechanized wear-resistant hard-facing. To solve the problem of providing repair workshops with electrode materials, the Plant decided to develop and master the technology for manufacture of cold-rolled alloyed strip. Use of the electrode strip as a hard-facing consumable provides high productivity of the process, small depth of penetration of the base metal, reliability of penetration of a roll being treated and stability of the process at a lower current density, as compared with the case of using hard-facing wires. Along with a high productivity, the process provides the deposited metal characterized by homogeneous composition and properties, which is determined by self-regulation of the efficiency of melting of flux and strip, as well as by intensive mixing of the metal pool under the effect of the arc moving along the tip.

Based on the results of investigations of properties of hard-facing medium-chrome steels conducted by the Branch Research Hard-Facing Laboratory of Priazovsky State Technical University in order to identify optimal composition and ensure the best combination of strength and ductile properties of a material to be used as a hard-facing strip, it was recommended that sparsely-alloyed steels should be used for this purpose. They make it possible to meet stringent requirements for production of thin cold-rolled strip and produce deposited metal with high technological and service properties.

In development of the technology for manufacture and utilization of the hard-facing alloyed strip, one often faces mutually exclusive requirements. To ensure the required properties (high strength and hardness), steel used for manufacture of the strip should be practically workable (ductile and of low hardness) at all stages of the metallurgical and rolling cycles. At the same time, the developed compositions of the surfacing strip did not correspond to the grades of steels mastered by the Plant for manufacture of thin plates.

Detailed analysis of technical capabilities of the Plant shops involved in production of rolled products of the required chemical composition and properties resulted in the development, in collaboration with the Plant associates, of the technology for manufacture of the cold-rolled strip. The technology provided for melting of steel of a preset chemical composition at a steel shape casting shop, rolling of ingots into slabs using the slabing-1150 mill at a roughing shop, and rolling of slabs into strip 3 mm thick using the NShS-1700 mill at a hot rolling shop. Cold rolling of the strip was done to achieving a final thickness of $1^{-0.2}$ mm, then the strip was cut into strips 30 mm wide. The works completed resulted in mastering the technology for manufacture of the cold-rolled alloyed hard-facing strip of the 18Kh3GMFA (C — 0.18; Cr — 3.0; Mn — 1.0; Mo — 1.0; V — 0.3 wt.%), 20Kh4GMFB (C — 0.2; Cr — 4.0; Mn — 1.0; Mo — 1.0; V — 0.5; Nb — 0.3 wt.%) and 25Kh3BMB (C — 0.25; Cr — 3.0; Mo — 0.5; W — 0.6; Nb — 0.6 wt.%) grades.

Tests were conducted on metal deposited by the submerged-arc hard-facing method using strip of steel 18Kh3GMFA and flux AN-60 (SiO_2 — 42.5 – 46.5; MnO — 47.0 – 41.0; CaO — 3.0 – 11.0; MgO — 0.5 – 3.0; CaF_2 — 5.0 – 8.0 wt.%) to identify the possibility of application of the alloyed strip for wear-

tions, to increase in fatigue limit of the joints in case of a symmetric cycle of loading by 12 – 25 %. At the same time the increase in the fatigue limit, set during testing of samples on the base of $2 \cdot 10^6$ cycles under the influence of the high-frequency peening reaches 200 % from the data of [4] (Figure 4).

Consequently, the reduction in concentration of effective stresses at the high-frequency peening is not, probably, a prevailing factor in the increase of the fatigue strength of the joints. The set increase in the fatigue limit of welded joints at the expense of the high-frequency peening, can, probably, be explained by the decrease in tensile and the creation of the favourable residual compressive stresses on the surface layer of the near-weld zone metal, as well as by the presence of the cold working effect (deformation hardening).

REFERENCES

1. Trufyakov, V.I. (1998) Increase in fatigue strength of welded joints and structures. *Avtomaticheskaya Svarka*, **11**, 11 – 19.
2. Statnikov, E.S., Muktepavel, V.O., Trufyakov, V.I. *et al*. Comparison of ultrasonic peening treatment (UPT) and other fatigue life improvement methods. *IIW Doc. XIII-1817–00*.
3. Mikheev, P.P., Nedoseka, A.Ya., Parkhomenko, I.V. *et al*. (1984) Effectiveness of application of ultrasonic treatment for increase in fatigue resistance of welded joints. *Avtomaticheskaya Svarka*, **3**, 4 – 8.
4. Statnikov, E.S., Trufyakov, V.I., Mikheev, P.P., *et al*. Specifications for weld toe improvement by ultrasonic peening treatment. *IIW Doc. XIII-1617–96*.
5. Mikheev, P.P. (1990) Improvement in fatigue resistance of welded joints and structures using ultrasonic peening treatment. In: *Problems of welding and special electrometallurgy*. Ed. by V.K. Lebedev. Kyiv: Naukova Dumka.
6. Trufiakov, V.I., Mikheev, P.P., Kudryavtsev, Yu.F. (1995) Fatigue strength of welded structures. Residual stresses and strengthening treatments. *Welding and Surfacing Rev.*, Vol. 3, Part 2. Harwood A.P.
7. Asnis, A.E., Ivashchenko, G.A. (1985) *Improvement of strength of welded structures*. Kyiv: Naukova Dumka.
8. Makhnenko, V.I., Mosenkis, R.Yu. (1985) Calculation of stress concentration factors in welded joints with butt and fillet welds. *Avtomaticheskaya Svarka*, **8**, 7 – 18.
9. (1990) *Strength of welded joints at alternating loads*. Ed. by V.I. Trufyakov. Kyiv: Naukova Dumka.

ROBUST DIGITAL SENSOR FOR ARC WELDING

G.A. TSYBULKIN
The E.O. Paton Electric Welding Institute, NASU, Kyiv, Ukraine

ABSTRACT

Modification of a digital arc sensor designed for a current estimation of the electrode deviation from the axial line of the joint being welded is suggested. The sensitivity of the sensor to some parametric disturbances of the welding process is reduced significantly due to the mounting of an additional digital unit.

Key words: *arc welding, lateral deviation of torch, digital arc sensor, parametric indeterminacy, serviceability*

When estimating the lateral deviation of the electrode from the axial line of the joint welded on the bases of measuring the welding current, using the so-called arc sensor [1], it is supposed usually that the parameters of the welding process are known with a sufficient accuracy and do not change practically during the arc welding. But actually, some parameters are not known accurately, and, besides, their values in the process of welding are changed unpredictably. Therefore, the estimation of the lateral deviation, obtained under the conditions of the parametric indeterminacy does not guarantee the required accuracy, that hinders greatly the solution of the next problem, namely the correction of movement of the welding torch on the basis of this estimate.

In [2] an effective method of estimation of deviation of the electrode has been suggested that possesses a low sensitivity to the changes in uncontrollable parameters. In particular, the estimate of the lateral deviation ε_n, which is obtained from the results of measurement of deviations δ_R and δ_L of welding current from its nominal value, respectively, in the right and left extreme points of the welding torch oscillations, is suggested to be found not using the known formula [3]

$$\hat{\varepsilon}_n = (\delta_R - \delta_L)\frac{M}{4av_n}, \qquad (1)$$

but using the relation

$$\hat{\varepsilon}_n = \frac{\delta_R - \delta_L}{\delta_R + \delta_L}(A - v_n T_c). \qquad (2)$$

In expressions (1) and (2) v_n is the rate of the transverse movement of the torch; M is the steepness of characteristic of electrode melting; A is the amplitude of transverse oscillations of the torch; T_c is the constant of time determined by formula

$$T_c = R/EM,$$

where E is the intensity of the electric field in the arc column; R is the general active resistance of the welding circuit; a is the parameter determining the shape of curve $F(n) = a(n - p)^2 + q (q > 0)$ forming at intersecting the free surface of the weld pool with the plane, passing through the longitudinal axis of

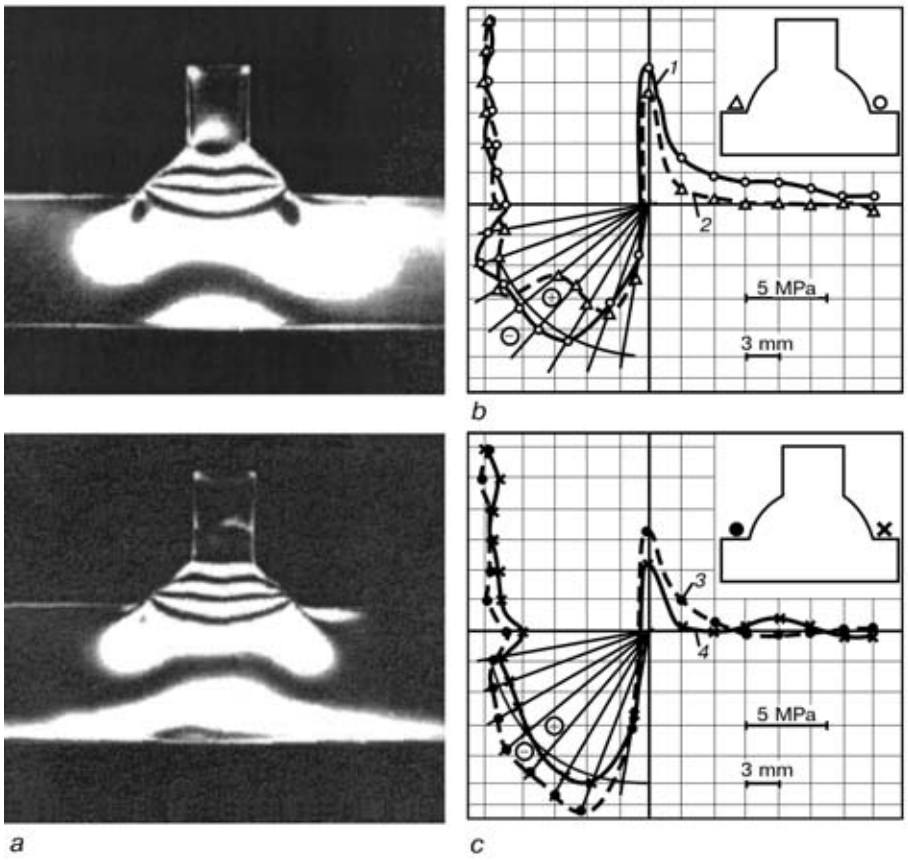

Figure 3. Patterns of isochromatic lines (*a*) and diagrams od stress distribution in near-weld zone of T-joint, obtained in models from optically-active materials, in initial state (*b*) and after high-frequency peening (*c*) at K_t = 2.0 (*1*), 1.8 (*2, 3*) and 1.6 (*4*)

This provides the most valid values of SCF taking into account the set relative radii of mating R/s, transition angles θ and relative legs h/s of the fillet weld (see Figure 1).

For comparison, the SCF was also determined experimentally using the photoelasticity method on models which reproduce the shape of the welded joint. The models of the welded joints were manufactured from the epoxy resin ED6-M. The adequacy of models and welded joints investigated was checked by the comparison of their configurations at a 12-fold increase using a spectral projector PS-18. When simulating welded joints, the conditions of a geometric similarity and performance of the joint material under the stress action were fulfilled. The stressed state of the models was investigated in the polarization installations «Mеorta» and KSP-5. The SCF were determined in the points of weld transition to the parent metal by measuring the optical path-length difference using the coordinate-synchronous polarimeter KSP-5. The patterns of isochromatic lines and distribution of stresses in the near-weld zone of the welded joint of models with fillet welds are shown in Figure 3.

Sample state	*SCF*	
	estimated	*experimental**
Initial	2.3	$\frac{2.0 - 1.8}{1.9}$
After high-frequency peening	1.8	$\frac{1.8 - 1.6}{1.7}$

*In numerator — range of values, in denominator — mean value.

The averaged SCF values, determined by using estimated and experimental methods for the welded joint with transverse fillet welds are given in the Table.

The comparison of estimated and experimental data of SCF showed that the discrepancy between them is negligible. Under the influence of the high-frequency peening, the SCF in welded joint with transverse fillet welds is decreased from 2.3 – 1.9 to 1.8 – 1.7.

The results of investigations [9] prove that this reduction in SCF values leads, at other equal condi-

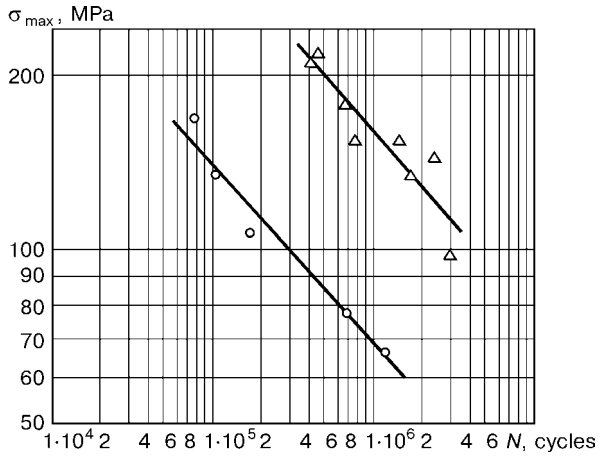

Figure 4. Results of fatigue tests at three-point bending of T-joints of high-strength steel at coefficient of asymmetry of loading cycle R_σ = –1 in initial state (○) and after high-frequency peening (△)

ROLE OF STRESS CONCENTRATION REDUCTION AT HIGH-FREQUENCY PEENING FOR FATIGUE RESISTANCE INCREASE IN WELDED JOINTS

P.P. MIKHEEV and **O.V. VOJTENKO**
The E.O. Paton Electric Welding Institute, NASU, Kyiv, Ukraine

ABSTRACT

Experimental values of stress concentration factor (SCF), determined using polarization-optical (photoelasticity) method, are compared with estimated values, determined by measurement of parameters of fillet welds of T-joints in initial state and after high-frequency peening. The relation between the SCF reduction under the action of the high-frequency peening and increase in the fatigue resistance of the welded joints is shown.

Key words: *welded joint, fillet weld, geometric parameters of weld, stress concentration factor, calculation methods, photoelasticity method, high-frequency peening, increase of fatigue resistance*

Among the known methods of improving the fatigue resistance of welded joints using the surface-plastic deforming of the near-weld zone, a method of the high-frequency peening is most effective [1, 2]. This method has been developed by «Kvant» (Severodvinsk, Russia) and the E.O. Paton Electric Welding Institute [3]. In case of welded joints without removed reinforcement and having intricate connections a compact hand ultrasonic tool with a multielement executive organ is used for the high-frequency peening [4]. The ultrasonic thyristor generator device with up to 1.2 kW output capacity is used as a tool power source with a mangnetostriction transducer [4].

The positive effect of the high-frequency peening on the fatigue resistance of the welded joints is attained at the expense of decrease in stress concentration, setting of compressive residual stresses in the zone of a stress raiser and deformation hardening of the near-weld metal [5, 6].

The aim of the present work is to investigate the change in stress concentration in the welded joint under the action of the high-frequency peening and to estimate the role of this factor for increasing the fatigue resistance of the joint.

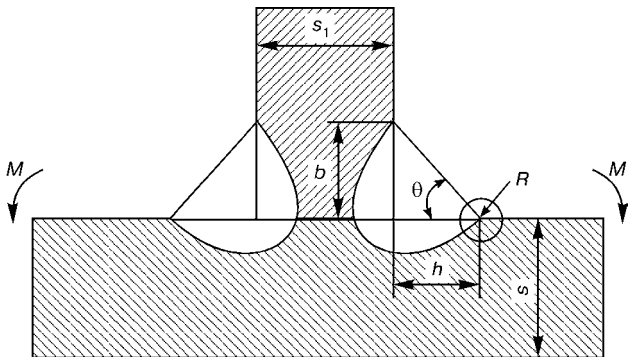

Figure 1. Geometric parameters of fillet weld of welded T-joint: M — moment of applied load; s, s_1 — thickness of plates being welded and welded-on, respectively; b, h — legs of fillet weld

The geometric parameters of the joint (Figure 1), required for determination of the SCF, were set by using a calculation method. Here, the samples with transverse fillet welds, made from high-strength steel, were used for the fatigue tests (Figure 2). The high-frequency peening of the transition zone from weld to the parent metal was performed using one of the technological variants providing the significant increase in the fatigue resistance of the welded joint. When determining the radius R of the weld metal transition to the parent metal and angle θ, the method of profilometry was used [7]. For each sample three profile lines of a local geometry of the fillet weld were plotted.

The estimated determination of SCF in initial joints and those after high-frequency peening was made using relation (1) from [8]:

$$K_t = 1 + \frac{1 - \exp\left(-0.9\theta\sqrt{\frac{s}{2h}+1}\right)}{1 - \exp\left(-0.45\pi\sqrt{\frac{s}{2h}+1}\right)} \times \left[\text{th}\left\{\frac{\left(\frac{2h}{s}\right)^{1/4}}{1-\frac{R}{s}}\right\}\right]\left[\frac{0.13 + 0.65\left(1-\frac{R}{s}\right)^4}{\left(\frac{R}{s}\right)^{1/3}}\right]. \quad (1)$$

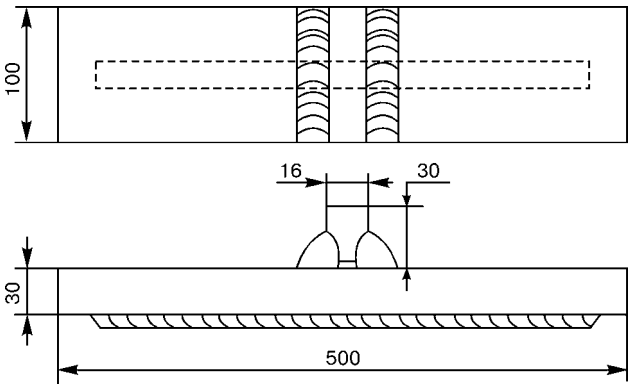

Figure 2. Welded high-strength steel sample for fatigue tests

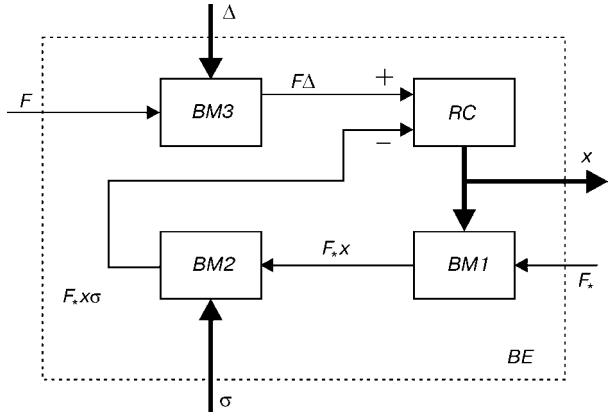

Figure 3. Schematic diagram of block of estimation

a rather simple scheme on binary multipliers, described formerly by Lundh [5]. We added an additional block of estimation *BE*, constructed on binary multipliers (Figure 3), into the diagram of the digital sensor device (Figure 2). In *BE* diagram three binary multipliers *BM1*, *BM2*, *BM3* and a reversible counter *RC* were used.

Sequences of pulses of similar frequency F and F_*, but being out-of-phase, are supplied to the binary multipliers to prevent the coincidence of pulses with time at outputs *RC*. Pulses with frequency F_* and some number x are supplied to *BM1*. At the output *BM1* the pulses of frequency F_*x are formed which are supplied to the input of the secondary of binary multiplier *BM2*. Number $\sigma = 2\Delta N_b$, obtained by shear for one charge to the left of number ΔN_b forming at the output *BCD*, is entered to the controllable inputs *BM2* (see Figure 2). At the output *BM2* the pulses of frequency $F_*x\sigma$ are occurred. Number $\Delta = \delta N_n$, obtained also at the *BCD* output, is entered to the third binary multiplier *BM3* through the controllable inputs. Pulses of frequency $F\Delta$ are formed at the output *BM3*.

If at the initial period of time the number $x = 0$, then $F_*x\sigma = 0$ and x begin to increase with entrance of pulses of frequency $F\Delta$ to the addition input of *RC*. Increase in x leads to a gradual increase in frequency $F_*x\sigma$. As soon as values of frequency $F\Delta$ and $F_*x\sigma$ become equal at both inputs *RC*, i.e. when the transition period is completed, the following relation will be set in the diagram:

$$F\Delta = F_*x\sigma,$$

from which it follows that

$$x = \frac{F\Delta}{F_*\sigma} = \frac{\Delta}{\sigma} = \frac{\Delta N_n}{2\Delta N_b}. \qquad (5)$$

The time of establishment of the transition process at twelve digit binary multipliers and frequency of pulses $F = F_* = 1$ MHz is 0.3 – 0.5 ms, as the calculations show, that is quite acceptable for practical use.

Thus, the number x at the output *RC* in each moment of time $t = kT$ at preset A, v_n and T_c characterize the lateral deviation ε_n, according to (4) and (5).

So, the modified arc sensor acquires a robust property with respect to the uncontrollable movement of the free surface of the weld pool at the expense of introducing an additional block constructed on simple counter-type structures.

REFERENCES

1. Inoue, K., Zhang, J., Kang, M. (1991) Analysis of detection sensitivity of arc sensor in welding process. *Transact. of JWRI*, **2**, 53 – 56.
2. Tsybulkin, G.A. (1999) About evaluation of current deviation of electrode from the line of joint being welded. *Avtomaticheskaya Svarka*, **12**, 53 – 54.
3. Cook, G.E. (1983) Robotic arc welding: research in sensory feedback control. *Transact. of IEEE on Ind. Electr.*, **30**, 252 – 268.
4. Tsybulkin, G.A. Digital device for direction of the welding robot along the weld. USSR author's certificate **1822042**, Int. Cl. B 23 L 9/10. Publ. 10.05.93.
5. Lundh, Y. (1959) Digital technique for small computations. *J. Brit. IRE*, **1**, 37 – 44.

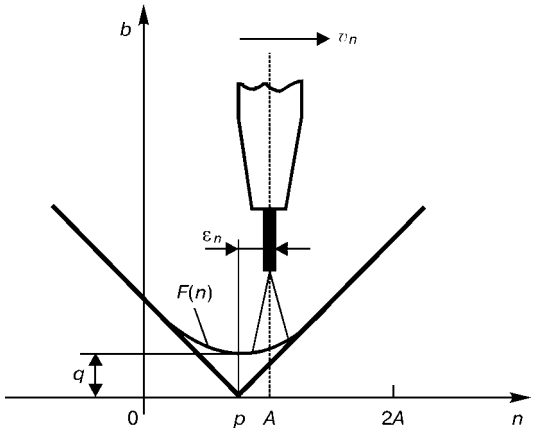

Figure 1. Scheme of torch movement across the line of joint being welded

the electrode and perpendicular to the axial line of the fillet joint welded (Figure 1). Parameter p, determining the shape and position of curve $F(n)$, and value ε_n are associated by the ratio $p = A - \varepsilon_n$.

Considering expressions (1) and (2) it is not difficult to note that estimate (2) unlike (1) does not depend absolutely on the parameter a which is, due to non-stationary movement of a free surface of the molten pool in the process of welding, subjected to uncontrollable changes and is not almost subjected to the current identification. Expression (2) includes only measurable values δ_R, δ_L, and also preset and known values A, v_n and T_c.

As was expected, the estimate of the lateral deviation possesses the similar property of robustness (low-sensitivity) as regards to changing the parameter a

$$\hat{\varepsilon}_n = \frac{\bar{\delta}_R - \bar{\delta}_L}{\bar{\delta}_R + \bar{\delta}_L}(A - v_n T_c), \qquad (3)$$

constructed by formula (2), but in which the mean values of deviations of welding current from nominal its value

$$\bar{\delta}_R = \bar{\delta}_L(\Delta n) \text{ and } \bar{\delta}_L = \bar{\delta}_L(\Delta n),$$

obtained not at the extreme points, but at some intervals of measurement $\Delta n \le A$ on the right and left from the middle position of the torch are figured instead of δ_R and δ_L.

These are mean values of the values measured which are calculated in many arc sensors, in particular in the digital sensor, suggested in [4] for the estimation of the deviation of the electrode end from the line of the joint welded. The digital arc sensor has the advantage over the arc sensor in an analog version, due to simplifying of its mating with systems of control of welding robots and automatic machines, which are made, as a rule, on the base of the digital engineering. But in design of the sensor, suggested in [4], not a robust algorithm (3) is used, but an algorithm (1) which has a drawback caused by sensitivity of estimate $\hat{\varepsilon}_n$ to the changes of parameter a.

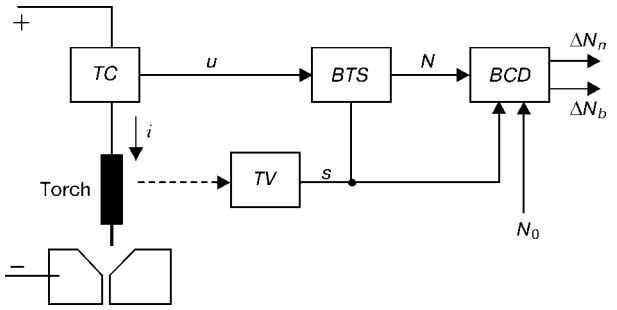

Figure 2. Schematic diagram of digital sensor

The present article will describe the modification of this sensor providing the robust estimation of the lateral deviation in the digital form. Figure 2 shows its simplified schematic diagram. The sensor includes transducers of welding current TC and voltage TV and also the blocks of transformation of signal BTS and calculation of deviations BCD. The scheme has the following designations: $u = u(t)$ is the voltage at output TC, proportional to welding current $i = i(t)$; N is the mean value of results m of voltage measurements $u(t)$ presented in unit-counting code and calculated by formula

$$N = \frac{1}{m}\sum_{j=1}^{m} N_j,$$

where N_j is the number of pulses entered the output BTS as a result of the j-th measurement; N_0 is the preset binary numbers corresponding to the rated welding current; s is the signal synchronizing the device operation; $\Delta N_n = \Delta N_n[kT]$ and $\Delta N_b = \Delta N_b[kT]$ are the binary numbers forming at the output BCD and characterizing $t = kT$ in each moment of time of torch deviation, respectively, in a lateral direction ε_n and along the electrode axis ε_b; T is the period of transverse oscillations of the welding torch; $k = 1, 2, \ldots, K$. In addition, according to [2]

$$\Delta N_n = N_1 - N_2, \quad \Delta N_b = \frac{N_1 + N_2}{2} - N_0.$$

In these expressions $N_1 = N_1[kT_1]$ and $N_2 = N_2[kT_2]$ are the numbers proportional to a mean value of the welding current in the periods of time of measurement T_1 and T_2 when the welding torch is located on the right and left from the mean its position, respectively, $T_1 = T_2 = A/v_n$.

It is evident, if now instead of estimate $\hat{\varepsilon}_n = K_1\Delta N_n$, where $K_1 = K_1(M, a, v_n)$, to calculate by any way the estimate $\tilde{\varepsilon}_n$ forming in accordance with relation

$$\tilde{\varepsilon}_n = \frac{\delta N_1 - \delta N_2}{\delta N_1 + \delta N_2}(A - v_n T_c) = \frac{\Delta N_n}{2\Delta N_b}(A - v_n T_c), \qquad (4)$$

similar to (3), then this value, the same as estimate (3), will be robust relative to changes in parameter a. (In expression (4) $\delta N_s = N_s - N_0$, $s = 1.2$.)

For technical realization of ratio $\Delta N_n / 2\Delta N_b$ included into formula (4) it possible to use, for example,